CHARACTERIZATION OF BROADBAND REGIONAL DISTANCE SEISMOGRAMS: USE OF GLOBAL, OPEN DATA TO STUDY REGIONS OF INTEREST

Terry C. Wallace
Susan L. Beck

Southern Arizona Seismic Observatory
University of Arizona
Tucson, Arizona 85721

June 1995

Final Technical Report

Accesion For	
NTIS CRA&I	☑
DTIC TAB	☐
Unannounced	☐
Justification	
By	
Distribution /	
Availability Codes	
Dist	Avail and / or Special
A-1	

DTIC QUALITY INSPECTED 2

19950821 041

REPORT DOCUMENTATION PAGE

Form Approved
OMB No. 0704-0188

Public reporting burden for this collection of information is estimated to average 1 hour per response, including the time for reviewing instructions, searching existing data sources, gathering and maintaining the data needed, and completing and reviewing the collection of information. Send comments regarding this burden estimate or any other aspect of this collection of information, including suggestions for reducing this burden, to Washington Headquarters Services, Directorate for Information Operations and Reports, 1215 Jefferson Davis Highway, Suite 1204, Arlington, VA 22202-4302, and to the Office of Management and Budget, Paperwork Reduction Project (0704-0188), Washington, DC 20503.

1. AGENCY USE ONLY (Leave blank)

2. REPORT DATE: June 1995

3. REPORT TYPE AND DATES COVERED: FINAL 15 July 92 - 15 January 95

4. TITLE AND SUBTITLE: Characterization of Broadband Regional Distance Seismograms: Use of Global, Open Data to Study Regions of Interest

5. FUNDING NUMBERS:
PE 61102F
Project 2309/AS
F49620-92-J-0416

6. AUTHOR(S)

Terry C. Wallace
Susan L. Beck

AFOSR-TR-95
0528

7. PERFORMING ORGANIZATION NAME(S) AND ADDRESS(ES)

Southern Arizona Seismic Observatory
Department of Geosciences
University of Arizona
Tucson AZ 85721

9. SPONSORING/MONITORING AGENCY NAME(S) AND ADDRESS(ES)

AFOSR/NM
110 Duncan Ave
Bolling AFB DC 20332-0001

10. SPONSORING/MONITORING AGENCY REPORT NUMBER

Monograph Series on Seismic Research 95-28

DTIC
ELECTE
AUG 2 2 1995
S D
F

11. SUPPLEMENTARY NOTES

12a. DISTRIBUTION/AVAILABILITY STATEMENT

APPROVED FOR PUBLIC RELEASE: DISTRIBUTION IS UNLIMITED

12b. DISTRIBUTION CODE

13. ABSTRACT (Maximum 200 words)

This research undertook scientific problem inherent in the monitoring of a comprehensive nuclear test ban treaty; establishing confidence that the seismograms from small and moderate-sized events are understood, thus, identifiable. This requires an understanding of broadband regional distance seismic phases from both explosions and earthquakes, the excitation of the various phases, and their dependence on source. Data from open broadband stations across the Andean Cordillera were used in research to evaluate the utility of the spectral characteristics of regional distance seismograms of phase ratio pairs (Pg/Lg; Pn/Lg). The entire regional waveforms for seismic events traversing the Andes were modeled providing detail of crustal thickness, the average crustal velocity, and propagation efficiency. Further, this report details research to treat a single regional distance station as a seismic observatory and to establish a relative location procedure in which to locate smaller magnitude events relative to an established epicentral coordinate. Finally, the results are reported of a temporary broadband deployment used to record the DOE hosted Non-Proliferation Experiment; exploration of how geologic environment changes affects discriminants.

14. SUBJECT TERMS

Seismology, regional discriminants, Andean Cordillera

15. NUMBER OF PAGES: 90

16. PRICE CODE

17. SECURITY CLASSIFICATION OF REPORT	18. SECURITY CLASSIFICATION OF THIS PAGE	19. SECURITY CLASSIFICATION OF ABSTRACT	20. LIMITATION OF ABSTRACT
UNCLASSIFIED	UNCLASSIFIED	UNCLASSIFIED	UNLIMITED

Chapter 1

Introduction

The two outstanding scientific problems in the arena of discrimination and verification of underground nuclear explosions are monitoring of a comprehensive test ban (CTBT) and developing "confidence" that the seismograms from small and moderate-sized events are understood and therefore identifiable. Both these problems require a fairly complete understanding of broadband regional distance seismic phases from both explosions (nuclear and chemical) and earthquakes. Most discrimination schemes are based on ratios of the excitation of various phases. Unfortunately, regional distance seismic phases are a complex combination of both propagation and source effects, and any discrimination algorithm requires both empirical and analytic development. There is a basic need to improve our understanding of regional distance wave propagation and the effects of Earth structure on the character of Pn, Pg, and Lg. Further, seismologists must improve their understanding of the excitation of the various phases and their dependence on source (earthquakes and explosions).

Open seismic stations equipped with very broadband sensors provide an outstanding experimental facility for improving our understanding of regional distance seismology. The stations are situated in a wide range of geological environments and allow a data base to be constructed for situations which are important for monitoring. This allows us to go to regions where there is direct monitoring interest, or to regions which may serve as analogs. Until recently, there was concern that certain South American countries had the capability of clandestine testing of a nuclear device. Little work has been done on the details of high-frequency, regional distance propagation along the Andean Cordillera, which is a complex mountain belt. Spectral characteristics of regional distance seismograms provide the most promising discriminants; this is based on the following: (1) Given the same zero frequency moment, an earthquake will be enriched in high frequencies as compared to an explosion, and (2) earthquakes excite more S wave type energy than explosions. Typically, spectral discriminants are based on the ratio of the amplitude of a particular regional distance phase (Pn, Pg, or Lg) in two narrow bands. Various

phase ratio pairs such as *Pg/Lg* and *Pn/Lg* show good separation of earthquake and explosion populations. Unfortunately, travel path has a strong influence on the "base line" of explosion–earthquake separation criteria. In Chapter 2 we model the entire regional waveforms for seismic events which traversed the Andean Cordillera. This analysis allowed us to detail crustal thickness, average crustal velocity, and efficiency of propagation.

One of the major problems with regional seismic events is that they are usually recorded at a limited number of stations. In fact, it is not unusual for an event to be recorded at a *single* regional distance station. In Chapter 3 we develop procedures to treat such a single station as a seismic observatory. We have developed a relative location procedure in which an established epicentral coordinate is used as a reference to locate smaller events. The procedure is stepwise: (1) Epicentral coordinates are determined from polarization analysis, and (2) focal mechanisms are determined from a waveform inversion.

Chapter 4 reports the results of a temporary broadband deployment used to record the Non-Proliferation Experiment (NPE). The profile was designed to investigate the development of regional seismic phases to explore how a change in geologic environment affects seismic discriminants.

Chapter 2

Crustal thickness variations in the Central Andes of South America determined from regional waveform modeling of earthquakes

Barbra K. Schuessler [1], Susan L. Beck [1], George Zandt [2], and Terry C. Wallace [1]
[1] *Dept. of Geosciences, University of Arizona, Tucson, AZ 85721, USA*
[2] *Lawrence Livermore National Laboratory, Livermore, CA 94550*

SUMMARY

The Central Andes of South America are a complex mountain belt associated with the subduction of the Nazca plate beneath the South American plate. The Peruvian Andes have an average elevation of over 5000 m, and the Altiplano Plateau has an average elevation of nearly 4000 m. Many models have been proposed to explain the uplift of the Peruvian Andes and the Altiplano, including magmatic addition, lithospheric thinning, crustal shortening, lithospheric delamination, and combinations of these mechanisms. Detailed determination of crustal thickness and average crustal velocities for the Central Andes provides important constraints for various thermal and mechanical uplift models. Using shallow to intermediate-depth, regional distance earthquakes, recorded at the digital stations NNA and ZOBO, first-order approximations of the crustal thickness and average crustal velocities have been obtained for parts of the Central Andes in Peru and Bolivia.

We modeled the entire regional waveform in the passband of 20 to 100 s with synthetic seismograms calculated with the reflectivity method. The observed and synthetic waveforms are compared using a grid search to maximize the fit in terms of average crustal thickness, crustal velocity, and mantle lid structure. Events located north of NNA, which are sensitive to the structure beneath the Peruvian Andes, are best modeled with a 48-km-thick crust and an average crustal *P*-wave velocity of 6.2 km s^{-1} above an ~40-km-thick lithospheric lid. These events sample an inactive region of the magmatic arc directly above a flat subducting slab. Events located above the area of slab dip transition are modeled with a 60-km-thick crust and an average *P*-wave

velocity of 6.1 km s^{-1}. Events with paths confined to the Altiplano show an average crustal thickness of 75 km, with a 50-km-thick mantle lid. Our results also suggest that the average crustal *P*-wave velocities are relatively low (5.95 km s^{-1}) under the Altiplano Plateau. A receiver function analysis of the data recorded at LPAZ in the Eastern Cordillera indicates a crustal thickness of only 55 km, much thinner than the nearby Altiplano Plateau.

Key Words: Altiplano Plateau, Peruvian Andes, crustal structure, reflectivity modeling

1 INTRODUCTION

The Andes of South America are a continuous mountain belt stretching over 4000 km along the convergent margin between the South American plate and the Nazca plate (Fig. 1). This convergent margin and associated structures are the type locality for many studies on ocean-continent subduction and mountain building processes. In this study, we present new seismological evidence on regional crustal thickness variations along the length of the Andes.

The major tectonic regions of the Peruvian Andes are a narrow coastal plain, the volcanic Cordillera Occidental, the Altiplano, the uplifted older fold-and-thrust belt of the Cordillera Oriental and the active fold-and-thrust belt of the sub-Andes. In the Peruvian Andes north of 10°S, an inactive volcanic arc and a fold and thrust belt form a single continuous mountain chain. Crystalline basement rocks outcrop in the coastal plain region, and the Ariquepa block, a Precambrian massif 1.8–2.0 b.y. old (Dalmayrac, Lancelot & Leyreloup 1977), outcrops from 14–17°S (Suarez, Molnar & Burchfiel 1983). A coastal range, the Cordillera Blanca, extends from 8° to 10°S, just NW of the Cordillera Occidental. The elevation of the range exceeds 5500 m and reaches 6800 m locally (Dalmayrac & Molnar 1981). The extreme topographic relief of the mountains and the presence of many young granitic plutons (3–12 m.y.) suggest that this range is a young feature (Stewart, Evernden & Snelling 1974; Dalmaryrac & Molnar 1981).

South of 10°S, the Peruvian Andes split into two branches, the Western and Eastern Cordillera, separated by the Altiplano high plateau (Fig. 2). At Lake Titicaca near La Paz, Bolivia, the width of this plateau reaches 350 km (Fukao, Yamamoto & Kono 1989). This denotes the

central portion of the Andes, where the Altiplano high plateau is located. The plateau has been an area of special interest since it is proposed to have an anomalously thick crust between 60–80 km thick, which supports a mean elevation of 4 km (James 1971b; Ocola, Meyer & Aldrich 1971; Isacks 1988). This study focuses on the Peruvian Andes and the northern section of the Altiplano Plateau (Fig. 2).

The western margin of South America has been the locus of subduction for at least 300 million years. During this long period of complicated subduction the slab–continent interaction has evolved with time. Currently, the subducting Nazca plate has two segments of relatively flat dip between 8° to 13°S and then again between 28° to 32°S (Haswega & Sacks 1981; Jordan *et al.* 1983; Chinn & Isacks 1983; Cahill & Isacks 1992). There is no active volcanism above the flat slab regions, presumably due to the absence of the asthenospheric wedge (Barazangi & Isacks 1979). The subducting slab is at an angle of 30° beneath most of the Altiplano Plateau, accompanied by active arc volcanism (between 13° and 28°S) (Cahill and Isacks 1992). North of 8°S and between 13° and 28°S the subducting slab has a normal dip of approximately 30°. The Peruvian Andes lie above a flat slab region with the abrupt transition zone in slab dip at 14° to 15°S (Barazangi & Isacks 1979; Grange *et al.* 1984; Lindo *et al.* 1992).

Many mechanisms have been proposed for the crustal thickening and uplift of the Peruvian Andes and Altiplano Plateau. The end-member models that have been proposed include underthrusting of the Brazilian craton (Suarez, Molnar & Burchfiel 1983; Jordan *et al.* 1983; Roeder 1988; Dorbath *et al.* 1993), distributed crustal shortening and telescoping (Isacks 1988; Allmendinger *et al.* 1990; Sheffels 1990, Schmitz 1994), lithospheric thinning (Froidevaux & Isacks 1984; Isacks 1988; Whitman *et al.* 1992), magmatic addition (James 1971b; Kono, Fukao & Yamamoto 1989), and combinations of these end member models. The crustal and upper mantle structure beneath the Andes has not been well constrained due to limited seismic station coverage and rugged terrain.

2 PREVIOUS GEOPHYSICAL STUDIES

There have been several geophysical studies of the Altiplano Plateau in Bolivia but much fewer studies in the Peruvian Andes and the Eastern Cordillera, due in part to the rugged terrane. Previous geophysical studies of the Altiplano have derived varying results for crustal thicknesses and average crustal velocities, but all studies find thick crust beneath the Altiplano. James (1971a) used phase and group velocities of Rayleigh and Love waves and found a 70-km-thick crust having an average crustal velocity of 6.15 km s^{-1} beneath the Western Cordillera, with the crust thinning to 50–55 km and having a crustal velocity of 5.95 km s^{-1} under the Eastern Cordillera. Seismic refraction studies (Ocola, Myer & Aldrich 1971; Ocola & Meyer 1972) were unable to constrain the crustal thickness since there was no clear evidence of a Moho reflection. However, this implied that the crust was greater than 70 km thick. A more recent seismic refraction study (Wigger 1988) indicates that crustal thickness is about 70 km beneath the Altiplano and the average crustal velocity is a low 6.0 km/s. These crustal parameters are supported by a teleseismic study of near-source depth-phase precursors sampling the southern Altiplano which determined a crustal thickness of 75-80 km and an average crustal velocity of 5.9-6.0 km/s (Zandt *et al.* 1994). Cabre (1983) used inversion of *P*- and *S*-wave residuals and Fernandez & Careaga (1968) used spectral analysis of longitudinal seismic waves to obtain a thickness of 65 km beneath La Paz, Bolivia. A recent study of travel-time residuals for teleseismic events by Dorbath *et al.* (1993) interprets a 10-km thinning of the crust from the Altiplano to the Eastern Cordillera near La Paz, Bolivia.

Gravity studies are important for constraining lateral density variations in the crust. Gravity surveys across the Peruvian Andes are modeled with a crustal thickness of 45 km in northern Peru, 55 km in central Peru, and 65 km in southern Peru (Fukao *et al.* 1989). For the Altiplano, the gravity is consistent with the crust being thickest beneath the Western Cordillera (about 75 km) and gradually thinning toward the Eastern Cordillera and Sub-Andean zone (Fukao *et al.* 1989). Lyon-Caen, Molnar & Suarez (1985) matched their observed Bouguer anomaly of –400 mGal across the Altiplano by using a 70-km-thick crust. Gravity results from 21°S to 25°S by Götze, Schmidt & Strunk (1988) show a 70-km-thick crust beneath the Altiplano and a 40-km-

thick crust beneath the Brazilian shield. Ocola and Meyer (1973) modeled gravity with a 75-km-thick crust beneath the Altiplano and a 70-km-thick crust in southern Peru. The transition to a 40-km-thick Brazilian Shield appears to be abrupt in Peru and more gentle in Bolivia (Ocola & Meyer 1973).

Although all these studies indicate relatively thick crust beneath the Altiplano, many of the estimates are not well constrained. We have modeled waveforms from regional distance earthquakes in order to help constrain the average crustal thickness along the Central Andes. We use regional data recorded at digital seismic stations NNA in Peru and ZOBO in Bolivia (Fig. 1). In addition, we modeled some teleseismic broadband data recorded at LPAZ, a new digital seismic station that replaced ZOBO.

3 DATA

Regional distance seismograms are sensitive to the details of the crust–mantle waveguide. At long periods, the relative timing of body and surface waves arrivals depend on the gross properties of the crust (thickness and mean velocity) and uppermost mantle. We have modeled the regional waveform (P_{nl} and surface waves) in the passband of 20 to 100 s. We use digital seismograms recorded from two permanent seismic stations in South America, NNA and ZOBO. NNA is a digital broadband station located near the coast of Peru and east of Lima, in Naña. This region is underlain by a flat segment of the subducting slab, just north of the transition zone where the slab dip becomes more steep. ZOBO was a digital Seismic Research Observatory (SRO) station, located northeast of the Altiplano, in the Eastern Cordillera, northeast of La Paz, Bolivia. Recently, a new digital broadband station LPAZ has been installed near ZOBO. We used the long-period channel of the ZOBO data and the broadband channel of NNA to model regional waveforms. An example of data from each station, filtered in the bandpass from 20 to 100 s, is shown in Fig. 3. The 21 events selected for the study all have magnitudes greater than 5.0, and their locations are shown in Fig. 1. Both shallow and intermediate-depth earthquakes are used, with most of the events located in the downgoing Nazca plate. Each record has a clear P-wave arrival and a high signal-to-noise ratio. We modeled the entire waveform, including both body and

surface waves, on the vertical, tangential, and radial components when possible. However, in a few cases the records were clipped beyond 100 s; therefore only the P-wave arrivals of the seismograms are modeled.

We compared the Harvard CMT locations and mechanisms with the U.S. Geological Survey Preliminary Determination of Epicenters (PDE) locations and mechanisms and only considered events in which there was good agreement. The event parameters for the nine events recorded at NNA and the parameters for the twelve events recorded at ZOBO are in Tables 1 and 2, respectively. In addition, we also analyzed receiver functions from four teleseismic events recorded at the new broadband station LPAZ (Table 8) located near ZOBO.

4 REGIONAL WAVEFORM MODELING

The gross lithospheric seismic structure of the Central Andes was estimated by comparing synthetic seismograms to observed regional distance waveforms. The synthetics, calculated in the passband of 20 to 100 s, were generated with the reflectivity method (Müller 1985) utilizing the formulaion of Kennett (1983) as implemented by Randall (1994). A horizontally stratified Earth model is assumed with a double-couple point source. We assumed a dissipative media where $Q_\alpha = 2.25\ Q_\beta$. The value of Q is defined for each layer using a Q model based on the estimates for upper mantle attenuation in South America by Whitman *et al.* (1992). The input model parameters include layer densities and a velocity–depth model using Poisson's ratio for the crust of $\nu = 0.24$ and for the mantle of $\nu = 0.27$. Other model input parameters are listed in Table 3.

The observed and synthetic waveforms are correlated to measure the goodness of fit. We used a grid search to maximize correlation in terms of average crustal thickness, crustal velocity, upper mantle velocity, and mantle lid thickness. For each event, a large range of thicknesses and velocities were tested in order to investigate the trade-off between various parameters.

The instrument response is added to the synthetics, and then both the data and synthetics are filtered between 20 and 100 s before comparison and the amplitude is normalized. Higher-frequency body waves are filtered out because they are sensitive to shallow crust variations, and our goal is to focus on larger-scale variations in the crust and upper mantle rather than local

complexities. Using relative amplitudes, the waveform comparison includes the relative timing between the body and surface waves, the overall waveform, and the travel time for the event. The synthetics are aligned with the data using the absolute travel times and are then cut to the same length and sampling rate for comparison. Each fit was compared visually and numerically using correlation coefficient calculations.

The correlation coefficient between the data and synthetic waveform is calculated using the following formula:

$$\frac{\int a(t)\, b(t-\tau)\, d\tau}{\left(\int a^2(t) \int b^2(t)\right)^{1/2}} \tag{1}$$

where a represents the observed time series and b represents the synthetic time series. If the observed and synthetic are aligned *a priori*, then the correlation coefficient reduces to

$$\frac{\sum ab}{\left[\left(\sum a^2\right)\left(\sum b^2\right)\right]^{1/2}} \tag{2}$$

A perfect fit would have a correlation coefficient equal to 1, and a completely out-of-phase fit would have a value of -1. Each component of the seismic record is compared separately, then the correlation coefficients for all three are averaged to give a single value for each model. Thus, the vertical, radial, and tangential components are weighted equally. With this approach, the correlation coefficient comparison is more sensitive to the match of the large-amplitude surface waves rather than the body waves. Occasionally this results in a maximum correlation coefficient with the P waves out of phase. When this happens, the correlation coefficient is disregarded, and only the solutions matching the P-wave polarity are considered. The correlation coefficient values are contoured to determine the best values of average crustal thickness and average crustal velocity for the path.

Since the synthetic seismograms are computed assuming flat layers, we find the best average thickness for the entire event–station path. For long paths that cross several tectonic

provinces with lateral heterogeneity, it is less clear how to interpret the average parameters. This is particularly true for coastal events and events located more than 10° from NNA or ZOBO since there are certainly regional dipping layers and lateral thickness changes in the crust.

4.1 Sensitivity Tests

There are trade-offs between various model parameters such as crustal thickness and mean velocity, so we investigated the resolution of various parameters with a series of synthetic tests. We did numerous sensitivity studies to investigate the behavior of the regional wave propagation, to look at trade-offs, and to ensure that the waveforms are sensitive to various parameters. We also investigated the sensitivity of the synthetic seismograms for event–station geometries for various crustal thicknesses. Fig. 4 shows the waveforms generated using a 40-, 50-, 60-, 70- and 80-km-thick crust for a regional distance event 277 km away, at a depth of 126 km, using an average crustal velocity of 6.0 km s^{-1}. As expected, as the thickness of the crust is increased, the arrivals are more dispersed. The shape of the body-wave arrivals change and the amplitude of the surface wave arrivals increase with increasing crustal thickness. These differences are large and should be observed in the data unless the average crustal velocity changes laterally. We reduced some of the trade-offs between crustal thickness and crustal velocity because we are utilized the entire waveform.

The location of events in South America often have large uncertainties, so we tested the effect of mislocations on the waveforms. Many of the events are located in the downgoing slab, between 120 and 140 km depth. The synthetic seismograms are relatively unaffected for mislocation errors of ±10 km in depth. Shifts of greater than ±10 km mostly affected the timing and amplitude of the surface wave arrivals. Similar mislocation errors in latitude and longitude had less affect on the synthetic waveform. The waveform was generally unchanged for changes of ±20 km in distance from the station.

Next, the sensitivity of the waveform to the attenuation parameters was tested. The synthetics are relatively insensitive to modestly varying values for Q_α and Q_β in the models, the effect mostly seen in the amplitudes of the arrivals. These changes were minor for all ranges of

distance and depth; hence we cannot constrain attentuation models in this study, and we fixed the Q values to those of Whitman *et al.* (1992).

The sensitivity of the V_P/V_S ratio was also investigated. Recently, Zandt *et al.* (1994) found that the V_P/V_S ratio is approximately 1.5–1.6 for a region in the southern Altiplano, just south of our study region. We tested one of the events in the central Altiplano region to determine if a lower V_P/V_S ratio was more appropriate. For a V_P/V_S ratio of 1.5, the relative timing of the arrivals was affected, which resulted in a poor fit. The best fit for the event is achieved using a ratio of 1.7. We used this value for our study. In general, we see no systematic evidence requiring an unusually lowV_P/V_S ratio.

We also investigated variations in mantle lid thickness to determine how sensitive the waveforms are to uppermost mantle structure. We generated synthetic waveforms using two models with no mantle lid, one with a half-space velocity of $\alpha = 7.9$ km s^{-1} and the other with a half-space velocity of 8.2 km s^{-1}. The difference in velocity structure mostly affected the timing of the early arrivals and the shape of the waveform on the tangential component. Fig. 5 shows the resulting waveforms calculated using mantle lid thicknesses ranging from 20 to 100 km. The presence of a lid affects the overall shape of the waveform and the timing of the body-wave arrivals on the vertical and radial components. The surface waves are less sensitive to lid structure and thickness. The tangential component is affected most as the lid thickness is varied (Fig. 5). As seen in the changing shape of the waveforms, we should be able to determine if a mantle lid is present. For most of the events, the lid appears to be within the range of 40–80 km thick. Similar tests were run for each event using various mantle lid thicknesses, and the results for the best fit of each event give an approximate thickness for the lid. However, the lid thickness is not well resolved from these data.

5 RESULTS

We have grouped the events based on similar event–station paths. Ideally, similar event–station paths would sample a relatively similar structure. The Peruvian Andes and Altiplano paths to NNA and ZOBO, respectively, are the most uniform. Therefore, these paths give the most

reliable average values for crustal thickness and crustal velocity. The transition paths discussed below are clearly more complicated because they are sampling multiple tectonic terranes. The transition path between the Peruvian Andes and the Altiplano probably has the largest lateral variation in crustal structure.

5.1 Peruvian Andes

The five events shown in Fig. 6a were used to model the crustal and upper mantle structure north of station NNA, beneath the Peruvian Andes. These events are all located within 3° of each other and sample similar paths. A wide range of crustal thicknesses and velocities were tested in order to determine a best fit between the data and synthetics. A two-layer crust, a mantle lid, and a high-velocity subducting slab layer were used to model each of the events. The results of our grid search are seen in Fig. 8, where the highest correlation coefficient indicates the best fit. For each event, Table 4 lists the parameters for the best-fit model, and Fig. 7 shows the corresponding waveform fits.

The two shallow events that occurred on 30 May 1990 are located 1 km apart at approximately the same depth. The seismogram for the first and larger event (m_b = 6.0) was clipped after 30 s; therefore only the first 30 s of the *P*-wave arrival were modeled. For the second 30 May event (m_b = 5.3), the entire waveform could be modeled. A good match was achieved for both events using the same model with a 25-km-thick upper crust, a 20-km-thick lower crust, and a 40-km-thick mantle lid underlain by a high-velocity mantle, representing the subducting Nazca slab (Table 4). However, the *P* wave of the first event was matched slightly better with a 50-km-thick crust, while the entire waveform of the second event was matched best using a 45-km-thick crust. The 21 October 1990 event (220 km depth) followed a similar but longer path (Fig. 6a). The best match was achieved using a 55-km-thick crust and a 40-km-thick upper mantle. The 4 May 1989 and 3 December 1989 events which are located farther east are matched using a 45-km-thick crust.

The average parameters for the Peruvian Andes are as follows: an average crustal thickness of 48 km and an average crustal velocity of 6.2 km s^{-1}. There is no asthenospheric wedge for this

area, due to the flat slab subduction from 8° to 13°S (Cahill & Isacks 1992); therefore we model a 40-km-thick upper mantle, underlain by the high-velocity subducting slab. Our data do not preclude a mantle wedge in this region, but the waveform fits were improved slightly using our model. A wide range of upper mantle values were tested, and the timing and amplitude of the surface waves are affected by changes in these parameters. However, the data are not as sensitive to the upper mantle parameters as to the crustal structure.

5.2 Transition South of NNA

The three events located south of NNA sample the transition zone between the flat and steeply dipping slab between the Peruvian Andes and the Altiplano (Fig. 6b). These events sample different regions from the coast to the Eastern Cordillera; hence, we would expect to find differences in crustal thickness and different upper mantle structure due to the presence of the asthenospheric wedge associated with the normal angle of subduction in this region. A two-layer crust model with a 30- to 40-km-thick mantle lid underlain by a low-velocity zone was used to model the events. The model parameters for the best fits of each event are in Table 5.

For the 7 January 1990 event, which occurred near the coast, two maximums of the correlation coefficients are seen, one for a 40-km-thick crust with a velocity of 6.1–6.15 km s^{-1} and the second for a 60-km-thick crust and a velocity of 6.4–6.5 km s^{-1}. Since it is a shallow coastal event, the 40-km-thick crust might be the more realistic; however, if the event was mislocated and actually occurred farther inland, then the thicker crust would be more probable. A thickness of 55 to 60 km and a velocity of 6.1–6.2 km s^{-1} is found for the 4 November 1990 event, which is located at the western edge of the Altiplano. The 16 March 1989 event, located beneath the Eastern Cordillera, is modeled with a 50–55 km crust and a crustal velocity of 6.05–6.25 km s^{-1}.

5.3 Transition Northwest of ZOBO

The 4 November 1990 event is an intermediate-depth event located beneath the boundary of the Western Cordillera and Axial Valley, so the path samples mostly the Altiplano and Cordillera

region (Fig. 9b). The best parameters are a 70- to 80-km-thick crust and a velocity of 5.91–5.95 km s^{-1} (Table 7). The three events located northwest of ZOBO (Fig. 9b) are at distances of greater than 10°. The closest event, 4 May 1989, shows a crustal thickness of 70 km and an average velocity of 5.95 km s^{-1} (Table 7). At 1200–1400 km from ZOBO, the 3 December 1989 and 20 April 1989 events both show crustal thicknesses of 65 km and an average crustal velocity of 6.2 km s^{-1} (Table 7).

5.4 Northern Altiplano South of ZOBO

The group of events located south of ZOBO (Fig. 9a), all have paths principally within the Altiplano and Western Cordillera. These six events are used to model the structure of the Altiplano, where we expect the crust to be very thick. For these events, a three-layer crust was used, with a 10-km-thick sedimentary layer with a *P*-wave velocity of 5.0 km s^{-1}, in addition to the two crustal layers. This value was obtained by taking the average of two sedimentary layer velocities of 4.8 km s^{-1} and 5.3 km s^{-1}, as estimated by Ocola & Meyer (1972) and Wigger (1988). This "low-velocity layer" is supported by several other studies: (1) Using explosion refraction data, Ocola, Myer & Aldrich (1971) found some evidence for a 7-km-thick layer of material with a velocity of 4.5 km s^{-1} for the Altiplano. (2) Ocola & Meyer (1973) propose 10 km of sedimentary and metamorphic material under the Altiplano. (3) The sediments and Tertiary volcanics near Lake Titicaca are proposed to be greater than 10 km thick (Newell 1949). (4) The Tertiary sediments and volcanics are up to 10 km thick on the Altiplano (James 1971b). (5) The Altiplano is proposed to have a maximum of 13–20 km of sedimentary cover thinning to 9 km on the western edge of the Western Cordillera (Dorbath *et al.* 1993). Therefore, an average of 10 km was used in this study for the Altiplano region, thinning away from the plateau. The addition of this sedimentary layer greatly improved the fit as compared to a two-layer crust. The models also include a mantle lid and low-velocity zone in the upper mantle. Table 6a shows the parameters for the best fits of each event, and Fig. 10 shows the corresponding waveform fits.

For the three events closest to ZOBO (Fig. 9a), we obtained a 75- to 85-km-thick crust with a velocity of 5.85–5.9 km s^{-1} for the 17 May 1990 event, a 75-km-thick crust and a velocity

of 5.85 km s^{-1} for the 9 May 1992 event, and a 65-km-thick crust and a 5.85 km s^{-1} crustal velocity for the 15 August 1990 event. The shallow 28 August 1990 event near the coast was modeled with a 70-km-thick crust and a velocity of 5.95 km s^{-1}, the 16 April 1992 event with a 65-km-thick crust and a crustal velocity of 5.85 km s^{-1}, and the 27 January 1992 event with a 80- to 85-km-thick crust and 5.85 km s^{-1} velocity. The path for the 27 December 1990 event sampled the thicker crust of the Altiplano as well as the thinner crust of the Coastal Range; hence, we are only determining an average crustal thickness. The grid search results indicate a crustal thickness of 65 km and an average crustal velocity of 6.05 km s^{-1} for the 27 December 1990 event. Several representative grid search results (Fig. 11) and the best average model values for all the events (Table 6b) are compiled to obtain an average model for the Altiplano and Western Cordillera. The average model has a 75-km-thick crust and an average crustal velocity of 5.9 km s^{-1}, with a 40-km-thick lid over a 50-km-thick low-velocity zone.

6 RECEIVER FUNCTION FOR LPAZ

An additional method of determining first-order discontinuities, such as the crust–mantle boundary, is teleseismic receiver function analysis using broadband seismic station seismograms (Owens & Zandt 1985). The source effects are removed, and the *P*-to-*S* conversion isolated by deconvolving the vertical component from the horizontals. The resultant receiver function is then convolved with a Gaussian filter to remove the high frequencies to emphasize the long-period signal. We stack receiver functions of similar azimuths to provide a single estimate of structure (Owens, Zandt, & Taylor 1984) beneath LPAZ. We are primarily interested in *P*-to-*S* wave conversions at major discontinuities such as the crust–mantle interface. The amplitude of the *P*-to-*S* conversion is a function of the contrast in velocity across the interface; therefore it is less sensitive to any smooth velocity variations with depth (Langston 1994). There is, of course, a trade-off between depth of the layer interface and the average velocity of the layer (Ammon, Randall, & Zandt 1990).

The new broadband seismic station LPAZ is located northeast of La Paz, Bolivia, in the Eastern Cordillera. We computed two receiver function stacks using two teleseismic seismograms

from the NW azimuth to Guerrero, Mexico, and two events from the NE azimuth to the mid-Atlantic Ridge (Fig. 12). The event parameters for these four events are in Table 8. These events do not sample the same region as the regional waveforms; however, they should give a good estimate of the crustal structure NE and NW of the station in the Eastern Cordillera.

For the NW stack, the *P*-to-*S* conversion is 7.6 s after the first *P* arrival (Fig. 12). We computed synthetic receiver functions fixing the average crustal velocity to match the low velocities seen in our reflectivity modeling. These data are matched with a three-layer model with a 54-km-thick crust and an average crustal velocity of 6.1 km s^{-1} (Table 9). On the NE stack the *P*-to-*S* conversion is at 7.3 s (Fig. 12), which is successfully modeled with a three-layer, 56-km-thick crust and an average crustal velocity of 6.2 km s^{-1} (Table 9). These crustal thicknesses of 54–56 km are nearly 20 km thinner than our results for the average crustal thickness of the Altiplano. There is a direct trade-off between average crustal velocity and crustal thickness. If we use an average crustal *P*-wave velocity of 6.5 km s^{-1}, then the resultant crustal thickness would be 64 km. In order to explain the *P*-to-*S* conversion with a 75-km-thick crust (similar to the Altiplano), the average crustal velocity would have to be greater than 7 km s^{-1}, an unrealistically high value. This suggests that the Eastern Cordillera crust is much thinner than that of the Altiplano even though, at least locally, the elevation is higher in the Eastern Cordillera northeast of La Paz.

7 DISCUSSION

Our first-order results indicate an average crustal thickness of 45–50 km for the Peruvian Andes, 60 km for the Peruvian segment of the Altiplano, and 75 km for the Altiplano in Bolivia, with an average crustal velocity of 6.15 km s^{-1}, 6.1 km s^{-1}, and 6.0 km s^{-1}, respectively (Fig. 13 and 14). Perhaps even more suprising is the large and rather sharp thinning of the crust beneath the Eastern Cordillera near La Paz, Bolivia. The average crustal *P*-wave velocities are relatively low and inconsistent with a large component of mafic lower crust. Our results also suggest a small decrease in average crustal velocity from north to south. This could be due to the presence of a thick sedimentary cover in the Altiplano region, or a change in the composition of the crust in each area. All the data sets require a mantle lid; however, we cannot resolve any variations in mantle lid

thickness along strike of the Andes. All areas can be effectively modeled with a 40- to 60-km-thick mantle lid (Tables 4–7).

If the above results for the Northern Altiplano are representative of the entire plateau, then these results can be used to constrain the mechanical and thermal models (Allmendinger 1986) proposed for the uplift of plateaus and thickening of the crust. Underplating or magmatic addition of mantle-derived mafic material to the lower crust has been proposed as a primary heat source and mechanism for thickening of the crust. The seismic signature of mantle derived melt emplaced in the lower crust depends upon the composition of the existing lower crust (Furlong & Fountain 1986). If the existing crust is primarily mafic, then the seismic velocity for the new layer will be similar to the original velocity despite the thickening of the crust. Furlong & Fountain (1986) suggest that for any region, underplating of mafic material could add up to 10 km to the lower crust, and the seismic velocity would reach 6.8–8.0 km s^{-1} at depths of 45–65 km. Our results of low average crustal velocities for the Altiplano suggest that underplating of mafic material is not a significant mechanism for thickening of the crust.

The importance of magmatic addition from the mantle to the crust is more difficult to evaluate. Baker & Francis (1978) propose a 10:1 ratio for intrusive to extrusive volumes in the Andes; however, they state that this would imply a very high rate of magmatic addition if the plateau was uplifted in the Cenozoic. Isacks (1988) estimates 0.3 km of extrusive material on the top of the plateau in Bolivia and Chile. James (1971b) proposed magmatic addition as the major component for plateau uplift and thickening of the crust, due to migration of magmatism from west to east. Kono, Fukao & Yamamoto (1989) proposed that magmatic addition predominates in the western part of the Altiplano. For the crust to reach the thickness of 65 km as proposed by Kono, Fukao & Yamamoto (1989), 15 percent of the mantle wedge must be melted for the necessary amount of magma addition. This implies a very high rate of magma generation of 0.14 km^3 yr^{-1} for the area. We would expect that this high amount of magmatic addition would also imply high lower crust velocities, which would increase the average crustal velocities for the Western Cordillera and the Altiplano. The results from this study suggest low average crustal velocities,

with lower crustal velocities of 6.3–6.5 km s^{-1}. These low crustal velocities imply that the crust does not contain large volumes of mafic magma.

However, the amount of mafic material in the lower crust beneath the Altiplano is still unknown. In the region of the western volcanic arc, where our data sample the crust, most of the active and recent volcanism consists of andesites and dacites, with limited mafic material (De Silva & Francis 1991). While magma addition is present to some degree beneath the Altiplano and Western Cordillera, our results do not support the hypothesis that it is the primary mechanism for thickening of the crust.

Froidevaux & Isacks (1985), Isacks (1988), and Whitman *et al.* (1992) all propose lithospheric thinning as a component for uplift of the plateau, primarily in the southern Puna Plateau. The existence of a thin mantle lid implies that elevation is supported by thermal thinning of the lithosphere, whereas a thick lid implies support due to crustal thickening (Whitman *et al.* 1992). Studying the Q structure of the mantle, Whitman *et al.* (1992) have determined that the lithosphere beneath the Puna has been considerably thinned as compared to the northern Altiplano. Froidevaux & Isacks (1984) state that thermally supported topography requires an asthenospheric root of thickness $H = (\rho_c/\Delta\rho_{la})h$, where h is the elevation of topography, ρ_c is the density of the crust, and $\Delta\rho_{la}$ is the density difference between the lithosphere and asthenosphere. It is assumed that the region is in isostatic equilibrium and that the weight of the topography and the buoyancy of the light root are equal (Froidevaux & Isacks 1984). For average density values, $H = 45h$, so for a normal mantle lithospheric thickness of 90 km, only 2 km of elevation could be supported (Froidevaux & Ricard 1987). Our results indicate the presence of a mantle lid, possibly thinner than 90 km, which would support even less elevation. This suggests that some other mechanism is responsible for at least part of the uplift of the Plateau. This other mechanism for uplift is crustal thickening by crustal shortening rather than magmatic addition from the mantle.

Various estimates of crustal shortening have been determined for the Altiplano and Eastern Cordillera. At 18°S, assuming a crustal thickness of 70 km for the Altiplano, thinning to 40 km in the east, Sheffels (1990) has found a lower bound of 210 km of shortening. Using the velocity

model of Wigger *et al.* (1993), Schmitz (1994) used a forward-modeling technique to create a balanced cross section at 21°S. His results show 320 km of shortening using an initial crustal thickness of 30–40 km; this would suggest that 20% of the volume beneath the Altiplano was derived from other means. All of these shortening estimates suggest that the crust beneath the Andes could be sufficiently thickened without extensive magmatic addition. Our low average crustal velocities are most consistent with large amounts of crustal shortening.

8 CONCLUSIONS

We have provided constraints on the average crustal thickness, average crustal velocity, and, to a lesser extent, the mantle lid structure from modeling regional seismograms sampling the Central Andes. The Peruvian Andes have an average crustal thickness of 48 km and an average crustal velocity of 6.2 km s^{-1}. The transition region from 12° to 16°S, where the Altiplano is narrow, has an average crustal thickness of 62 km with an average crustal velocity of 6.1 km s^{-1}. The crust thickens southward on the Altiplano Plateau, where it reaches a thickness of 75 km between 16° to 21°S with an average crustal velocity of 5.95 km s^{-1}. The Eastern Cordillera near La Paz, Bolivia, is consistent with a crustal thickness of ~55 km assuming an average *P*-wave velocity of 6.1 km s^{-1}. This is a remarkably sharp transition from 75-km-thick crust on the Altiplano to 55-km-thick crust in the Eastern Cordillera, at least locally (Fig. 14).

If our Altiplano values are representative of the entire Plateau, then the low average crustal velocities for the Altiplano region suggest a limited amount of magmatic addition from the mantle for the Plateau. These low crustal velocities are more consistent with distributed shortening within the crust. The results for the upper mantle beneath the Peruvian Andes and the Altiplano weakly suggest that there is a mantle lid, though not well defined. This implies that the asthenosphere does not lie directly below the crust, which suggests that the Plateau is primarily being supported by a crustal or lithospheric root rather than a thermal one. Hence, crustal shortening and/or underthrusting of the Brazilian craton may the primary mechanisms for the thickening of the crust and uplift of the Altiplano Plateau.

Acknowledgments

We would like to thank Bob Butler for his contributions and for reviewing this manuscript. We would also like to thank George Randall for providing his computer programs for the reflectivity modeling and Bill Walter for providing programs and valuable advice for this study. This study was supported by Air Force grant number F49620-92-J-0416. GZ was supported by IGPP at LLNL. SASO contribution 54.

REFERENCES

Allmendinger, R., Figueroa, D., Snydes, D., Beer, J., Mpodozis, C. & Isacks, B., 1990. Foreland shortening and crustal balancing in the Andes at 30° latitude, *Tectonics*, **9**, 789–809.

Allmendinger, R., 1986. Tectonic development, southeast border of the Puna plateau, northwestern Argentine Andes, *Geol. Soc. Am. Bull.*, **97**, 1070–1082.

Ammon, C.J., Randall, G.E. & Zandt, G., 1990. On the non-uniqueness of receiver function inversions, *J. geophys. Res.*, **95**, 15,303–15,318.

Baker, M.C.W. & Francis, P.W., 1978. Upper Cenozoic volcanism in the central Andes—Ages and volumes, *Earth planet. Sci. Lett.*, **41**, 175–187.

Barazangi, M. & Isacks, B., 1979. Subduction of the Nazca plate beneath Peru: Evidence from spatial distribution of earthquakes, *Geophys. J. R. astr. Soc.*, **57**, 537–555.

Cabre, R., 1983. Geophysical studies in central Andes, in *Geodynamics of the Eastern Pacific Region, Carribean and Scotia Arcs, Geodyn. Ser.*, vol. 9, pp.73–77, ed Cabre, R., American Geophysical Union, Washington, DC.

Cahill, T. & Isacks, B., 1992. Seismicity and shape of the subducted Nazca plate, *J. geophys. Res.*, **97**, 17,503–17,529.

Chinn, D. & Isacks, B., 1983. Accurate source depths and focal mechanisms of shallow earthquakes in Western South America and in the New Hebrides island arc, *Tectonics*, **2**, 529–563.

Dalmayrac, B. & Molnar, P., 1981. Parallel thrust and normal faulting in Peru and constraints on the state of stress, *Earth planet. Sci. Lett.*, **55**, 473–481.

Dalmayrac, B., Lancelot, J.R. & Leyreloup, A., 1977. Two-billion year granulites in the late Precambrian metamorphic basement along the Peruvian coast, *Science,* **198,** 49–51.

De Silva, S. & Francis, P., 1991. *Active Volcanoes of the Central Andes*, Springer-Verlag, New York.

Dorbath, C., Granet, M., Poupinet, G. & Martinez, C., 1993. A teleseismic study of the Altiplano and the Eastern Cordillera in Northern Bolivia: New constraints on a lithospheric model, *J. geophys. Res.,* **98**, 9825–9844.

Fernandez, L.M., & Careaga, J., 1968. The thickness of the crust in Central U.S. and La Paz, Bolivia, from the spectrum of longitudinal seismic waves, *Bull. seism. Soc. Am.,* **58,** 711–741.

Froidevaux, C. & Isacks, B., 1984. The mechanical state of the lithosphere in the Altiplano–Puna segment of the Andes, *Earth planet. Sci. Lett.,* **71**, 305–314.

Froidevaux, C. & Ricard, Y., 1987. Tectonic evolution of high plateaus, *Tectonophysics,* **134**, 227–238.

Fuenzalida, A., Pardo, M., Cisternas, A., Dorbath, L., Dorbath, C., Comte, D. & Kausel, E., 1992. On the geometry of the Nazca plate subducted under Central Chile (32–34.5 S) as inferred from microseismic data, *Tectonophysics*, **205**,1–11.

Fukao, Y., Yamamoto, A. & Kono, M., 1989. Gravity anomaly across the Peruvian Andes, *J. geophys. Res.*, **94** (B4), 3867–3890.

Furlong, K.P. & Fountain, D.M., 1986. Continental Crustal Underplating: Thermal considerations and seismic-petrologic consequences, *J. geophys. Res.,* **91**, 8285–8294.

Gotze, H.J., Schmidt, S. & Strunk, S., 1988. Central Andean gravity field and its relation to crustal structures, *The Southern Central Andes, Lect. Notes Earth Sci.*, vol. 17, pp. 201–209, eds Bahlburg, H., Breitkreuz, C. & Giese, P.

Grange, L., Hatzfield, F., Cunningham, D., Molnar, P., Roecker, P., Suarez, S., Rodrigues, G. & Ocola, A., 1984. Tectonic implications of the microearthquake seismicity and fault plane solutions in Southern Peru, *J. geophys. Res.,* **89**, 6139–6152.

Haswega, A. & Sacks, I., 1981. Subduction of the Nazca plate beneath Peru as determined from seismic observations, *J. geophys. Res.*, **86**, 4971–4980.

Isacks, B., 1988. Uplift of the central Andean plateau and the bending of the Bolivian orocline, *J. geophys. Res.*, **93** (B4),3211–3231.

James, D. E., 1971a. Andean crustal and upper mantle structure, *J. geophys. Res.*, **76**, 3246–3271.

James, D. E., 1971b. Plate tectonic model for the evolution of the Central Andes, *Geol. Soc. Am. Bull.*, **82**, 3325–3346.

James, D.E. & Snoke, J.A., 1994. Structure and tectonics in the region of flat slab subduction beneath Central Peru: Crust and uppermost mantle, *J. geophys. Res.*, **99**, 6899–6912.

Jordan, T., Isacks, B., Allmendinger, R., Brewer, J., Ramos, V. & Ando, C., 1983. Andean tectonics related to geometry of subducted Nazca plate, *Geol. Soc. Am. Bull.*, **94**, 341–361.

Kennett, B.L.N., 1983. *Seismic Wave Propagation in Stratified Media*, Cambridge University Press.

Kono, M., Fukao, Y. & Yamamoto, A., 1989. Mountain building in the central Andes, *J. geophys. Res.*, **94** (B4), 3891–3905.

Langston, C.A., 1994. An integrated study of crustal structure and regional wave propagation for Southeastern Missouri, *Bull. seism. Soc. Am.*, **84**, 105–118.

Lindo, R., Dorbath, C., Cisternas, A., Dorbath, L., Ocola, L. & Morales, M., 1992. Subduction geometry in central Peru from a microseismicity survey: First results, *Tectonophysics*, **205**, 23–39.

Lyon-Caen, H., Molnar, P. & Suarez, G., 1985. Gravity anomalies and flexure of the Brazilian Shield beneath the Bolivian Andes, *Earth planet. Sci. Lett.*, **75**, 81–92.

Müller, G., 1985. The reflectivity method: A tutorial, *J. Geophys.*, **58**, 153–174.

Newell, N.D., 1949. Geology of the Lake Titicaca region, Peru and Bolivia, *Mem. Geol. Soc. Am. 36*, 111 pp, Geological Society of America, Boulder, Colo.

Ocola, L.C., Meyer, R.P. & Aldrich, L.T., 1971. Gross structure under Peru–Bolivia Altiplano, *Earthquake Notes*, **42, 3–4,** 33–45.

Ocola, L.C. & Meyer, R.P., 1972. Crustal low-velocity zones under the Peru–Bolivia Altiplano, *Geophys. J. R. astr. Soc.,* **30**, 199–209.

Ocola, L.C. & Meyer, R.P., 1973. Crustal structure from the Pacific Basin to the Brazilian shield between 12° and 30° latitude, *Geol. Soc. Am. Bull.,* **84,** 3378–3404.

Owens,T. J., Taylor, S. & Zandt, G., 1987. Crustal structure at regional seismic test network stations determined from inversion of broadband teleseismic *P* waveforms, *Bull. seism. Soc. Am.,* **77**, 631–662.

Owens, T. J. & Zandt, G., 1985. The response of the crust–mantle boundary observed on broadband teleseismic receiver functions, *Geophys. Res. Lett.,* **12,** 705–708.

Owens, T.J., Zandt, G. & Taylor, S., 1984. Seismic evidence for an ancient rift beneath the Cumberland Plateau, Tennessee: A detailed analysis of broadband teleseismic *P* waveforms, *J. geophys. Res.,* **89**, 7783–7795.

Randall, G. E., 1994, Efficient calculation of complete differential seismograms for laterally homogeneous earth models, *Geophys. J. Int.*, **118**, 245-254.

Roeder, D., 1988. Andean-age structure of Eastern Cordillera (Province of La Paz, Bolivia), *Tectonics,* **7**, 23–39.

Schmitz, M., 1994. A balanced model of the southern Central Andes, *Tectonics*, **13**, 484–492.

Sheffels, B.M., 1990. Lower bound on the amount of crustal shortening in the central Bolivian Andes, *Geology,* **18**, 812–815.

Stewart, J.S., Evernden, J.F. & Snelling, N.J., 1974. Age determinations from Andean Peru: A reconnaissance survey, *Geol. Soc. Am. Bull.,* **85**, 1107–1116.

Suarez, G., Molnar, P. & Burchfiel, B., 1983. Seismicity, fault plane solutions, depth of faulting, and active tectonics of the Andes of Peru, Ecuador, and southern Columbia, *J. geophys. Res.,* **88**, 10403–10428.

Whitman, D., Isacks, B., Chatelain, J., Chiu, J. & Perez, A., 1992. Attenuation of high-frequency seismic waves beneath the Central Andean plateau, *J. geophys. Res.*, **97**, 19,929–19,947.

Wigger, P. J., 1988. Seismicity and crustal structure of the Central Andes, *The Southern Central Andes, Lect. Notes Earth Sci.*, vol. 17, pp. 209–229, eds Bahlburg, H., Breitkreuz, C. & Giese, P.

Wigger, P. J., Schmidtz, M., Araneda, M., Asch, G., Baldzuhn, S., Geise, P., Heinsohn, P., Martinez, E., Ricaldi, E., Roiver, P. & Viramonte, J., 1993. Variation of the crustal structure of the southern Central Andes deduced from seismic refraction investigation, in *Tectonics of the Southern Central Andes*, pp. 23–48, ed Reutter, K.-J. *et al.*

Zandt, G., Velasco, A. & Beck, S., 1994. Composition and thickness of the southern Altiplano crust, Bolivia, *Geology*, 22, 1003-1006.

Figure captions

Figure 1. A map of the Central Andes of South America showing the Altiplano-Puna Plateau (from 14° to 30°S) which has a mean elevation of nearly 4 km. The black dots represent the locations of the events used in this study. The white squares represent the locations of seismic stations NNA and ZOBO. The gray triangle shows the location of the new digital station LPAZ.

Figure 2. A map showing the tectonic regions of the Central Andes. The stippled region represents the Atiplano–Puna Plateau. Also shown is the location of the seismic stations ZOBO and LPAZ. The inset box shows the location in South America.

Figure 3. (a) An Example of data from the 30 May 1990 event recorded at the broadband station NNA, bandpass filtered from 20 to 100 s. (b) An example of data from the 28 August 1990 event recorded at the long-period station ZOBO, also filtered from 20 to 100 s. The traces are plotted as vertical, radial and tangential components.

Figure 4. Comparison of vertical and tangential component waveforms computed with crustal thicknesses between 40 and 80 km, for an event at a depth of 126 km. Note the significant shift of the surface wave arrivals with increasing crustal thickness.

Figure 5. Comparison of waveforms computed with various mantle lid thicknesses. The top set of waveforms are computed with no mantle lid (half-space only). The bottom set of waveforms are computed for mantle lid thicknesses from 20 to 100 km. The tangential component shows the most sensitive to mantle lid thickness.

Figure 6. (a) Locations of events 1 and 2 of 30 May 1990 and events of 21 October 1990, 4 May 1989, and 3 December 1989 recorded at NNA. These events were used to model the structure

beneath the Peruvian Andes. (b) Locations of the 7 January 1990, 4 November 1990, and 16 March 1989 events recorded at NNA. These events were used to model the structure beneath the transition from the Peruvian Andes to the Altiplano.

Figure 7. comparison of waveform fits between the data (solid line) and synthetics (dashed line) for the events shown in Fig. 6(a). Both data and synthetics are bandpass filtered at 20 to 100 s. The model parameters used for each fit are shown in Table 4. The tangential component of the 30 May 1990 was not used since the record is clipped.

Figure 8. Comparison of the correlation coefficient between the data and synthetics from our grid search for the 21 October 1990, 3 December 1989, 4 May 1989, and 30 May 1990 events recorded at seismic station NNA. The best fit model parameters for average crustal thickness and average crustal velocity are shown by the highest values. A perfect fit has a value of 1.

Figure 9. (a) Location of the events on 17 May 1990, 9 May 1992, 28 August 1990, 15 August 1990, 16 April 1992, 27 December 1990, and 27 January 1992 recorded at station ZOBO. These events are used to model the structure beneath the Altiplano and Western Cordillera region in Bolivia. Model parameters are shown in Table 6(a). (b) Location of events on 4 May 1989, 3 December 1989, 4 November 1990, and 20 April 1989 events recorded at ZOBO and used to model the region northwest of ZOBO. The model parameters are shown in Table 7.

Figure 10. Comparison of waveform fits between the data (solid line) and synthetics (dashed line) for the events shown in Fig. 9(a). Both data and synthetics are bandpass filtered at 20 to 100 s. The model parameters used for each fit are seen in Table 6(a).

Figure 11. Comparison of the correlation coefficient between the data and synthetics from our grid search for the 28 August 1990, 27 January 1992, 17 May 1990, and 9 May 1992 events

recorded at seismic station ZOBO. The best fit model parameters of average crustal thickness and average crustal velocity are shown by the highest values. A perfect fit has a value of 1.

Figure 12. (a) Plot of the radial and tangential components for each receiver function stack. The NW stack is for two events near Chiapas and Guerrero, Mexico, and the NE stack is for two events along the central Mid-Atlantic Ridge (Table 8). The peaks on the radial components that are above the level of the tangential component are considered reliable arrivals to model. (a) Comparison of the receiver function data stack and the synthetic for events from the NW and NE azimuths. For the NW stack the *P*-to-*S* conversion from the Moho occurs at 7.6 s after the *P*-wave arrival and for the NE stack the Moho conversion occurs at 7.3 s.

Figure 13. Average crustal thicknesses for each path determined from modeling regional waveforms recorded at stations NNA and ZOBO.

Figure 14. Composite crustal thickness estimates and corresponding average crustal velocities for the Peruvian Andes, transition region, and the Altiplano. Also shown is the average crustal thicknesses and velocities for the receiver function analysis done for LPAZ.

Table 1: Parameters for events recorded at NNA

EVENT mm/dd/yy	TIME hh:mm:ss	LAT (S)	LON (W)	DEPTH km	mb	Mo dyne-cm	STRIKE (o)	DIP (o)	RAKE (o)
3/16/89	17:12:21.1	16.86	64.93	35.4	5.1	8.81E+23	171	9	127
5/4/89	10:30:06.6	6.66	75.79	36.3	5.6	6.00E+23	130	35	66
12/3/89	14:16:48.8	7.64	74.53	150.9	5.9	7.30E+25	192	40	-70
1/7/90	09:06:43.3	15.91	74.28	30.2	5.9	1.85E+24	161	52	140
5/30/90	02:34:07.0	6.01	77.229	23.2	6	7.65E+25	188	24	122
5/30/90	16:49:28.2	6.02	77.127	23.1	5.3	3.36E+24	169	29	130
10/21/90	15:10:43.6	4.01	77.31	108.1	5.7	1.51E+24	354	32	-69
11/4/90	18:13:42.4	15.70	72.7	140.5	5.4	4.92E+24	278	51	42

Table 2: Parameters for events recorded at ZOBO

EVENT mm/dd/yy	TIME hh:mm:ss	LAT (S)	LON (W)	DEPTH km	mb	Mo dyne-cm	STRIKE (o)	DIP (o)	RAKE (o)
4/20/89	08:08:51.2	9.20	79.04	63.1	5.7	3.11E+24	335	40	-84
5/4/89	18:32:55.9	13.02	76.17	84	5.3	5.42E+23	172	21	103
12/3/89	14:16:48.8	7.64	74.53	150.9	5.9	7.30E+25	192	40	-70
5/17/90	11:03:24.6	18.08	69.135	126.2	5.4	4.98E+24	190	14	-52
8/15/90	13:23:36.3	18.83	69.09	136.5	5.1	1.09E+24	215	32	-43
8/28/90	08:58:06.6	19.83	70.09	65.1	5.2	9.00E+23	334	45	-88
11/4/90	18:13:42.4	15.70	72.7	140.5	5.4	4.92E+24	278	51	42
12/27/90	16:08:34.8	22.77	70.4	63.9	5.2	1.82E+24	229	20	-50
1/27/92	09:52:58.5	21.49	68	145.6	5	4.85E+24	2	46	-108
4/16/92	18:33:04.6	20.11	68.53	130.1	5.6	5.48E+24	207	28	-37
5/9/92	00:20:55.9	18.34	69.34	130.3	5.4	8.39E+23	214	18	-9

TABLE 3. Model parameters

phase velocity window	1.69492	1.78571	40	100
slowness window	0.01	0.025	0.4	0.5
frequency window	0	1 Hz		
Nyquest frequency	1 Hz			

Table 4. Model parameters for events used to model the Peruvian Andes

event	distance	depth		event	distance	depth		event	distance	depth	
10/21/90	883.8 km	108.1 km		5/30/90. 1	661.83 km	23.2 km		5/30/90.2	660.95 km	23.1 km	
th (km)	a (km/s)	b (km/s)	r (kg/m3)	th (km)	α	β	ρ	th (km)	α	β	ρ
25	6.1	3.47	2.72	25	6.1	3.47	2.72	25	6.1	3.474	2.72
55	6.3	3.588	2.82	45	6.4	3.64	2.82	50	6.4	3.645	2.82
85	8	4.49	3.3	85	8.1	4.6	3.3	90	8.1	4.5	3.3
175	8.2	4.6	3.22	175	8.2	4.61	3.22	180	8.2	4.615	3.22
235	8.3	4.659	3.32	235	8.21	4.615	3.32	240	8.21	4.615	3.32
0	8.4	4.71	3.35	0	8.4	4.71	3.35	0	8.4	4.71	3.35
event	distance	depth		event	distance	depth		Average for Peruvian Andes			
5/4/89	600.5 km	36.3 km		12/3/89	543.63 km	150.9 km					
th (km)	α	β	ρ	th (km)	α	β	ρ	th (km)	α	β	ρ
25	6.1	3.47	2.72	20	5.8	3.3	2.72	24	6.04	3.43	2.72
45	6.3	3.64	2.82	45	6.2	3.53	2.82	48	6.32	3.65	2.82
85	8.1	4.5	3.3	85	8.1	4.602	3.3	86	8.08	4.65	3.3
175	8.2	4.615	3.22	175	8.2	4.615	3.22	176	8.2	4.623	3.22
235	8.2	4.61	3.32	235	8.21	4.615	3.32	236	8.23	4.659	3.32
0	8.4	4.71	3.4	0	8.4	4.71	3.35	0	8.4	4.71	3.35

Table 5. Model parameters for events used to model south of NNA

event	distance	depth		event	distance	depth	
1/7/90	514.7 km	30.2 km		11/4/90	607.6 km	140.5 km	
th (km)	a (km/s)	b (km/s)	r (kg/m3)	th (km)	α	β	ρ
1	5	2.847	2.5	20	6.1	3.47	2.72
27	6.2	3.53	2.72	60	6.3	3.64	2.82
60	6.8	3.872	2.82	100	8.1	4.6	3.3
90	8.1	4.546	3.3	130	7.75	4.47	3.22
120	7.9	4.434	3.22	200	8.2	4.61	3.32
190	8.4	4.71	3.32	0	8.4	4.7	3.34
0	8.6	4.827	3.35				
event	distance	depth					
3/16/89	1388 km	35.5 km					
th (km)	α	β	ρ				
20	5.8	3.3	2.72				
50	6.2	3.53	2.82				
90	8.1	4.546	3.3				
130	7.55	4.237	3.22				
200	8.4	4.71	3.32				
0	8.6	4.827	3.35				

Table 6A. Model parameters for the events used to model the Altiplano and Western Cordillera

event	distance	depth	
5/17/90	276.9 km	126.2 km	
th (km)	a (km/s)	b (km/s)	r (kg/m3)
10	5	2.847	2.52
47	5.8	3.3	2.72
80	6.2	3.53	2.82
130	8	4.49	3.3
180	7.55	4.23	3.22
250	8.4	4.71	3.32
0	8.6	4.88	3.34

event	distance	depth	
5/9/92	267.8 km	130.2 km	
th (km)	α	β	ρ
10	5	2.847	2.52
40	5.8	3.3	2.72
75	6.2	3.53	2.82
125	8	4.49	3.3
175	7.55	4.237	3.22
245	8.4	4.71	3.32
0	8.6	4.827	3.35

event	distance	depth	
8/15/90	311.1 km	136.5 km	
th (km)	α	β	ρ
10	5	2.847	2.52
40	5.8	3.3	2.72
75	6.2	3.53	2.82
125	8	4.49	3.3
175	7.55	7.238	3.22
245	8.4	4.71	3.32
0	8.7	4.88	3.34

event	distance	depth	
5/4/89	600.5 km	36.3 km	
th (km)	α	β	ρ
10	5	2.847	2.52
35	5.8	3.3	2.72
70	6.5	3.702	2.82
110	8.2	4.6	3.3
160	7.55	4.237	3.22
230	8.4	4.71	3.32
0	8.7	4.88	3.4

event	distance	depth	
12/3/89	543.6 km	150.9 km	
th (km)	α	β	ρ
10	5	2.847	2.52
30	5.8	3.3	2.72
65	6.2	3.53	2.82
95	8.1	4.546	3.3
145	7.55	4.237	3.22
215	8.4	4.71	3.32
0	8.7	4.88	3.4

event	distance	depth	
8/28/90	445.6 km	65.1 km	
th (km)	α	β	ρ
10	5	2.847	2.52
40	5.8	3.3	2.72
80	6.2	3.53	2.82
110	8.1	4.546	3.3
160	7.55	4.237	3.22
230	8.4	4.71	3.32
0	8.6	4.827	3.35

event	distance	depth	
12/27/90	758.08 km	63.9 km	
th (km)	α	β	ρ
20	5.8	3.3	2.72
65	6.2	3.53	2.82
105	8.2	4.649	3.3
155	7.55	4.238	3.22
235	8.4	4.65	3.32
0	8.6	4.75	3.34

Table 6b. Average values for Altiplano

th	α	β	ρ
10	5	2.847	2.52
39	5.8	3.3	2.72
75	6.3	3.588	2.82
117	8.06	4.52	3.3
167	7.55	4.237	3.22
237	8.4	4.71	3.32
0	8.65	4.85	3.34

Table 7. Model parameters for events northwest of ZOBO

event	distance	depth		event	distance	depth	
5/4/89	938.13 k	84 km		12/3/89	1182 km	150.9 km	
th (km)	a (km/s)	b (km/s	r (kg/m3)	th	α	β	ρ
5	5	2.847	2.52	2	5	2.847	2.5
40	5.8	3.3	2.72	30	6	3.359	2.72
70	6.4	3.643	2.82	65	6.3	3.588	2.82
110	8.1	4.546	3.3	105	8.1	4.546	3.3
160	7.55	4.237	3.22	155	7.55	4.237	3.22
230	8.4	4.71	3.32	225	8.4	4.65	3.32
0	8.6	4.827	3.4	0	8.6	4.827	3.34
event	distance	depth		event	distance	depth	
4/20/89	1419.4 k	63.1 km		11/4/90	493.73 km	140.5 km	
th	α	β	ρ	th	α	β	ρ
2	5	2.847	2.5	5	5	2.847	2.52
30	6	3.359	2.72	40	5.8	3.3	2.72
65	6.4	3.645	2.82	75	6.2	3.53	2.82
105	8.1	4.546	3.3	115	8.1	4.546	3.3
155	7.55	4.237	3.22	165	7.55	4.237	3.22
225	8.4	4.65	3.32	245	8.4	4.71	3.32
0	8.6	4.827	3.34	0	8.6	4.88	3.34

Table 8. Teleseimic event parameters used in receiver function stacks

date (mm/dd/yy)	lat (degrees)	lon (degrees)	mag mb	depth (km)	dist (km)	baz (degrees)
9/19/93	14.3 N	93.2 W	6.1	33	4364.1	319.47
9/20/93	0.9 N	29.4 W	5.9	10	4659.8	69.621
10/24/93	16.8 N	98.6 W	6.5	33	4957.5	316.17
3/14/94	1.4 N	24.0 W	6.3	10	5228.6	72.2

Table 9. Model parameters used to model the NW and NE stacks

NW stack model				NE stack model			
th	α	β	ρ	th	α	β	ρ
(km)	(km/s)	(km/s)	(kg/m3)	(km)	(km/s)	(km/s)	(kg/m3)
3	5	2.847	2.52	8	5	2.847	2.52
26	6	3.53	2.72	31	6	3.53	2.72
54	6.3	3.64	2.82	56	6.3	3.64	2.82
114	8.1	4.65	3.3	96	8.1	4.65	3.3
154	7.55	4.327	3.22	136	7.55	4.327	3.22
0	8.3	4.659	3.32	0	8.3	4.659	3.32

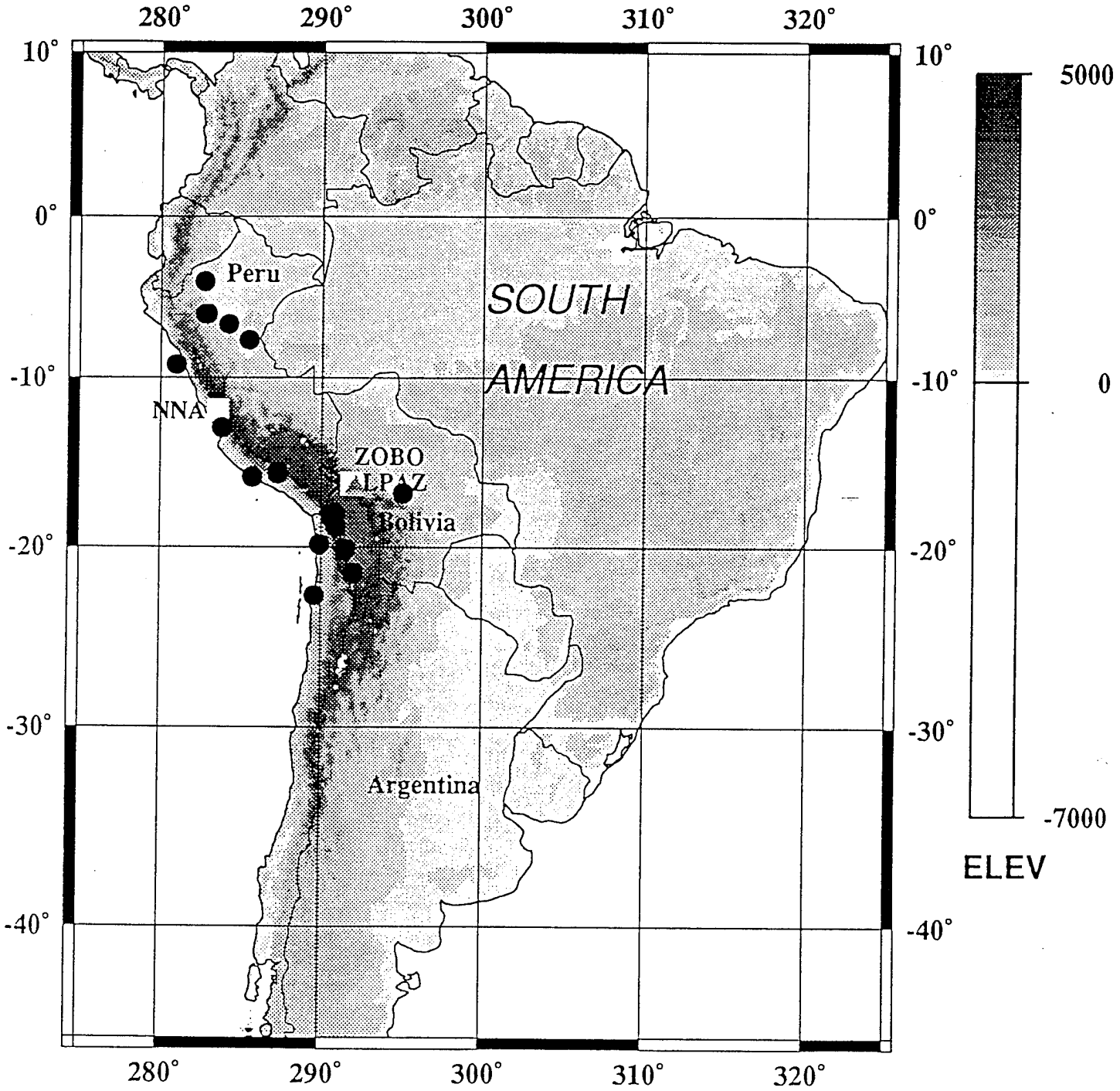
280°
290°
300°
310°
320°
10°
0°
-10°
-20°
-30°
-40°
Peru
NNA
ZOBO
ALPAZ
Bolivia
SOUTH
AMERICA
Argentina
5000
0
-7000
ELEV

Figure 1

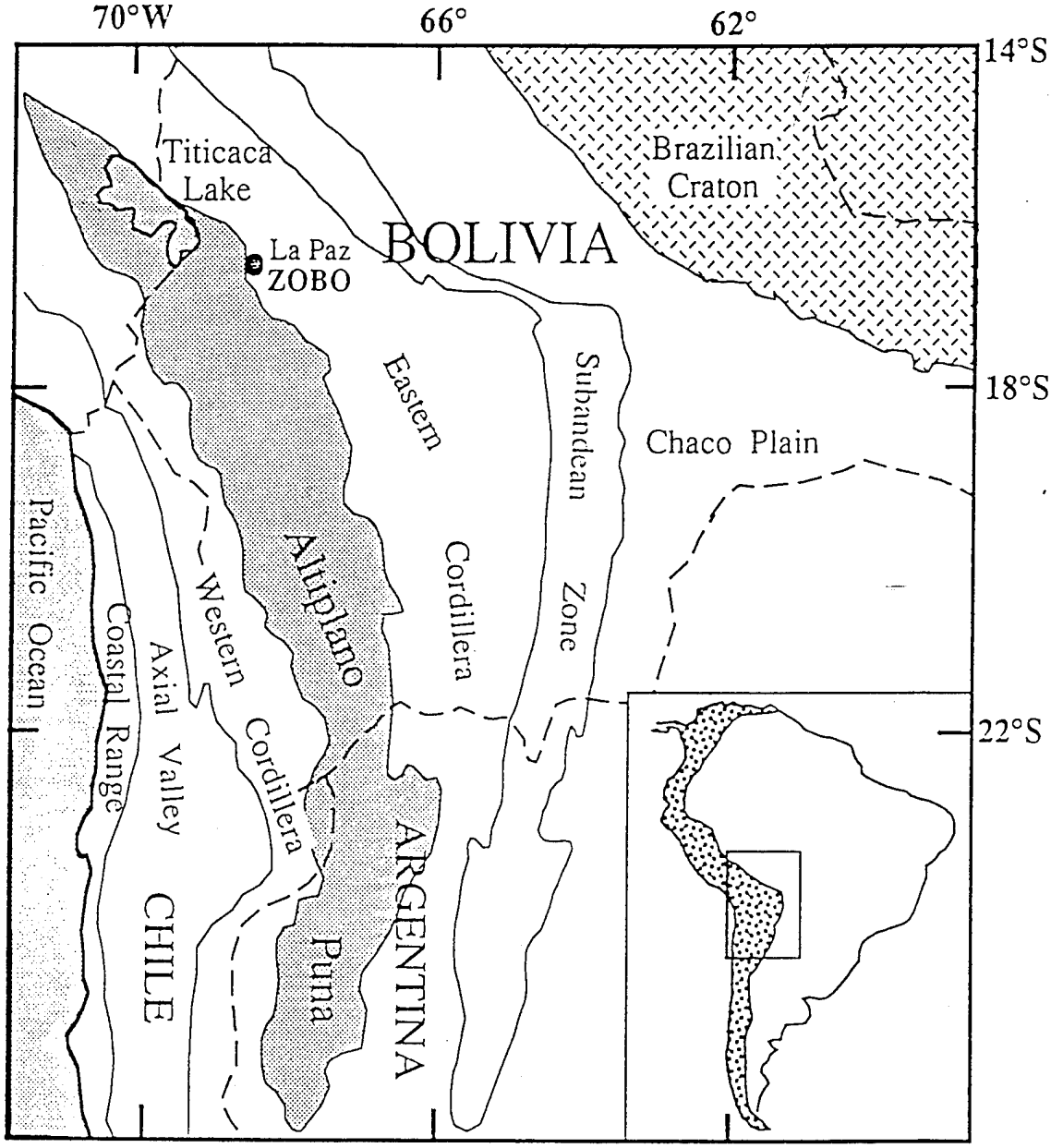
70°W
66°
62°
14°S
18°S
22°S
Brazilian Craton
Titicaca Lake
La Paz
ZOBO
BOLIVIA
Eastern Cordillera
Subandean Zone
Chaco Plain
Altiplano
Western Cordillera
Puna
ARGENTINA
Pacific Ocean
Coastal Range
Axial Valley
CHILE

Figure 2.

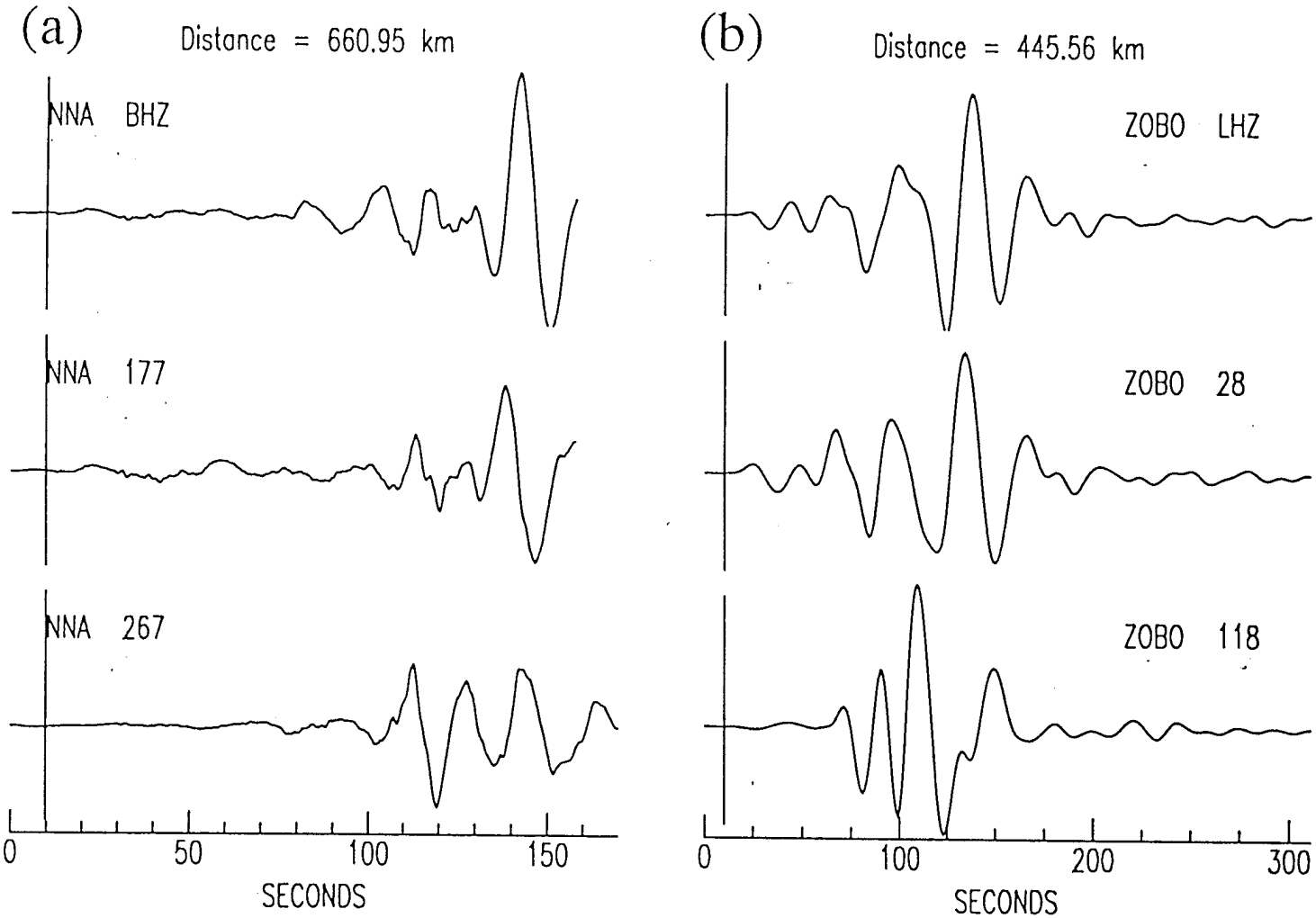
(a)
Distance = 660.95 km
NNA BHZ
NNA 177
NNA 267
0
50
100
150
SECONDS
(b)
Distance = 445.56 km
ZOBO LHZ
ZOBO 28
ZOBO 118
0
100
200
300
SECONDS

Figure 3

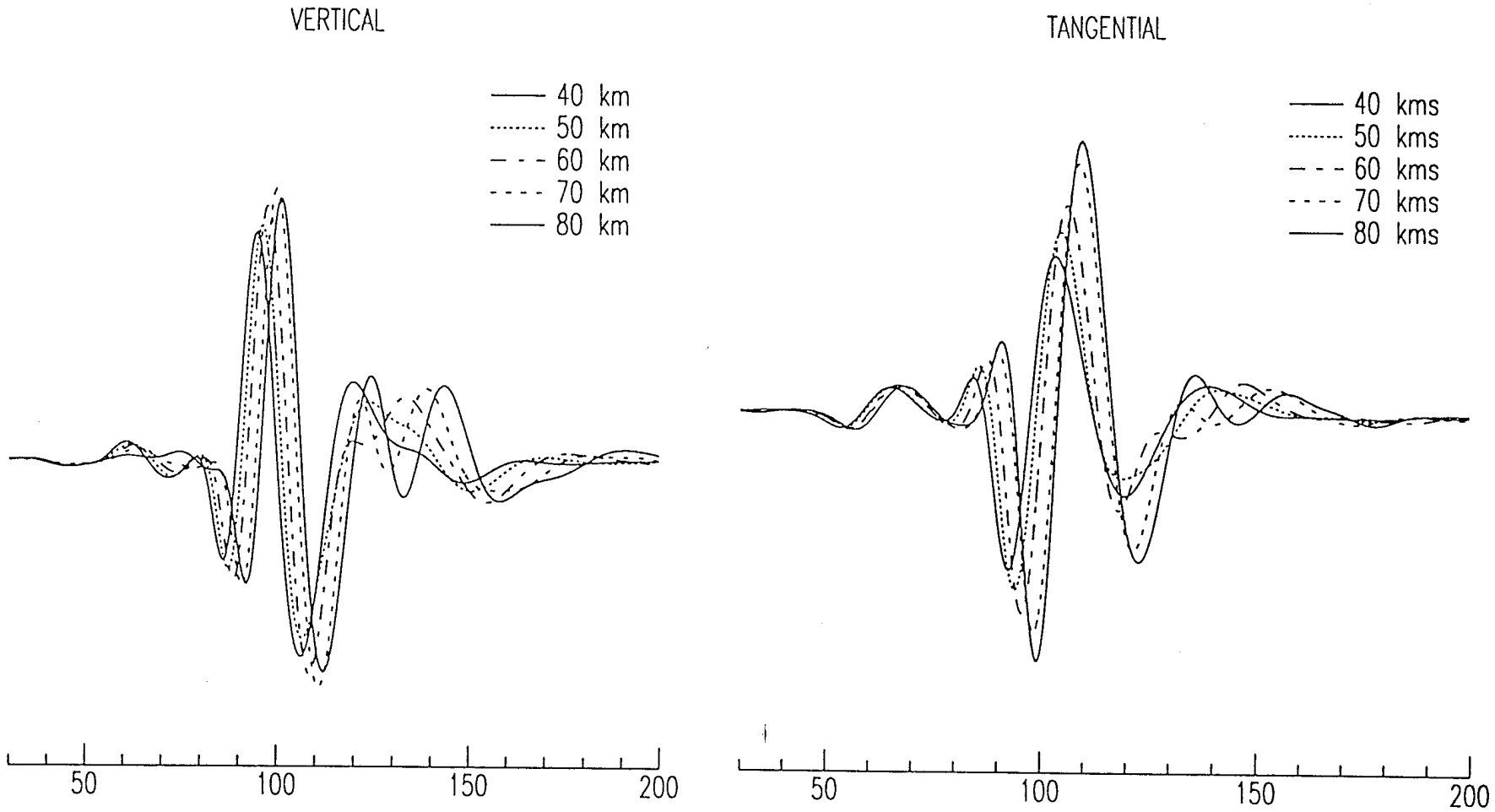
VERTICAL
40 km
50 km
60 km
70 km
80 km
50
100
150
200
TANGENTIAL
40 kms
50 kms
60 kms
70 kms
80 kms
50
100
150
200

Figure 4

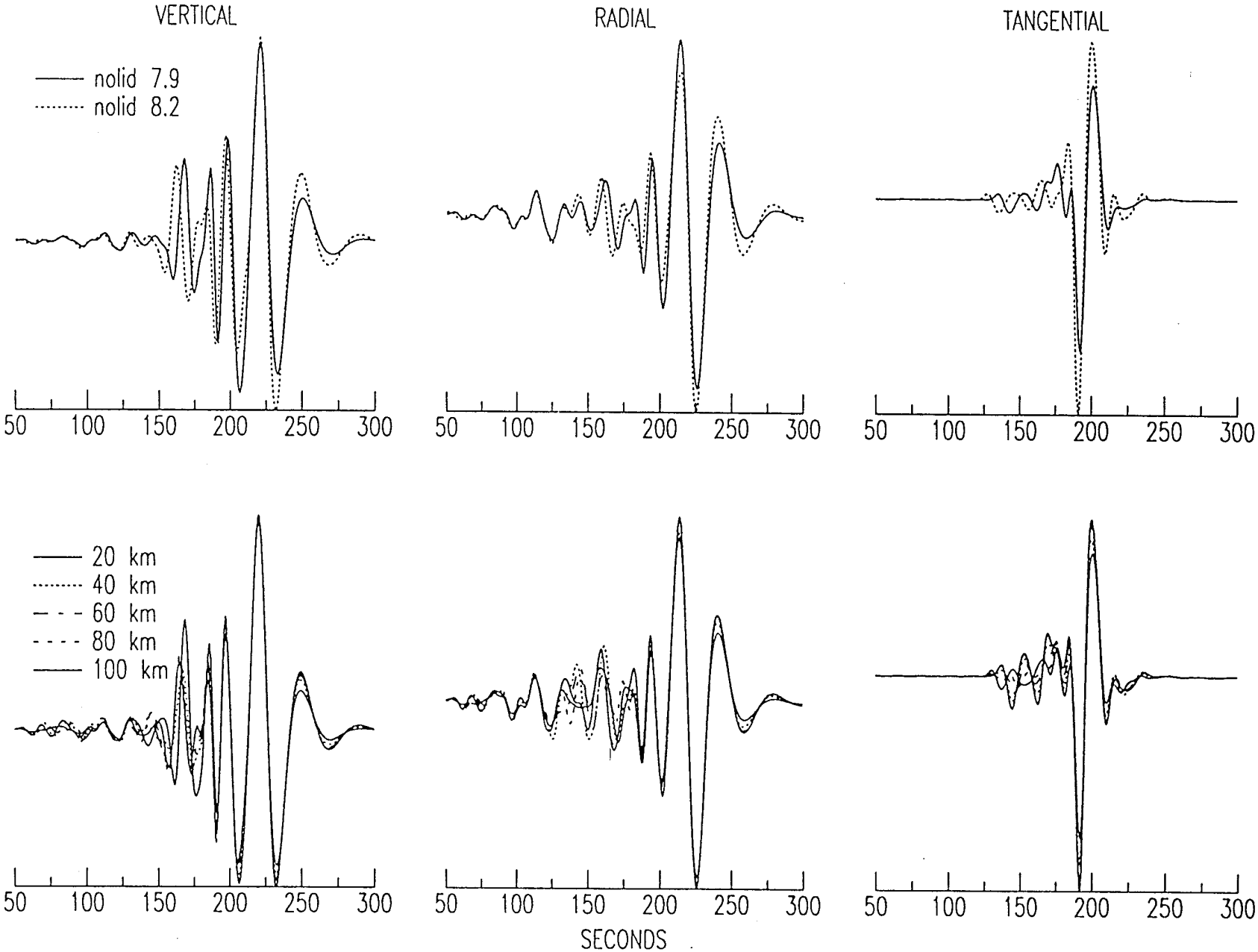
VERTICAL
RADIAL
TANGENTIAL
nolid 7.9
nolid 8.2
20 km
40 km
60 km
80 km
100 km
50
100
150
200
250
300
SECONDS

Figure 5

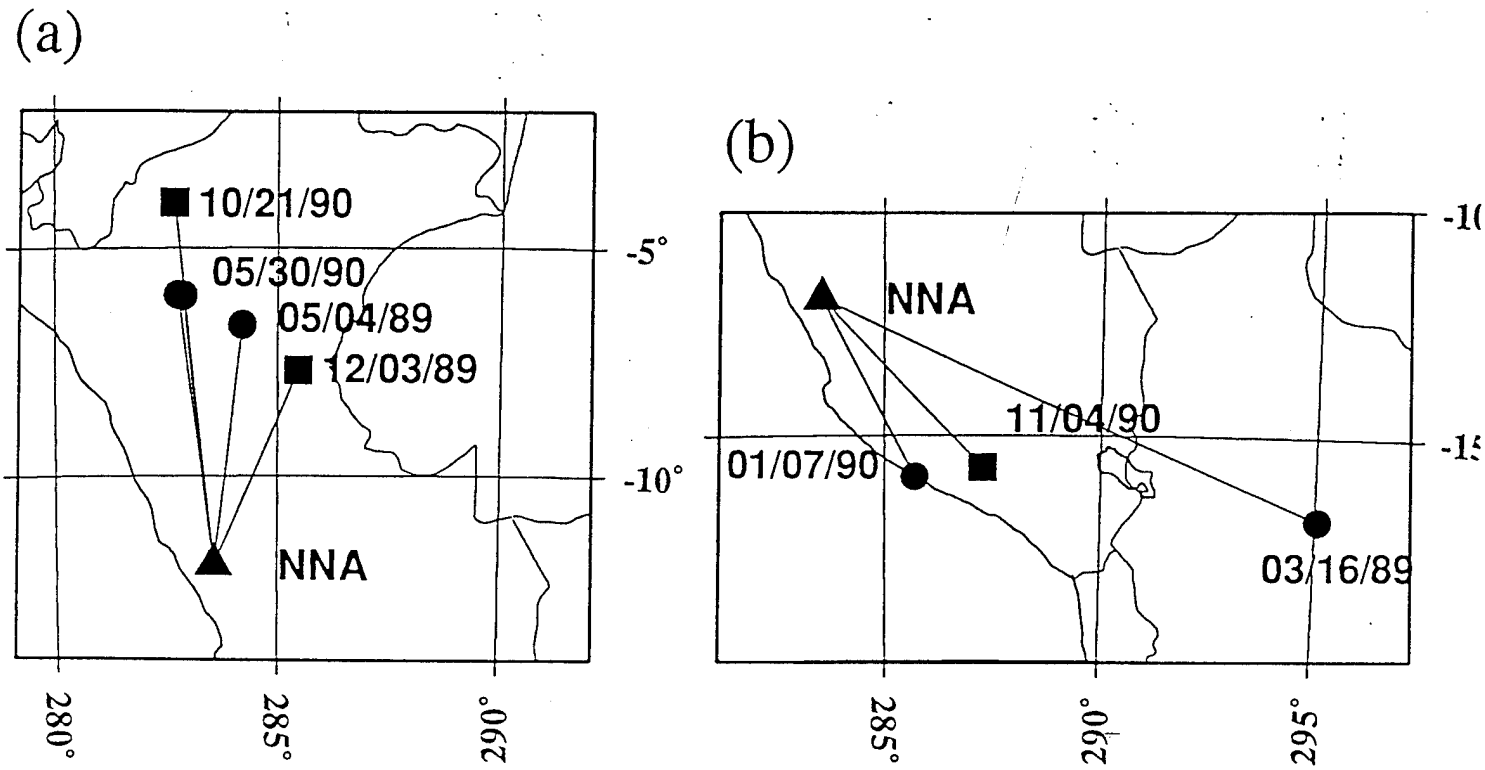
(a)
10/21/90
05/30/90
05/04/89
12/03/89
NNA
-5°
-10°
280°
285°
290°
(b)
NNA
11/04/90
01/07/90
03/16/89
285°
290°
295°

Figure 6

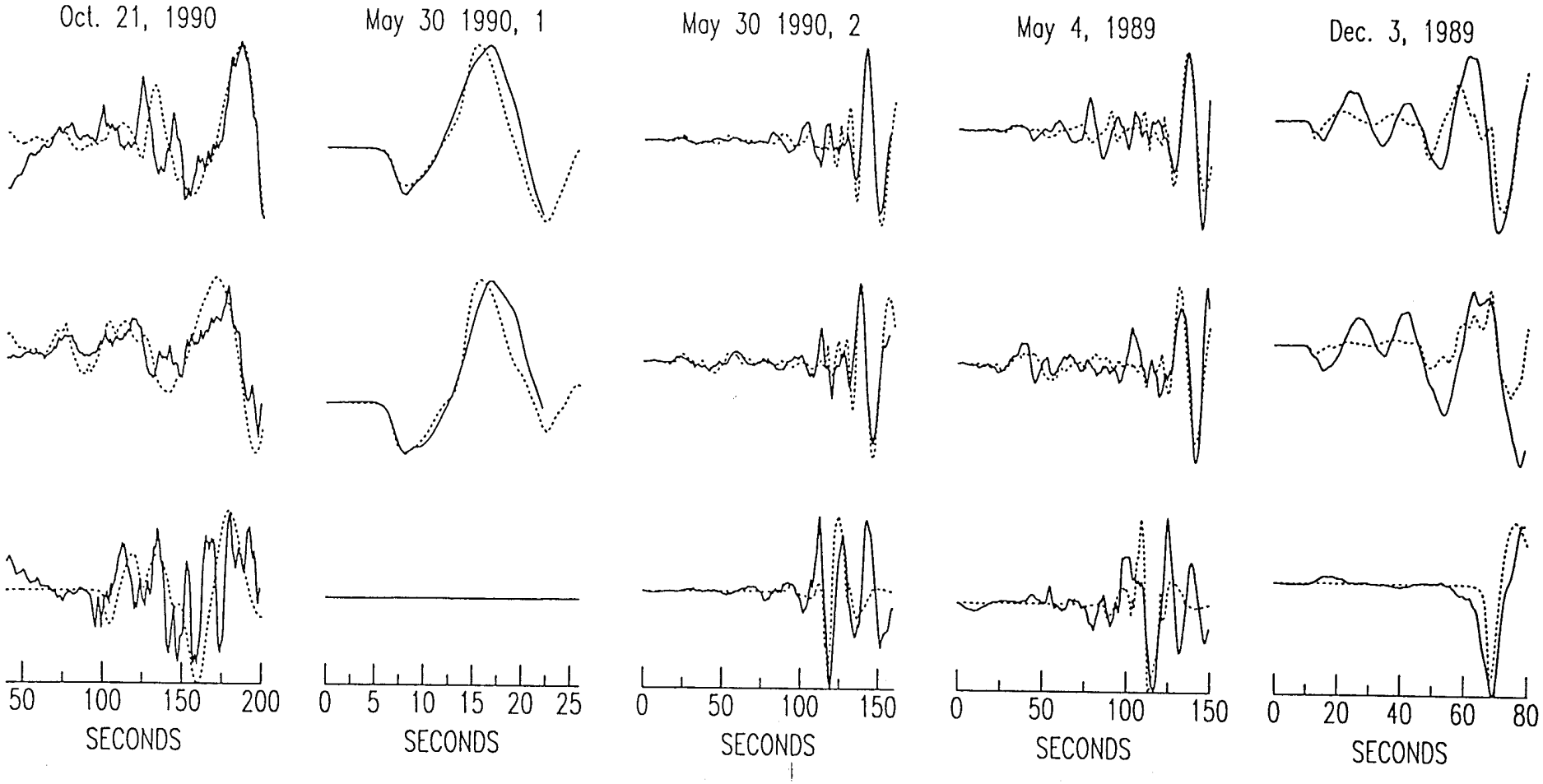
Oct. 21, 1990
May 30 1990, 1
May 30 1990, 2
May 4, 1989
Dec. 3, 1989
50 100 150 200
SECONDS
0 5 10 15 20 25
SECONDS
0 50 100 150
SECONDS
0 50 100 150
SECONDS
0 20 40 60 80
SECONDS

Figure 7

Correlation Coefficient Comparison

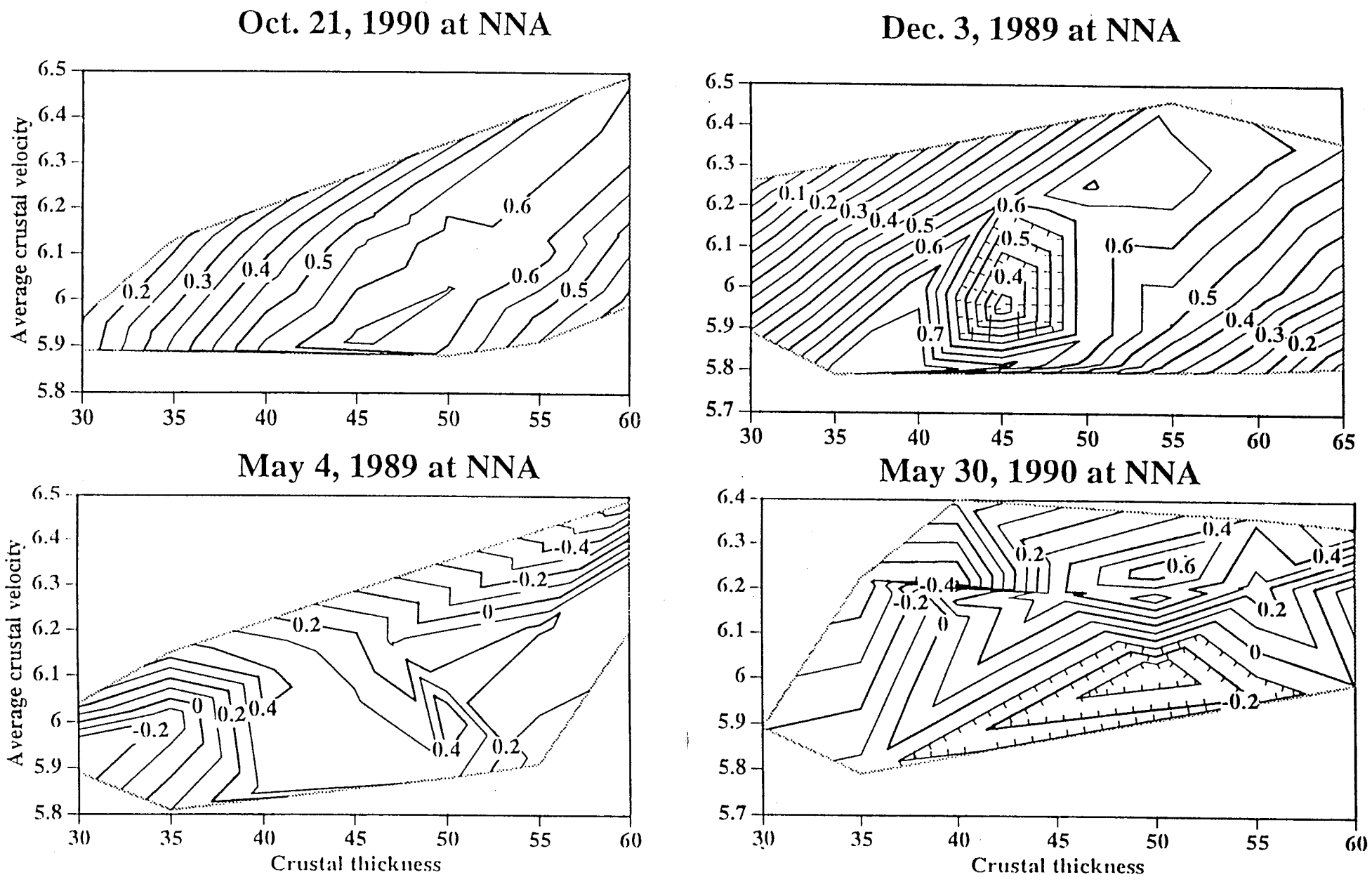

Figure 8

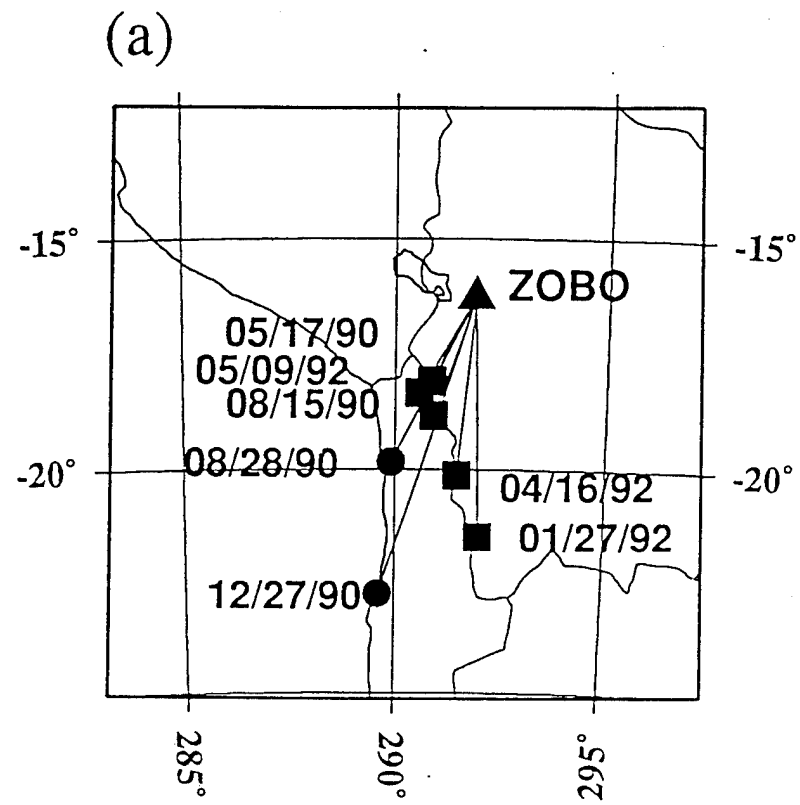
(a)
-15°
-15°
ZOBO
05/17/90
05/09/92
08/15/90
-20°
08/28/90
-20°
04/16/92
01/27/92
12/27/90
285°
290°
295°

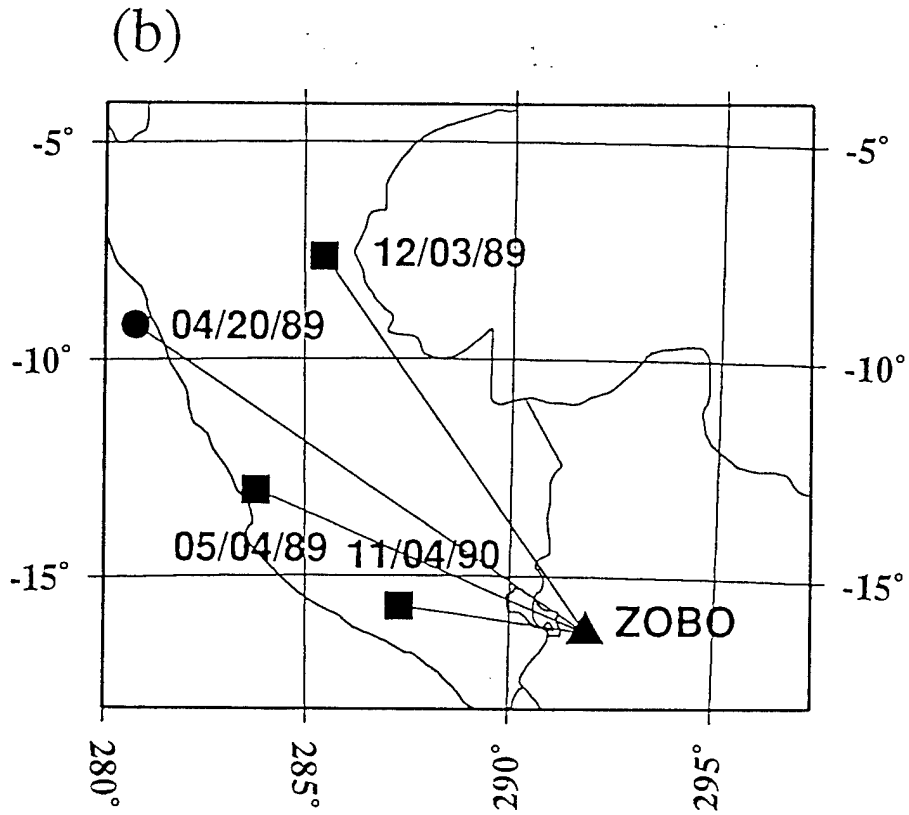
(b)
-5°
-5°
12/03/89
04/20/89
-10°
-10°
05/04/89
11/04/90
-15°
-15°
ZOBO
280°
285°
290°
295°

Figure 9

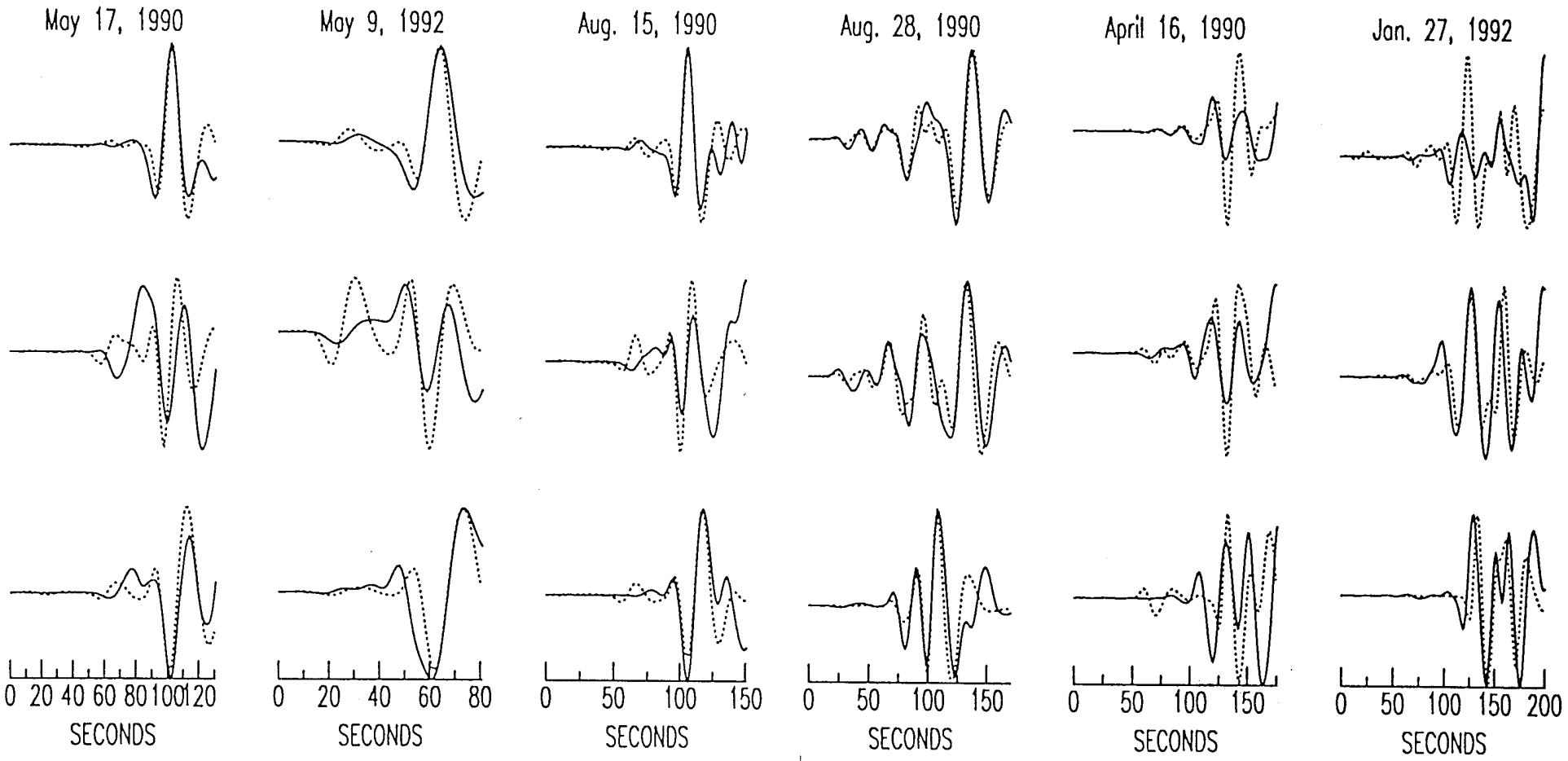
May 17, 1990
May 9, 1992
Aug. 15, 1990
Aug. 28, 1990
April 16, 1990
Jan. 27, 1992
0 20 40 60 80 100 120
SECONDS
0 20 40 60 80
SECONDS
0 50 100 150
SECONDS
0 50 100 150
SECONDS
0 50 100 150
SECONDS
0 50 100 150 200
SECONDS

Figure 10

Correlation coefficient comparison

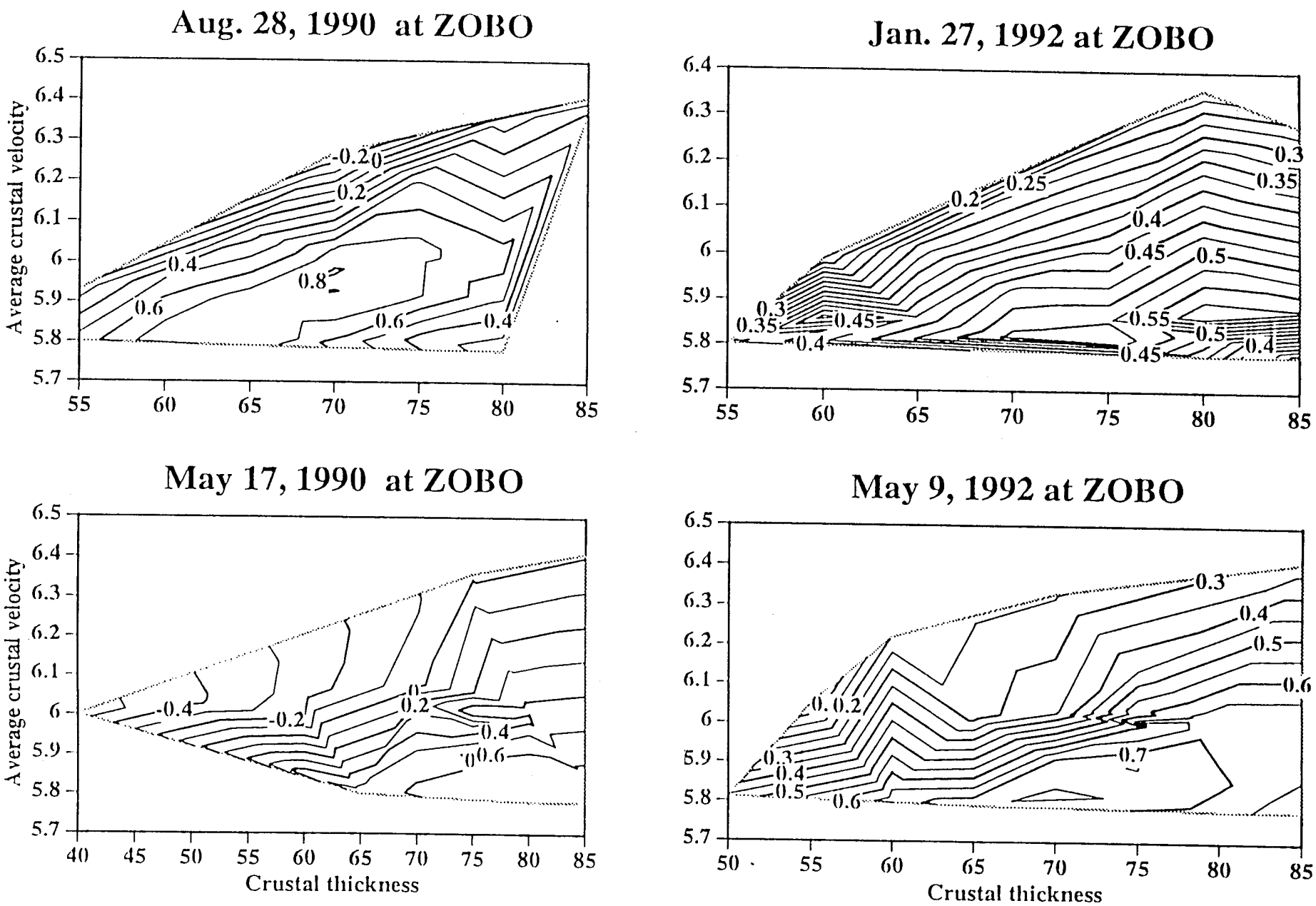

Figure 11

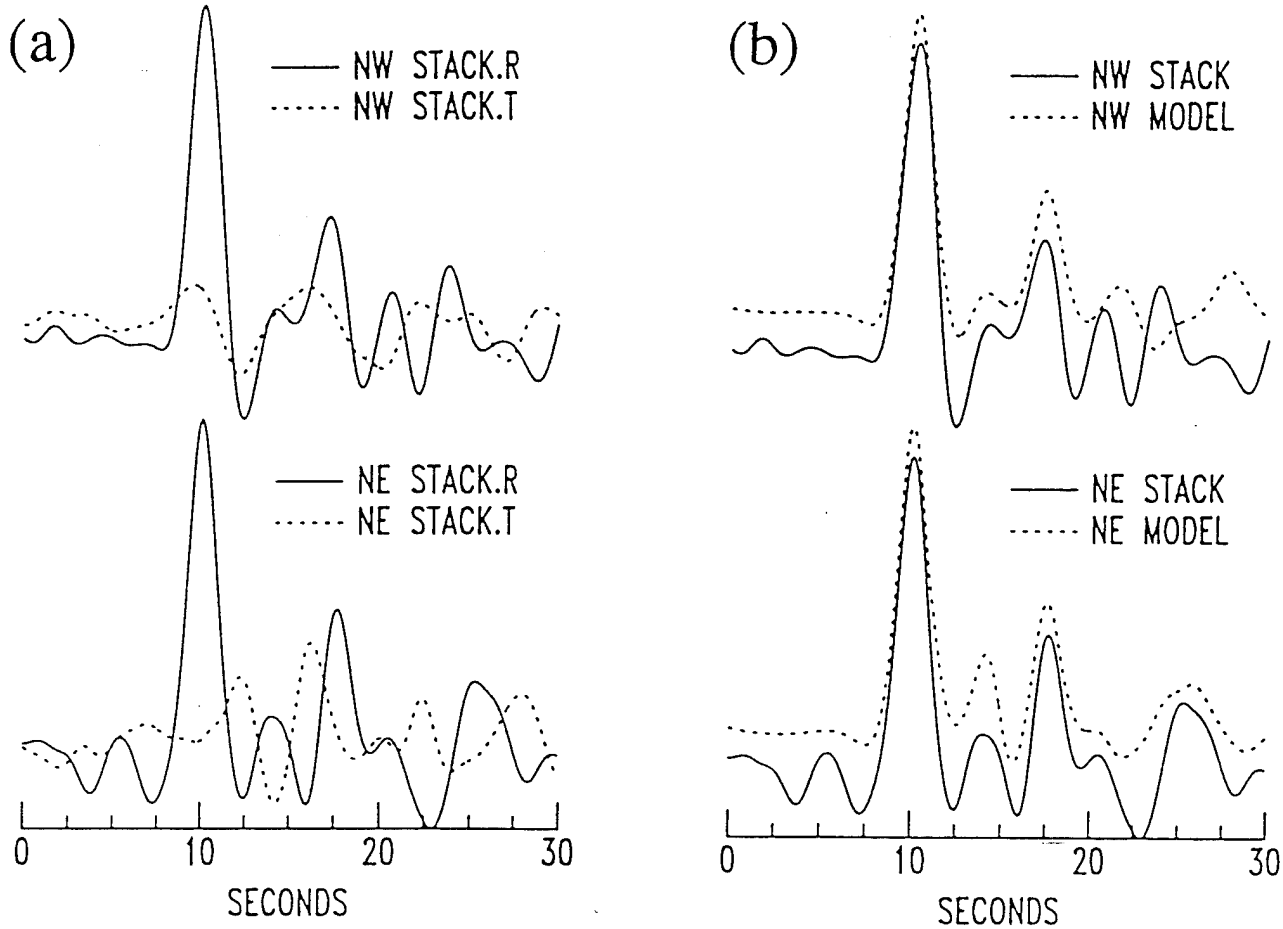
(a)
NW STACK.R
NW STACK.T
NE STACK.R
NE STACK.T
0
10
20
30
SECONDS
(b)
NW STACK
NW MODEL
NE STACK
NE MODEL
0
10
20
30
SECONDS

Figure 12

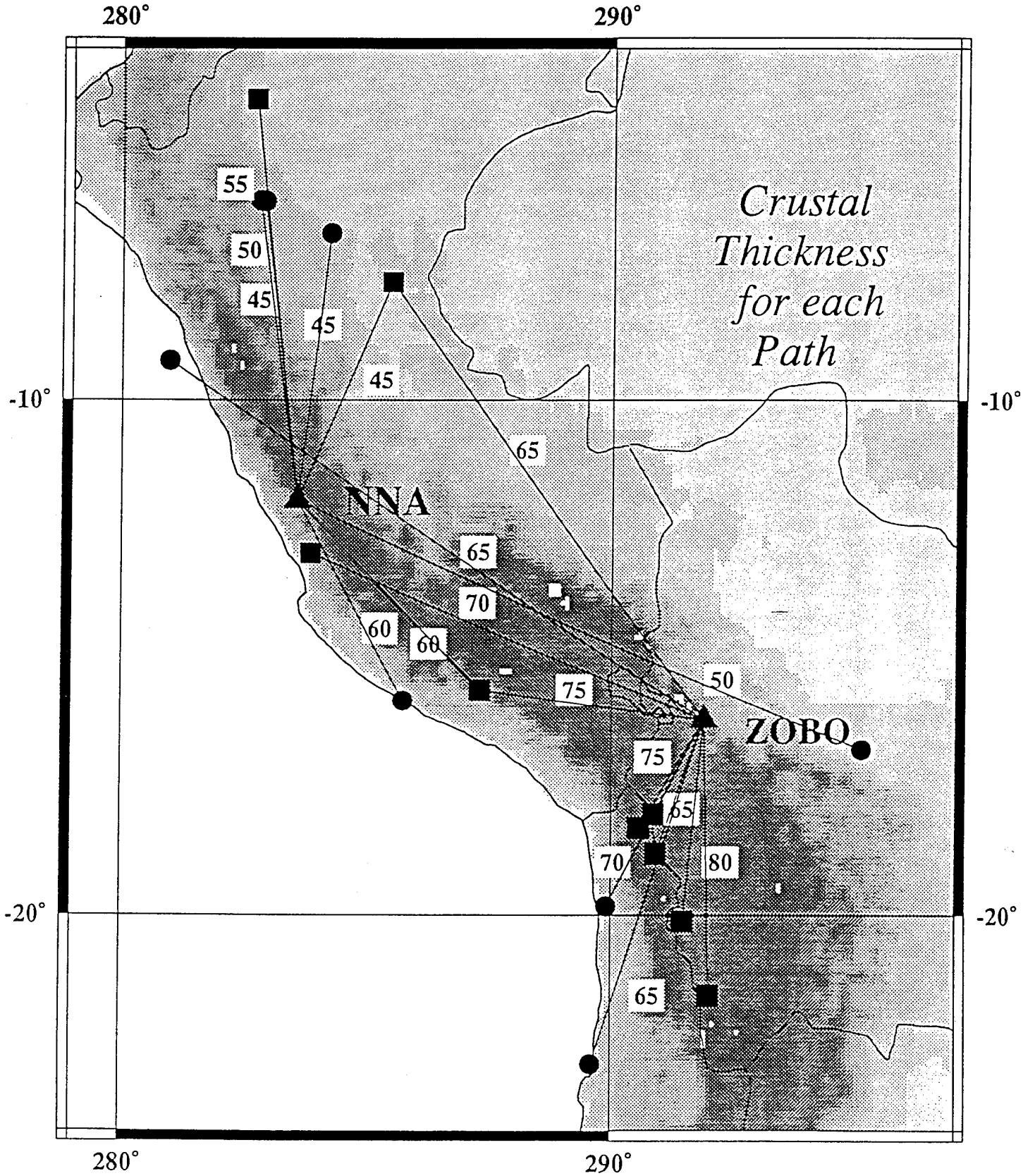
280°
290°
Crustal Thickness for each Path
-10°
-20°
NNA
ZOBO
55
50
45
45
45
65
65
70
60
60
75
50
75
65
70
80
65

Figure 13

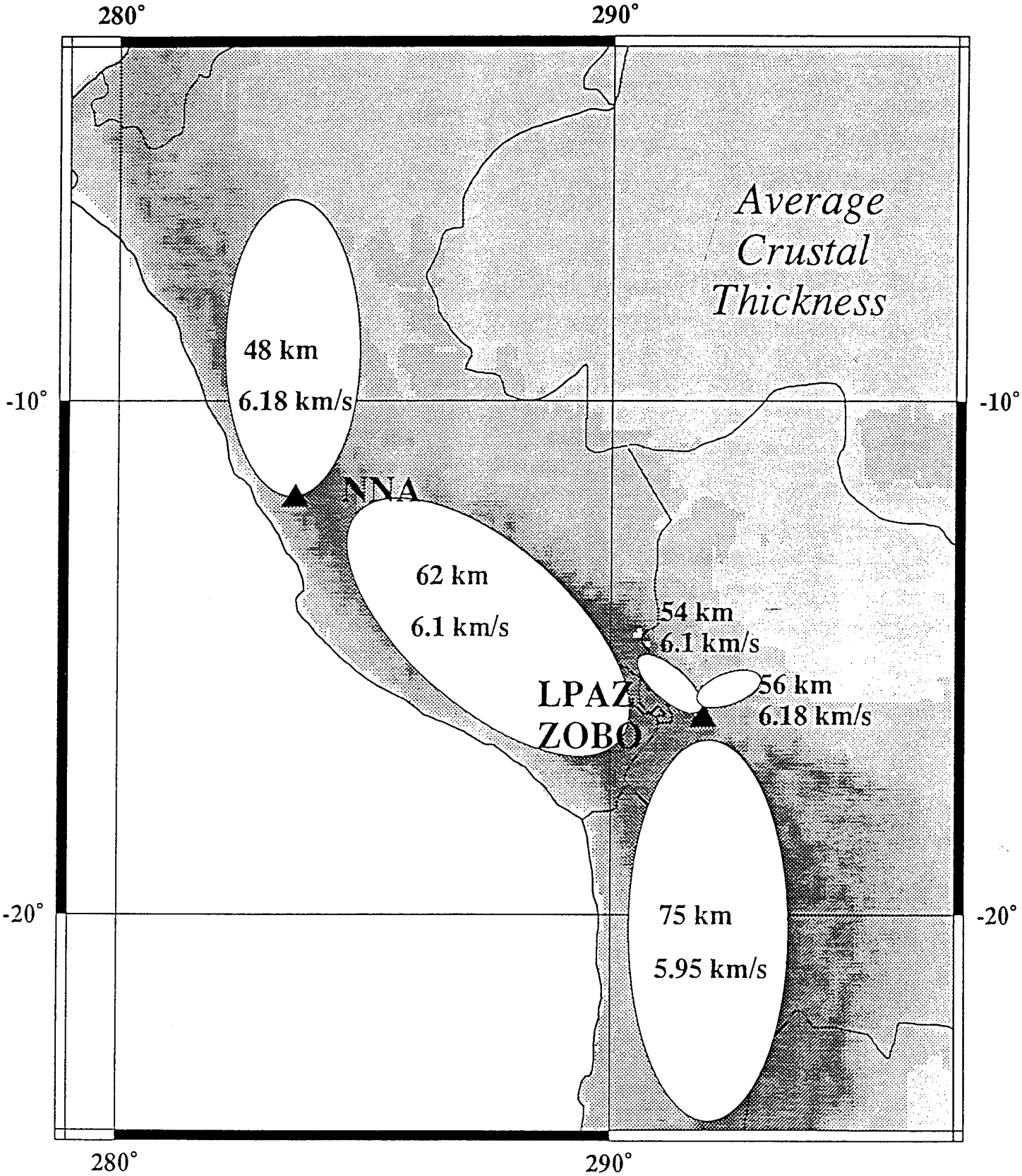
280°
290°
Average
Crustal
Thickness
48 km
6.18 km/s
-10°
-10°
NNA
62 km
6.1 km/s
54 km
6.1 km/s
LPAZ
ZOBO
56 km
6.18 km/s
-20°
-20°
75 km
5.95 km/s
280°
290°

Figure 14

Chapter 3

Using a Single Broadband Seismic Station as a Seismic Observatory

SUMMARY

Small earthquakes and mining explosions are often recorded at a limited number of seismic stations located at regional distances. This means that stations need to be treated as individual seismic observatories. In September 1993, a strong earthquake swarm began in northern Sonora, Mexico. This protracted seismic sequence was well recorded only on a single broadband station(TUC), approximately 300 km away. The nine largest magnitude events of the sequence are as follows: October 5 (M_L 4.0), October 8 (M_L 2.5), October 10 (M_L 3.3), October 19 (M_L 3.2). October 230 (M_L 2.8), M_L 3.5), October 26 (M_L 2.8) and October 31 (M_L 3.7). The events were located with single-station procedures that utilize the entire broadband waveform. Larger events ($M_L \geq 3.5$) were located with a sequential method that determines azimuth to the event, epicentral distance, and focal depth. A relative location technique was used to locate smaller ($M_L < 3.5$) events of the swarm, using a master event.

The epicentral region of the swarm lies within the southernmost extent of the Basin and Range Province. The individual events of the swarm are approximately equidistant to the TUC station (300) km) but are scattered over an east–west trend 30 km long. A focal mechanism for the largest event was obtained by performing a grid search and appears to be dominantly normal-slip. This is consistent with the local tectonic setting. The resolution of the locating techniques was assessed by locating several aftershocks of the January 17, 1994 Northridge earthquake. Station Barett (BAR), with an epicenter distance of approximately 264 km, was used to locate several aftershocks well located by SCSN. A resolution of ±20 km was inferred from this test.

Introduction

An onset of increased seismicity in Sonora, Mexico in the later half of 1993 was recorded at the Southern Arizona Seismic Observatory (SASO). This activity reached its peak in October 1993, although it continues today. The largest events in the Sonoran earthquake swarm are: September 11 (M_L 2.8), October 5 (M_L 4), October 8 (M_L 2.5), October 10 (M_L 3.3), October 19 (M_L 3.2), October 20 (M_L 2.8), (M_L 3.5), October 26 (M_L 2.8) and October 31 (M_L 3.7). Events of October 5, October 20, and October 31, 1993, ($M_L \geq 3.5$) triggered the regional network; the epicentral coordinates for these events were calculated by NEIC. The broadband waveforms for the events were available from IRIS stations TUC and ANMO. The events of October 8, October 10, October 19, October 20, and October 26 with magnitudes $M_L < 3.5$ were only recorded at TUC. Events of this size typically are not well located within areas with the sparse seismic network coverage. Using single-station data and a relative location technique, the coordinates of the smaller magnitude events of the swarm were determined.

The task of obtaining seismic source parameters for regional distance events consists of: a) epicentral coordinates determination from polarization analysis, and b) focal mechanism determination from a waveform inversion. This two-part problem has been addressed previously in the literature [*Magotra et al.,* 1987; *Thurber et al.,* 1989], although recent advances in instrumentation, in particular, frequency bandwidth, hold great promise for using single stations to extract detailed seismic source parameters.

The October 1993 activity provides a very good opportunity to test procedures for source location and analysis using a single broadband seismic station. The method we developed and used, allowed us to locate smaller magnitude events with respect to a larger master event where epicentral coordinates are assumed known. The method involves an assessment of the relative azimuth and relative distance to an event and focal mechanism determination from band-passed data.

Geological Setting and Seismicity

The epicentral region of the swarm lies within the southernmost extent of the Basin and Range province, in Northern Sonora, Mexico in the vicinity of the towns of Bacerac, Huachineras, Huasabas, and Granados. Figure 1 shows the location of the events on a simplified regional tectonic map. The region is located within a large extension zone and has a number of normal faults thought to be active in the Quaternary (Figure 1). Figure 2 shows local topography and locations of the October 1993 events.

Northern Sonora generally has a low level of seismicity. However, the earthquakes of 1887 (the great Sonoran $M = 7.8$) that ruptured the Pitaycachi fault, and one in 1924 that occurred along the Bavispe fault, caused significant damage. Recent activity in the region around Bavispe in June 1988, May 1989, and June 1989 has been described [*Wallace et al.* 1988, *Wallace and Pearthree* 1989]. These were four small earthquakes (magnitudes of 4.2, 3.4, 2.4, and 2.8) that caused no damage and occurred over a period of two years. These events were associated with faulting in vicinity of southern part of San Bernardino Valley (northern segment) and northern part of Bavispe and El Tigre Valley junction (southern segment). It has been suggested [*Wallace and Pearthree* 1989] that there is a significant "slip-deficit" from the 1887 event along the southern segment, although the fault segments may be independent.

Beginning in October 1993, we noted a marked increase of seismicity in the region. The felt reports that followed the events, varied. Some claimed that events were not noticed at all, in some cases vibrations of the windows are mentioned, along with a sound of "air through a hall". During one event, plates slid in a student dining room. The event of October 5, 1993 is said to have caused cracks in a wall. No significant damage, however, was reported [1]. The monthly average is one event every four days -

[1]The felt reports are based on reports in the newspaper El Imparcial, October 21, 1993.

the highest level of seismicity experienced in recorded history (since the mid 1920s) in this region of Sonora.

Data and Hypocenter Location

The installation of very broadband seismic stations has generated interest in using single station as "seismic observatories". The task of source location with a single station, or a sparse network, is especially interesting and important in the case of low-magnitude events ($M_L \leq 4$). The larger magnitude events of the October 1993 swarm, namely October 5, October 20, and October 31 were separated by a sequence of smaller magnitude events. Figure 3 shows vertical components of the individual earthquakes of the swarm recorded at TUC. The magnitudes of the events were estimated to be: October 5 (M_L 4), October 8 (M_L 2.5), October 10 (M_L 3.3), October 19 (M_L 3.2), October 20 (M_L 2.8), (M_L 3.5), October 26 (M_L 2.8), and October 31 (M_L 3.7). Magnitude values were calculated at Tucson (TUC) approximately 300 km away. The larger magnitude earthquakes (Figure 3a) triggered the USNSN regional network and their coordinates were calculated by National Earthquake Information Center (NEIC) with a standard triangulation method. The smaller events (Figure 3b), however, were not located. The epicentral coordinates of the weaker events were obtained by means of a relative location method, used by Southern Arizona Seismic Observatory (SASO). The method is a three-step procedure: (1) azimuth determination, (2) distance determination, and (3) focal mechanism and depth determination. The procedure requires a pair of events. One is a reference, or master event, and the epicenter of the other event is determined relative to the master event.

Azimuth Determination

The method for determination of the horizontal angle or azimuth to the source of seismic energy is based on methodology introduced by Magotra *et al.* [1987], where a

vector of ground displacement is determined from a three-component waveform polarity analysis. It is well known that in heterogeneous media the azimuth of an arriving wave does not always coincide with an expected direction. However, for events that are sufficiently close to one another, the difference in the azimuth will be preserved. The waveforms of the reference and tested events are analyzed with a standard polarity method to assess values of the instantaneous azimuth as a function of time. The values of the residual azimuth, or difference between azimuth to the master event, is calculated for all events in the swarm. Figure 4 shows an example of the azimuth determination for one of the events. Shown are the values of instantaneous azimuth averaged over the time windows as a function of time. The statistical estimates of the mean and standard deviation allow a "pick" of the best value of the azimuth.

Distance Determination

Distance determination at regional distances has traditionally been a difficult task. Arrival times of individual phases are difficult to pick, and further, show variability due to heterogeneity in the earth, and are quite dependent on source orientation. We have developed a procedure which correlates the entire shape of a broadband waveform with distance; an envelope function which depends on the strength of regional phases such as P_n, P_g, L_g, and R_g is compared to a catalogue of synthetic envelopes calculated for a regional structure. The "best" distance is determined by maximizing the cross-correlation between synthetics and observed data. We have found that this procedure removes much of the ambiguity in picking arrival times. Further, envelope functions are much less sensitive to actual source mechanism than direct synthetics.

In a multi-layered medium there are a variety of seismic phases that have lower amplitudes individually, but collectively interfere and make it difficult to pick the onset of specific arrival. It has been noted [*Wallace* 1986], that at regional distances a simplified model, that averages crustal velocities, is representative enough for purposes

of source parameter inversion and distance determination. Relative timing of the P_g, S_g and L_g phases appears to be a function of the average crustal velocity. Two events that have similar epicentral distances will have similar timing of the P_g, S_g and L_g phases. An increase or decrease of relative timing between the corresponding P_g, S_g and L_g phases is indicative of the increase or decrease in distance from the epicenter. Using the fact that relative timing of the phases is a pseudo-linear function of distance, one can assess its value with respect to a master event, the coordinates and epicentral distance of which are known. Within the framework of the task of obtaining relative coordinates of the tested events from the waveforms of the reference earthquakes, we have found our approximation to be adequate.

Generally, two different focal mechanisms produce different relative amplitudes for various regional distance phases. Although the timing is independent of mechanism, the influence of source mechanism makes it impossible to directly compare observations to a catalogue of synthetics.

We attempt to minimize the amplitude variability by constructing a vector describing the total displacement. We then use the time dependent "length" of this vector as an envelope. In other words, we take the sum of the squares of the amplitudes of the various components as follows:

$$X(t) = \sqrt{x_1^2(t) + x_2^2(t) + x_3^3(t)} \tag{1}$$

The new time series $X(t)$ represents all three components. Then we obtain the envelope of the $X(t)$ and all further analysis is performed on it. An important quality of the $X(t)$ is that it has multiple distinct maxima, corresponding to arrival of the various regional phases. The separation of these phases is related to a distance that seismic wave travels away from the source.

For the Sonoran earthquakes we assumed a simple model - one layer over a half space. The layer velocity was assumed to be an average velocity of typical three-layered

continental crust. This simplification was based on practical reasons, as well as some useful approximations [*Wallace* 1986]. Crustal heterogeneity requires the use of the azimuth to the seismic source before estimating the distance to the event. The structure used for these events is based on a model for Southern Arizona introduced in a thesis by Hiller [1989]. The minimized misfit is given by the maximized value of coefficient of correlation;

$$\xi_j = \frac{\sum_{i=0}^{N}[d_{i+j}m_i]}{\sqrt{\sum_{i=0}^{N}[d_{i+j}^2]\sum_{i=0}^{N}[m_i^2]}} \tag{2}$$

with

$$\delta_j = 1 - \xi_j$$

ξ_j and δ_j are the correlation coefficient and misfit, respectively, over the time interval j; d represents N discrete values of envelope in the interval j; m represents N discrete values of synthetic envelope of the same interval.

The distance determination for the individual events of the seismic swarm was conducted with a relative location technique. The earthquake of October 31, 1993 was chosen as a reference event, and the other events were treated as earthquakes with unknown epicentral coordinates. It appeared that all of the events had approximately the same epicentral distance. Figure 5 shows that relative timing between the P_g and S_g, L_g phases is very similar which implies similarity in epicentral distance.

Focal Mechanism and Depth Determination

Once the epicentral coordinates are determined, we can solve for seismic moment tensor. This procedure is based on methodology developed by Fan and Wallace [1991] and by Walter [1993] for regional waveforms, where a catalog of Green's functions representing the individual moment tensor terms is used. Each Green's function is a numerical representation of a double-couple force in a particular orientation. A linear

combination of Green's functions represents the elastic response of a point source or arbitrary fault geometry. This can be written as a linear equation for source parameters m:

$$Am = d \tag{3}$$

where A is a linear combination of Green's functions, d is observed data vector and m is vector containing the moment tensor elements. However, instead of constructing an inverse operator and using it to assess model parameters by applying it to the vector of observed data, we used grid search to obtain best fitting moment tensor. The minimum value of the L_2 norm, the difference synthetic minus observed data, was used as a criteria for the search:

$$\mu = ||(d_i - a_i)||_2 = \frac{\sqrt{\sum_{i=0}^{N}(d_i - a_i)^2}}{N} \tag{4}$$

where μ represents misfit, d_i is an observed data series and a_i is the synthetic time series.

The depth of the event has been determined by considering sets of Green's functions calculated for a number of focal depths. The "best" depth was chosen, for the lowest value of misfit between observed data and the model given by the equation (4).

Resolution Assessment

To assess the resolution of the single station methodology, we decided to locate a number of aftershocks of the January 1994, Northridge earthquake. The event is one best recorded in the history with the broadband recordings at TERRAscope and the various short-period networks in Southern California. Good spatial and azimuthal coverage of the region with Southern California Seismic Network gave a number of aftershocks which are located with a high degree of confidence. Records from seismic station Barett (BAR) were chosen for analysis. The reason for the choice was based on similarity of

the epicentral distances with events of the Sonoran seismic swarm of October 1993. The aftershocks that are being considered and the corresponding magnitudes are as follows: January 17, 23:33:30.31 $M_L = 5.6$, 23:40:52.93 $M_L = 3.2$, 23:49:25.08 $M_L = 4.0$; January 18, 04:01:26.73 $M_L = 4.3$, 15:19:54.10 $M_L = 3.9$, 15:23:46.88 $M_L = 4.8$; and January 19, 04:40:47.99 $M_L = 4.3$.

The implications of the resolution analysis to our task of locating smaller events of the October 1993 seismic swarm are as follows: even though, the relative timing of the P_g, S_g and L_g phases of different events of the swarm (Figure 5) implies that events are equidistant to the station TUC, we do allow small errors in distance determination. We also think that we see insignificant localized event scattering off the azimuth due to near source effect.The topography of the area where we predict event locations (Figure 2) shows that this events are localized around some structural form of Basin and Range type. This implies that our results are in agreement with local geology. In the light of this comments we do not dissmiss the posibility of the October 1993 seismic swarm to be more localized that we are predicting, however, wave forms for all of the events appear to have very distinct "signatures". This implies change in focal mechanism or location of each events.

The epicentral coordinates were our main concern in this test. The result of the test showed reasonable resolution of the method with an exception of one event where the mislocation was of the order of 20 km. This value was taken as the resolution of the method of relative source location. Figure 7 shows the epicenters located with our method and locations determined by the TERRAscope network. Table 1 presents these results.

Discussion

Small earthquakes are often recorded by a single stations, which greatly limits their analysis. We have developed a relative location procedure where an earthquake with an

established epicentral coordinate is used as reference events to locate smaller magnitude ones. The results of analysis of the sonorian swarm had a grouping of epicenters, consistent with the general east-northeast trend (determined by NEIC) of the strongest events of the swarm, and somewhat consistent with the available felt reports. We also conducted a test on well-located aftershocks of the January 17, 1994 Northridge earthquake, which allowed us to obtain resolving capabilities of the method. The value of $\pm$ 20 km was assumed to be the resolution of the method for relative epicentral location. This value was taken into account in determining the tectonic implications of the swarm. The tectonic setting in Northern Mexico is somewhat complicated. There are a number of normal fault segments that are not connected and, in spite of the generic north-northwest orientation, are not colinear. The focal mechanism for the largest event was obtained through grid-search and moment tensor inversion procedures. The solutions showed consistent P axis, and variable T axis. The prefered mechanism is strike = 204.5, dip = 58.6, and slip = -51.9.

The normal-slip mechanism is consistent with the general tectonic setting, although the relationship to the Bavispe faulting is uncertain. The intensity of the swarm is very unusual for the southern Basin and Range, where earthquakes seldom have any aftershocks. Since 1987, northern Sonora area has experienced a number of similar magnitude ($M_L \leq 4.2$) events, however, this swarm represents the most concentrated release of seismic energy in the area to date. At this stage it is difficult to assess level of potential hazard associated with seismic activity in the region. If the seismicity is associated with a southern extension at the Pitaycachi fault, which did not experienced as much slip as the northern segment during the earthquake 1887, then a moderate size earthquake (> 5.0) may occur to accomodate the associated strain.

Acknowledgements

The authors' gratitude and appreciation go to Silvia Torres for her willingness and active participation in translating from Spanish, also to Susan Beck and Steve Sorenson for their active technical support. We also greatful to Dave Wald and Charles Langston, whose comments helped to improve the quality of the presentation. The research was partially funded by grant from AFOSR F49601-92-J-0416 to the University of Arizona. SASO contribution No. 43.

References

Fan, G. and T. Wallace, The determination of source parameters for small earthquakes from a single station, *Geoph. Res. Lett.*, *18*, 1385-1388, 1991.

Hiller, J., Seismic structure of Arizona, University of Arizona., *MS thesis work.*, , , 1989.

Magotra, N., Ahmed N., and E. Chael, Seismic event detection and source location using single-station (three-component) data., *Bull. Seism. Soc. Am.*, *77*, 958-971, 1987.

Thurber, C., Given H., and J. Berger, Regional seismic event location with a sparse network: application to eastern Kazhakhstan, USSR, *J. Geophys. Res.*, *94*, 17,767-17,780, 1989.

Wallace, T., Domitrovic, A., and P. Pearthree, Southern Arizona earthquake update, *Arizona Geology*, *18*, 6-7, 1988.

Wallace, T., and P. Pearthree, Recent earthquakes in Northern Sonora, *Arizona Geology*, *19*, 6-7, 1989.

Wallace, T., Some useful approximations to generalized ray theory for regional distance seismograms, *Geophys. J. R. astr. Soc.*, *85*, 349-363, 1986.

Walter, W., Source parameters of the June 29, 1992 Little Skull Mountain earthquake

from complete regional waveforms at a single station., *Geoph. Res. Lett.*, *20*, 403-406, 1993.

Table 1. Resolution Assesement

	Relative Location		SCSN		Errors		
Event	Lon.	Lat.	Lon.	Lat.	δ Lat.^{o}	δ Lon.^{o}	δ Dist. (km)
1	241.31	34.38	241.31	34.38	0.0	0.0	0.0
2	241.37	34.38	241.32	34.34	0.02	0.040	3.5
3	241.39	34.39	241.37	34.34	0.02	0.050	5.5
4	241.38	34.38	241.41	34.21	-0.03	0.170	18.0
5	241.50	34.43	241.45	34.39	0.05	0.040	6.5
6	241.49	34.41	241.45	34.40	0.04	0.010	4.0

Coordinates of the events as determined by relative location method and SCSN locations. The estimates of errors are given in degrees of latitude, longitude and in km.

Figures

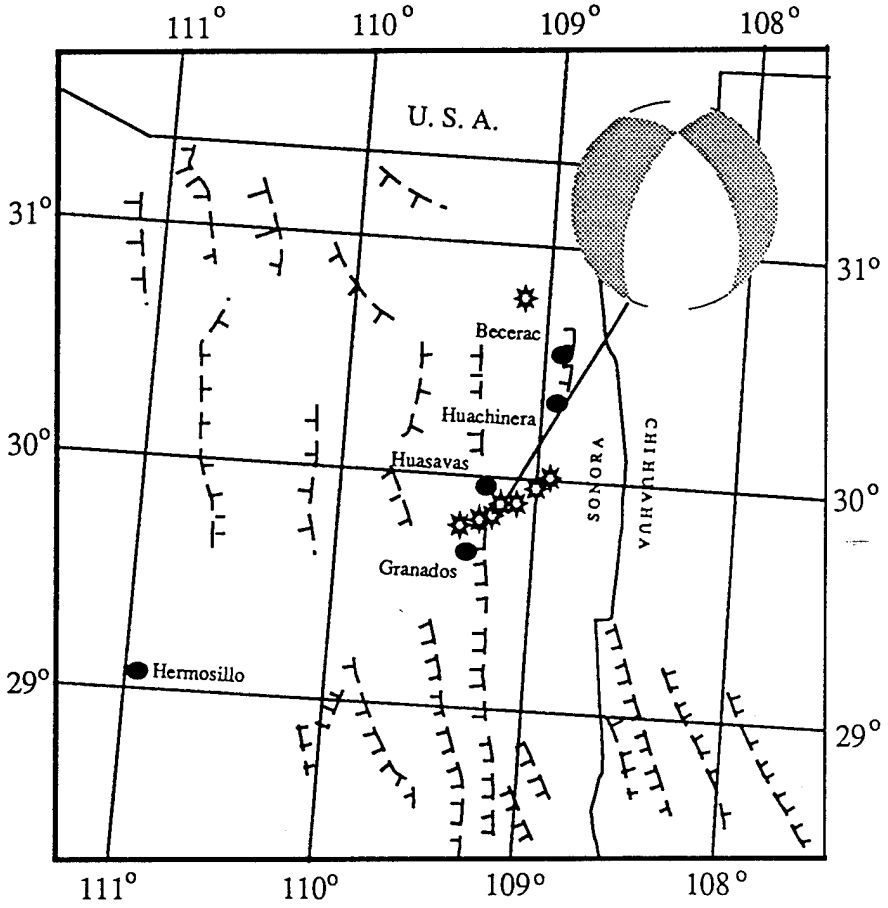

Figure 1. Events of the October 1994 swarm overlaying a simplified tectonic map of Mexico. The events of the swarm are marked with stars. One can see general east - northeast trend of the events. The 1887 Great Sonoran Earthquake is represented by a star north of the swarm. The cities mentioned in the text are marked with black circles.

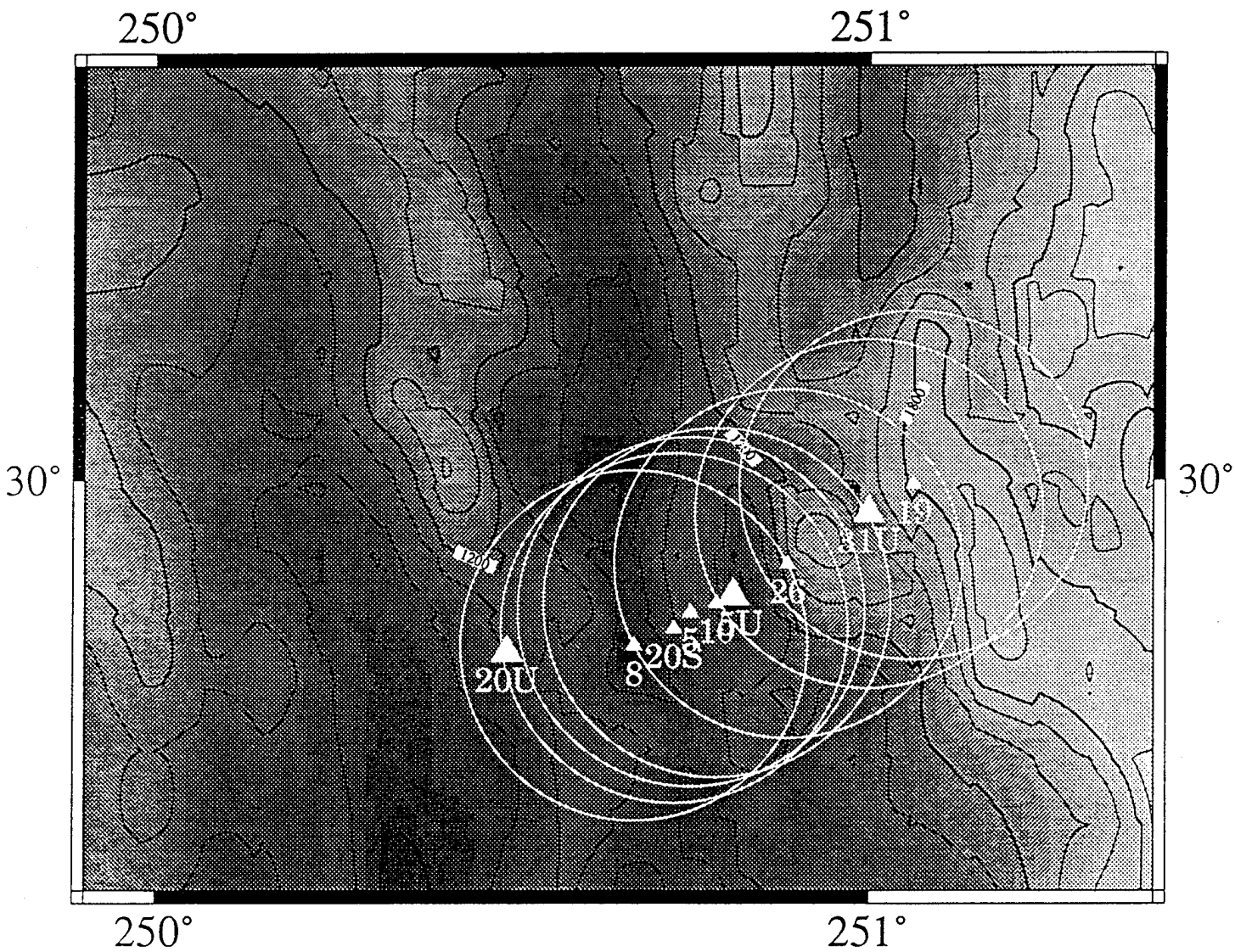

Figure 2. This close up of the regional topo map shows the locations of the individual events of the October 1993 seismic swarm in northern Mexico. Seismic events are represented with triangles. The associated number corresponds to the day the earthquake occurred. Locations of the reference earthquakes, namely October 5, October 20, and October 31 (larger triangles were used to obtain epicentral coordinates of the smaller magnitude events (smaller triangles). Large circles represent the area where solution could reside. The error circles of the events 8 and 19, which are the most distant to one

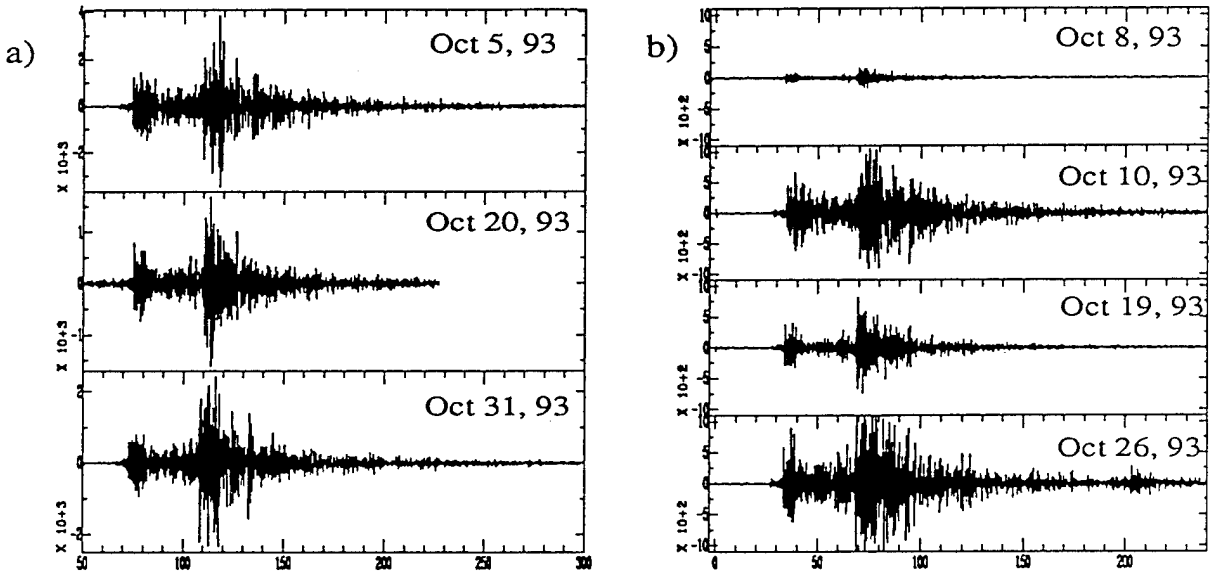

Figure 3. The earthquakes of the October 1993 seismic swarm, a) Larger magnitude events $M_L \geq 3.5$, October 5, October 20, October 31; and b) Smaller magnitude $M_L < 3.5$ October 8, October 10, October 26

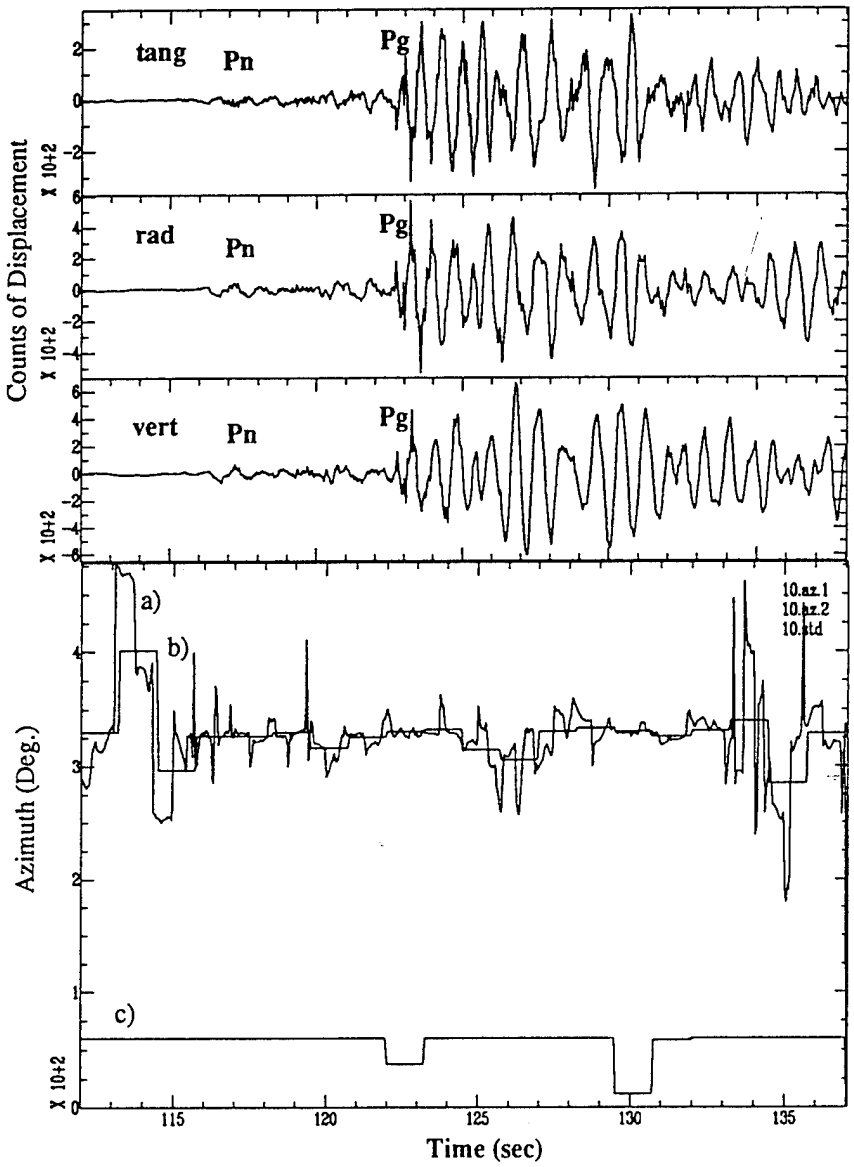

Figure 4. Waveforms and azimuth determined from the set. Statistical analysis of the values of azimuth is used for azimuth determination. Curves on the lower part of the figure represent: a) Values of instantaneous azimuth plotted as a function of time; b) Values of instantaneous azimuth are averaged over a time window to assess mean value of azimuth over the window; c) Standard deviation of the instantaneous azimuth from the mean is plotted to show the zones of stable and reliable value of azimuth. Values of standard deviation do not exceed 60 on this plot.

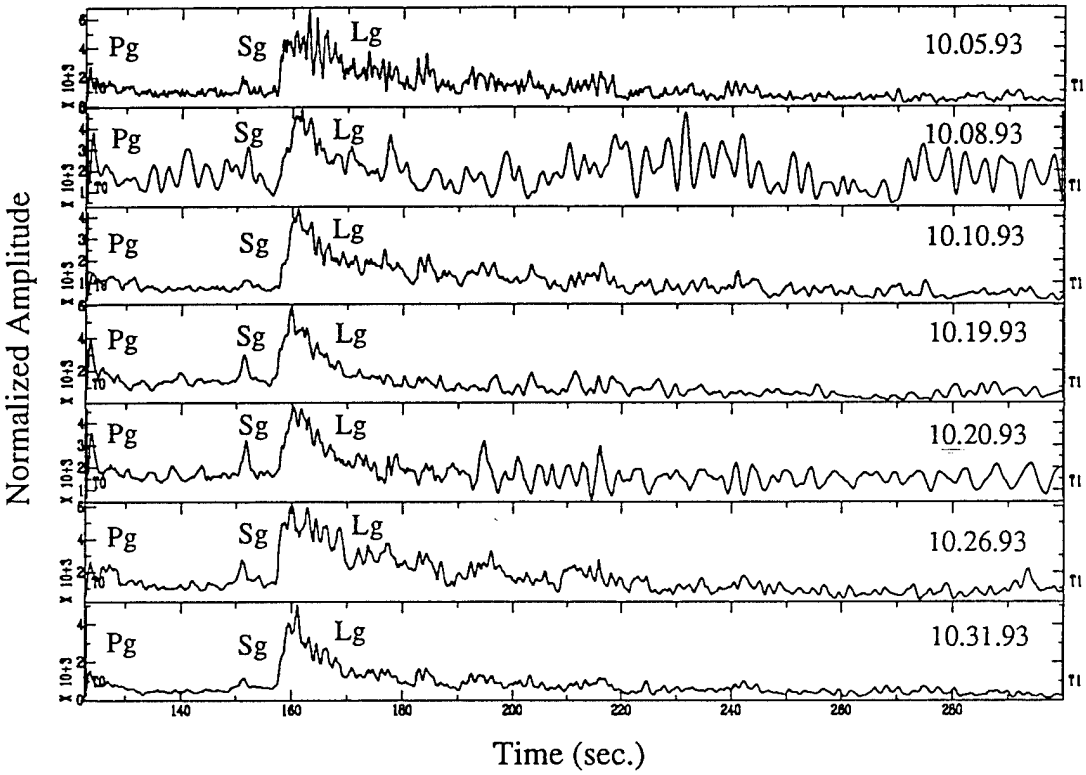

Figure 5. Normalized waveforms are used for distance determination. Waveforms of individual events of the swarm are presented and marked with corresponding day when the event has occurred.

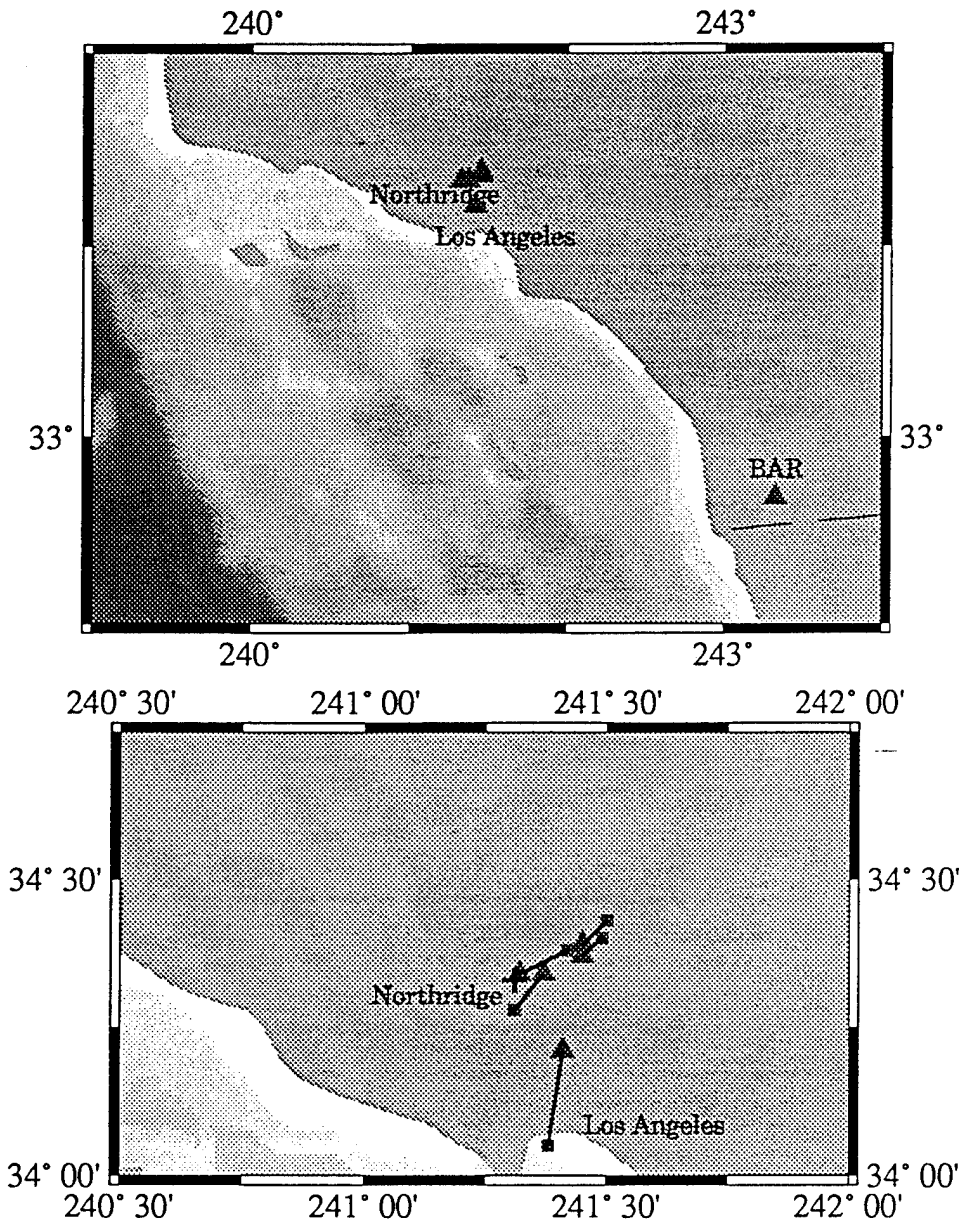

Figure 6. Locations of the aftershocks of the January 17, 1994 earthquake. The triangles represent locations of the events determined by SCSN and squares represent locations of the same events determined by our method. Line connecting a triangle and the corresponding square represents the mislocation for the given event. The largest mislocation, (the most southern event) is of the order of 18 km.

Chapter 4

Regional Phase Development of the Non-Proliferation Experiment Along a Broadband Seismic Profile

Mark Tinker, Terry Wallace, George Zandt and Steve Myers

SUMMARY

The Non-Proliferation Experiment (NPE), a large chemical explosion (1.3 x 10^6 kg of ANFO) detonated at the Nevada Test Site on September 22, 1993, was conducted to verify possible differences between the seismic signature from a nuclear and chemical explosion. The University of Arizona recorded NPE along an east-west profile between NTS and the Lawrence Livermore National Laboratory station KNB (Kanab, Utah). There were 10 stations in the profile equipped with very broadband seismometers (STS-2), spaced at approximately 20 km. The close spacing was essential to tract regional seismic phase development without aliasing. Data were sampled at 100 and 20 sps.

Analysis of the waveforms yields three generalities: (1) the seismic phases change character dramatically at the Colorado Plateau-Basin and Range transition. (2) NPE produced a significant non-isotropic wavefield (SH energy). NPE was detonated only 500 m from a nuclear explosion of similar yield (HUNTER'S TROPHY, September 18, 1992); although the P waves for the two explosions are similar, the S-waves are different, reflecting the finitness of the source. The regional wavefield recorded on open broadband stations located throughout the US, shows remarkable similarity to that of HUNTER'S TROPHY. (3) the m_{bLg} from the stations along the profile are consistent with a yield of a 1.6 kt nuclear explosion.

The stations along the profile also recorded a number of teleseismic and regional earthquakes. We have used these recording to determine the receiver structure beneath all the stations. The crustal structure varies from 50 to 31 km; there is strong correlation between the thickness and amount of geologic extension which occurred during the last 20 million years.

INTRODUCTION

Regional distance seismology is the primary tool used for dectection and identification of explosions, either nuclear or chemical. However, regional distance waveforms are also the most complicated. Due to the large number of explosions and earthquakes at the Nevada Test Site, a thorough analysis of various discrminants and source effects is possible, but only at the limited number of stations (in other words, limited distances and azimuths) that have been in operation for many years thereby acquiring such data (Walter et al., submitted to *BSSA*). Of course, stations located at these same distances and azimuths about another test site in another country could produce an entirely different set of results. Therefore, it is necessary to have a solid understanding of how regional phases develop within different tectonic regimes (azimuthal dependence) and at different distances to effectivly monitor an active test site (prior data exists) or a potential test site (no prior data). Such monitoring is necessacry, in terms of verification, if the world is to reenter into a comprehensive nuclear test ban treaty. Furthermore, such monitoring would also attempt to provide discrimination between eartquakes, legitimate chemical explosions, and nuclear explosions.

To address such critical non-proliferation issues, on September 22, 1993, a large chemical explosion was detonated at the Nevada Test Site. This explosion was known as the Non-Proliferation Experiment (NPE). The purpose of this experiment was multi-fold, from measuring hydrodynamic shock waves and free field particle velocities, accelerations, and stresses to measuring electromagnetic pulses, gas samples, and atmospheric waves. A large portion of the experiment focused on local and regional seismic surface measurements. The purpose of these include, 1) verifying possible differences between the seismic signature from a nuclear and chemical explosion, 2) investigating the evolution of regional seismic phases as they propagate across major tectonic provinces, and 3) determining the effects a change in geologic environments has on seismic discriminates.

Members of the Southern Arizona Seismic Observatory at the University of Arizona participated in NPE by recording the explosion on an east-west broad band seismic profile. Ten broad band stations were installed on a line trending east from the Nevada Test Site to the Lawrence Livermore National Laboratory permanent seismic station KNB at Kanab, Utah (figure 1). The purpose of this profile was to investigate the development of regional seismic phases and to explore the effects a change in geologic environments has on seismic discriminantes. Furthermore, the Chemical Kiloton Explosion (hereafter referred to as NPE) was the most instrumented non-classified explosion in history. Fifty broad band stations recorded the event, allowing not only for investigation of phase development at greater distances, but also as a function of azimuth (Fig. 2). Finally, NPE was detonated less than 500 meters from a nuclear explosion (Hunter's Trophy) of similar magnitude. Therefore, comparisons can be made between source effects since the ray paths are (or were) virtually the same.

THE NON-PROLIFERATION EXPERIMENT

The United States Department of Energy excavated a large cylindircal chamber (15.2 meters in diameter by 5.5 meters in height) 390 meters under Rainier Mesa at NTS. The cylinder was filled with approximately 1.29 million kilograms of a pasty looking 30/70 emulsion to ANFO (ammonium nitrate and fuel oil) blend. This entire volume was detonated sucessfully at one minute past midnight on September 22, 1993, and recorded at 50 seismic stations.

The University of Arizona seismic profile consisted of 10 broad band STS-2 seismometers (frequency band 40 - 0.05 Hz), Reftek digitizers, and GPS clocks. Nine of the ten stations were operational during the explosion. The closest station to the shot point is 73 km, from which the remaining stations were located at approximately 20 km intervals. Station KNB is 302 km from the shot point. Thus, the profile covers the transition between the Basin and Range and the Colorado Plateau. Station 1 is the furthest and Station 10 is the closest to the shot point. The remaining stations that recorded NPE are permanent stations operated by Incorporated Research Institutions in Seismology (IRIS)/Global Seismograph Network (GSN), Lawerence Livermore National Lab (LLNL), Sandia National Lab, TERRAScope, the Berkeley Digital Seismic Network (BDSN), and

another portable broad band profile (trending 320° from NTS, 250km long) deployed by Priestley, McCormack, and Patton, for a total of 50 stations. These stations range in distance 73km to 1029km from NTS. For Hunter's Trophy, we have 14 permanent stations from IRIS, LLNL, BDSN, and TERRAScope, ranging in distance from 217km to 1029km.

ANALYSIS

NPE Pn, Pg, and Lg Phase Development

The University of Arizona seismic profile (UA) recorded NPE at 9 stations. Station 2 was not operational. However, by sheer coincidence, it was at the same distance and nearly the same azimuth as permanent station LDS. The entire UA profile is shown in Figure 3. The Pg velocity is 6.04 km/sec as determined from a least squares fit. The apparent Pn velocity is a slow 7.6 km/sec. This is expected on a down-dipping structure such as the thickening Colorado Plateau. However, also notice the variation in Pn amplitude. The crustal transition from the Basin and Range to the Colorado Plateau is not a smooth one. This results in a focusing and defocusing of Pn energy as it travels the down-dipping Moho. Finally, the shaded region is a Lg velocity window between 3.55 and 3.0 km/sec. Lg does not emerge until Station 6 at 166 km. From Station 6 to station KNB (302km), the Lg/Pn spectral ratio gradually increases.

The same is true for the Reno profile (Figure 4). The Lg/Pn ratio increases with distance out to the furthest station at 364 km. However, the apparent Pn velocity is a fast 8.5 km/sec, especially for the Basin and Range. Perhaps, there is an up-dip component to the Moho from NTS to the north-northwest. Furthermore, the Pg velocity is the same at 6.06 km/sec. Regardless, the Moho again appears not to be sooth, as there is a pronounced focusing effect of Pn energy at station BRH and defocusing of energy at COX and LRV.

Inverting the Pn and Pg times from both profiles, we find the Moho does dip downward to the east and upward to the north-northwest. We constrained the Moho to be flat and used a Pn velocity of 7.8 km/sec for the Reno profile and 7.9 increasing to 8.0 km/sec for the UA profile. However, since this is an extremely non-unique problem, we inverted for a Moho structure consisting of 3 to 5 line segments over the 400 km length of the model. This resulted in a crustal thickness under

NTS of approximately 30 km. From NTS, out to 300 km on the UA line (the furthest distance sampled), the crust stepped downward to a thickness of 40 km. Likewise, out to 370 km on the Reno line, the crust shallowed to 18 km.

NPE Spectral Ratios versus distance and azimuth

Both of the previously mentioned profiles share similar characteristics of interest to a verification problem They are deployed along 2 different azimuths from NTS and therefore, in this case, incorporate 2 different geologic/tectonic environments. As a result, the 2 profiles have different phase velocities. In spite of their different locales, azimuths, and distances, their spectral ratios each appear to behave as predicted. The Pn and Lg spectra decrease with distance, while the Lg/Pn ratio increases with distance along the two respective azimuths . However, it is necessary to ask it "how do these ratios compare between azimuths absolutely"? For the same distance, is the Lg/Pn ratio different at different azimuths? In other words, what effect does azimuth have on spectral discriminates within highly variable tectonic regimes? Furthermore, do spectral discriminates vary as a function of distance?

The Lg and Pn spectral values were determined for the 50 stations that recorded NPE (Figure 1) at different frequency bands (0.5Hz-1.0Hz, 1-2Hz, 2-4Hz, 4-6Hz, 6-8Hz, 8-10Hz). Lg/Pn at different frequency bands and the Lg and Pn spectral ratios were evaluated versus distance. In Figure 5, the Pn spectral ratio (0.1-10Hz/2-4Hz) is plotted as a function of distance. It is clearly seen that Pn decreases with distance independent of azimuth and reasonably independent of frequency band. The same is true of Lg at 0.1-10Hz/2-4Hz (Fig. 6). However, the Lg/Pn ratio shows a remarkably different character (Fig. 7). From 1-2Hz, Lg/Pn increases out to 400 km and then tapers off. Thus, from about 250 km to 500 km, the Lg/Pn ratio is large and highly scattered, making it an extremely variable discriminant within this distance range. This scattering occurs independent of azimuth, therefore, it cannot be tied to tectonic environment. This is also observed in the Lg/Pn ratio of different frequency bands. Figure 8 shows Lg from 1-2Hz ratioed with Pn at 6-8Hz. In the distance range of 250 to 500 km, the values are highly scattered.

Hunter's Trophy phase comparison

We compared NPE to Hunter's Trophy, a nuclear explosion at the NTS of approximately the same magnitude and virtually the same location. Walter et al. (submitted to *BSSA*) performed a thorough analysis of short-period phase and spectral ratio discriminates for 130 underground nuclear explosions, NPE, and 50 earthquakes that occurred at NTS. However, they have only two stations that recorded this activity. We use 14 permanent stations that recorded both Hunter's Trophy and NPE. Figure 9 shows 9 stations that recorded Pn from both NPE and Hunter's Trophy. The waveforms not only show remarkable similarity in terms of shape, but amplitude as well. The ratio value indicated in each box is the ratio of the first swing of Pn from Hunter's Trophy (HT) to NPE. The mean ratio of the 9 stations is 0.99, however, there is slight deviation between the stations. KNB has the maximum value of 1.32 and PFO has the smallest value of 0.58. There appears to be no correlation of ratio value with distance or azimuth. Pg could be distinguished at 5 stations (Fig. 10). The mean ratio value is 1.45, with a maximum of 1.7 at station GSC and a minimum of 0.93 at KNB. Once again, there appears to be no pattern of ratio values, as emphasized by KNB having the maximum Pn value and the minimum Pg value.

Likewise, P/S ratios were compared for the two explosions. The amplitude ratios for Pg/Sh at 5 stations and Pn/Sh at 7 stations were determined for a frequency window of 1 to 2 Hz and the values plotted as a function of distance and azimuth. There was strong correlation between HT and NPE implying that P to S ratios would be a poor method to discriminate between nuclear and chemical explosions. No pattern is apparent in the ratio values as a function of azimuth. There is a large increase in the Pg/S ratios at a distance range of approximately 400 km. However, this observation is only based on one station and may be unreliable, yet it is intriguing how this was also observed for the Lg/Pn ratios of NPE.

Crustal and Mantle Structure

On Septmber 19, 1993, several days prior to NPE, and earthquake at Chiapas, Mexico (distance to the profile is about 20^0), was recorde by nine stations of the profile. A teleseismic P wave propagating up to a seismic stations generates converted S waves at significant impedance contrasts (e.g., the Moho) beneath the station. Receiver functions are waveforms computed by

deconvolving the vertical component from the radial component of the P wavetrain to isolate converted phases within the coda. We used a time domain deconvolution procedure (Ammon, 1992) to compute reciever functions on oure profile. The raw data were low-pass filtered at about 3 s to emphasize the Moho P-to-S converted wave and to reduce the effects of a heterogeneous crust. The low-frequency band pass of the rceiver function eliminates most effects of crustal heterogeneity yet is sufficient to accurately measure the crustal Ps stravel time. Most of the low-pass receiver functions hav e one lare Ps arrival in the time window of 4-7 seconds, which we interpret as the converted Ps wave from the crust-mantle boundary (figure 11). Assuming a constant average crustal velocity of 6.25 km/s and Vp/Vs of 1.73 (for a Poisson solid), the observed Ps-P time can be used to estimate crustal thickness using the equation:

$$T_{Ps} - T_P = h/Vp * (Vp/Vs*\cos j - \cos i)$$

where i and j are the angles of incidence for the P and S waves, respectively. Receiver functions have an inherent non-uniqueness due to the trade-off between crustal velocity and thickness (Ammon et al., 1990). Therefore we also tabulate crustal thicknesses correspondings to curstal velocities of 6.0 and 6.5 km /s (Table 1). The crustal thickness profile determined from this simple travel time calculation reveals a crustal thinening from the Basin and Range to Colorado Plateau of approximately 20 km. The range of crustal thickness we sampled in the central part of the Basin and Range is 30-33 km, increasing to 35-38 km in the eastern side of the Basin and Range. This thickness reached the range of 49-53 km on western edge of the Colorado Plateau. Considering the large range in average crustal velocity we considered, the crustal thickness estimates should be fairly robust.

One final check on the crustal thickness comes from constraining the Vp/Vs ratios, and the variability along the profile. The crustal P wave velocity average varies from 6.0 to 6.6 km/sec in North America (Braile et al., 1989), which could change the thickness estimates from receiver function analysis by up to 3 km (see table 1). The average Vp/Vs ratio varies for 1.73 to 1.85, although extreme of 1.6 and 2.0 have been reported (Zandt and Ammon, 1995; Zandt et al., 1994). Our analysis of the NPE profile shows a variation of at least 13% (1.65-1.85), which could

significantly influence our crustal thickness estimates made from Ps-P travel times. Higher than normal Vp/Vs will result in a thinner crustal estimate and visa versa. However, higher Vp/Vs rocks tend to be associated with more mafic compositions and high average velocities, thus the high Vp tends to counteract the effect of Vp/Vs.

We estimate the crustal Vp/Vs along our profile using travel times of crustal multiples identified in our receiver functions there are two significant crustal multiples: one is a multiple with two P wave legs and one S wavbe leg, and the other is a multiple with one P wave leg and two S wave legs (see figure 11). The two P wave leg multiple PpPms (here after referred as the P multiple) is the phase that refelcts off the surface then is converted to an S wave on reflection from the Moho. The travel time difference between the P multiple and Ps is simple the two-way travel time through the crust for a ray with rap parameter *p*:

$$T_{PpPms} - T_{Ps} = 2h\,(1/V^2 - p^2)^{1/2}$$

The two S leg multiple (here after called the S multiple) is composed of two kinematically similar waves PpSms + PsPms, which have identical travel times in a uniform layer (again, see figure 11). The travel time difference between this S multiple and direct P wave is the two-way S wave travel time through the crust;

$$T_{PsPms} - T_p = 2h(1/V^2{}_s - p^2)^{1/2}$$

The ratio of the travel time multiples is proportional to Vp/Vs, independent of crustal thickness, but the S wave multiple is generall difficult to identify, prolavley becuase it is composed of two seperate rays and has a greater chance of being affected by lateral heterogeneity and adding out of phase.

On the basis of the receiver function multiple, we suggest that the Colorado Plateau stations are located on crust with a significantly above average Vp/Vs -- which is 1.84-1.86. In contrast, the western most Basin and Range stations are located on crust with a low Vp/Vs, or 1.62-1.64. Vp/Vs is near normal at the middle stations. The crustal thickness variations between stations of our selected grouping is less than 2-3 km for all models, except stations 9 and 10 which differ by 5 km. The Ps phase at station 9 may be smapling a local crustal rot beneat the northen end of the

high She p Range similar to local crustal roots imaged in the southern Basin and Range (McCarth et al., 1991; Myers and Beck, 1994). The Ps phase is sampling the curst out to 5-10 km fromthe station, buth the multiple sample 2-3 time that distance (see figure xx). We did some simple calculations to exame the possible effects of the crust that increases in thickness by 5 km over the distance sample by the P multiple We found that the estra 5 km of crustal thickness would result in about a 3.5 % underestimate of Vp/Vs. Our estimatesd deviation from normal for this group is maginally greater than the estimated error, but we note that some htis deviation may be due to the breakdown of the uniform curst assumption.

In summary, we found model B in table 1 is most consistent with teleseismic travel times, Bouguer gravity and isostatic elevations. In model B, the crustal velocity is 6.25 km/s (Vp/Vs = 1.85) in the Plateau, 6.1 km/s (1.73) in the estern Basin and Range, and 6.0 km/s (1.73) in the central Bansin and Range. The prefered crustal thickness results are shouw in figure xy with thickness plotted approximately where the receiver function samples the Mohon along the source-receiver great circle path, offset from the receiver towards the soure. The crust is between 30 and 35 km in the Basin and Range and thickens to about 44 km in the Colorado Plateay which is also characterized by a high Vp/Vs ratio of 1.85.

Conclusions

We have made seismic recordings of the NPE explosion along a profile cross the Basin and Range on to the Colorado Plateau. The profile, which contained 10 stations, showed remarkable character in terms of Pn and Pg amplitudes, although at all stations the waveforms were consistent with those expected for an explosion. However, when the waveforms from all the stations in the Western U.S. are considered, there is a strong anomoly in the Lg to Pn amplitude at 400 to 450 km. Although this effect needs to be investigated more fully, it suggests that discrimination based on a single station must be calibrated for distance.

References

Ammon C. J., G.E. Randall and G. Zandt (1990). On the non-uniquess of receiver function inversions, *J. Geophys. Res.*, *95*, 15,303-15,318.

Braile, L.W., W.J. Hinze, R.R. B. von Frese and G.R. Keller (1989). Seismic properties of the curst and uppermost mantle of the coterminous United Sates and adjacent Candada, in Geophycisl Framework of the Continental United States, editied by L.C. Pakiser and W.D. Mooney, *Mem. Geol. Soc. Am., 172,* 655-680.

Myers, S.C. and S.L. Beck (1994). Evidence for a local crustal root beneath the Santa Catalina metamorphic core complex, Arizona, *Geology, 22,*223-226.

Zandt, G. and C.J. Ammon (1995). Continental crustal compostion constrained by measurements of crustal Poisson's ratio, *Nature,* in press.

Figure Captions

Figure 1: Maps of station deployment, simplified geology (from Wernicke et al., 1988), and major geogrpahic features. Heavy line are Cenozoic faults, oppoising arrow s indicate sense of slip on strike-slip faults and D/U indicates the down and up thrown sides of normal faults. In bold nubers are our preferred estimates from crustal thicness (in km) at approximate locations show.

Figure 2: Broad band stations which recorded NPE.

Figure 3: Reduced travel time profile for NPE along SASO profile. Pn velocity (7.58 km/s), Pg (6.04 km/s) and Lg window are shown.

Figure 4: Reduced travel time profile for NPE along an NE azimuth from NTS. Pn velocity (8.58 km/s), Pg (6.27 km/s) and an Lg window are shown.

Figure 5: Pn spectra ratioed at two different frequencies. The ratio increases with distance due to attenuation. In general, paths to the west show more attenuation than those to the south.

Figure 6: Lg spectra ratioed at two different frequencies. Lg is apparently not well developed before 300 km.

Figure 7: Lg to Pn spectra ratio. This is one of the best discriminates, although there are two distance effects. Note that as distance increases the ratio increases (looks more earthquake like); further, at 400 km Lg becomes abnormally large.

Figure 8: Comparision of Pn for HUNTER'S TROPHY and NPE.

Figure 9: Comparison of Pg for HUNTER'S TROPHY and NPE.

Figure 10: (a) Synthetic radial component receiver function for a simple layer over halfspace model. Main phases and multiples corresponding to the ray path shown below. (b) Ray paths for converted Ps phase and major multiples for a simple layer over half-space model.

Figure 11:

Table 1. Crustal Thickness and V_p/V_s Estimates From Travel Times of Converted Phases and Multiples Picked From Receiver Functions of the September 19, 1993, Chiapas, Mexico Earthquake

Station	Ps-P, s	H, km			Pm-Ps, s	V_p/V_s			H, km		V_p/V_s	H, km Model C
		6.25 km/s	6.00 km/s	6.50 km/s		6.0 km/s	6.25 km/s	6.5 km/s	Model A	Model B		
KNB	6.20	49.0	47.4	50.6					44.2	42.3		44.9
1	6.50	51.4	49.7	53.1					46.4	44.4		47.1
2	6.40	50.6	48.9	52.3					45.7	43.7		46.3
Stk1-2	6.45	51.0	49.3	52.7	12.3	1.86	1.85	1.84	46.0	44.1	1.80	46.7
3						no data						
4	4.60	36.4	35.2	37.6					36.4	34.7		35.2
5	4.85	38.4	37.1	39.6					38.4	36.6		37.1
6	4.50	35.6	34.4	36.8					35.6	34.0		34.4
Stk4-6	4.65	36.8	35.6	38.0	10.1	1.75	1.73	1.73	36.8	35.1	1.73	35.6
7	3.90	30.8	29.8	31.9					29.4	29.4		29.8
8	4.20	33.2	32.1	34.3					31.7	31.7		32.1
Stk7-8	3.95	31.2	30.2	32.3	8.65	1.74	1.72	1.72	29.8	29.8	1.73	30.2
9	4.20	33.2	32.1	34.3					36.5	34.9		32.1
10	3.60	28.5	27.5	29.4					31.3	29.9		27.5
Stk9-10	4.05	32.0	31.0	33.1	10.2	1.64	1.62	1.62	35.2	33.6	1.73	31.0

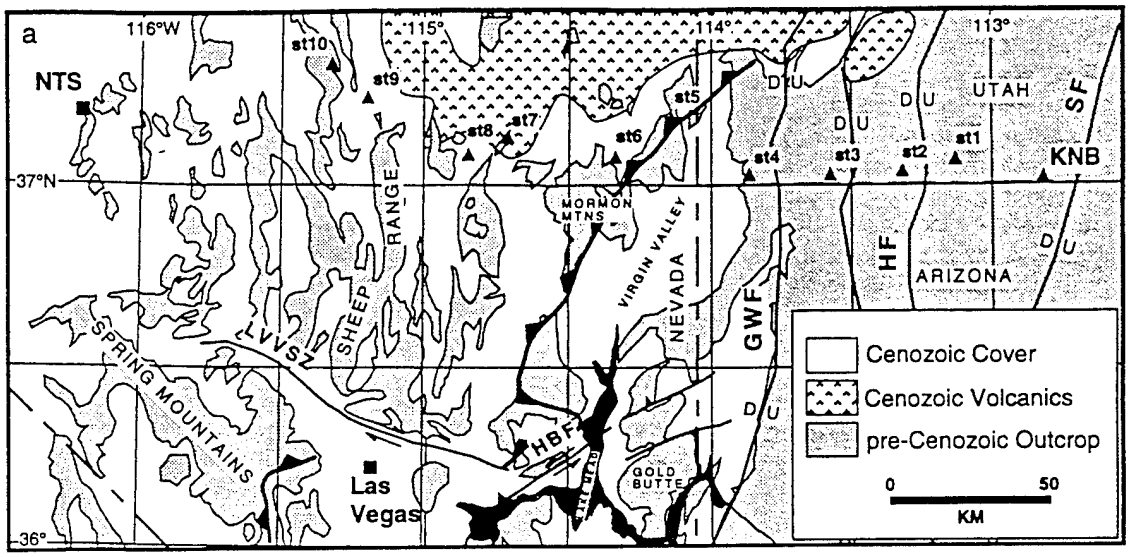
a
116°W
115°
114°
113°
37°N
36°
NTS
st10
st9
st8
st7
st6
st5
st4
st3
st2
st1
KNB
UTAH
ARIZONA
NEVADA
SF
HF
GWF
HBF
LVVSZ
SHEEP RANGE
SPRING MOUNTAINS
MORMON MTNS
VIRGIN VALLEY
GOLD BUTTE
Las Vegas
Cenozoic Cover
Cenozoic Volcanics
pre-Cenozoic Outcrop
0
50
KM

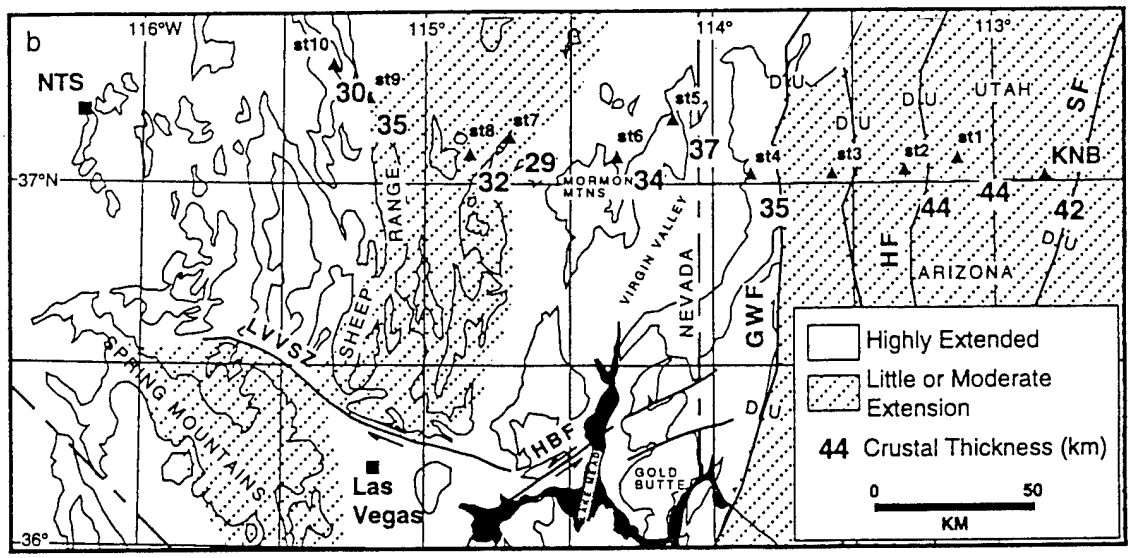
b
116°W
115°
114°
113°
37°N
36°
NTS
30
35
29
32
34
37
35
44
44
42
KNB
UTAH
ARIZONA
NEVADA
SF
HF
GWF
HBF
LVVSZ
SHEEP RANGE
SPRING MOUNTAINS
MORMON MTNS
VIRGIN VALLEY
GOLD BUTTE
Las Vegas
Highly Extended
Little or Moderate Extension
44 Crustal Thickness (km)
0
50
KM

Stations That Recorded NPE

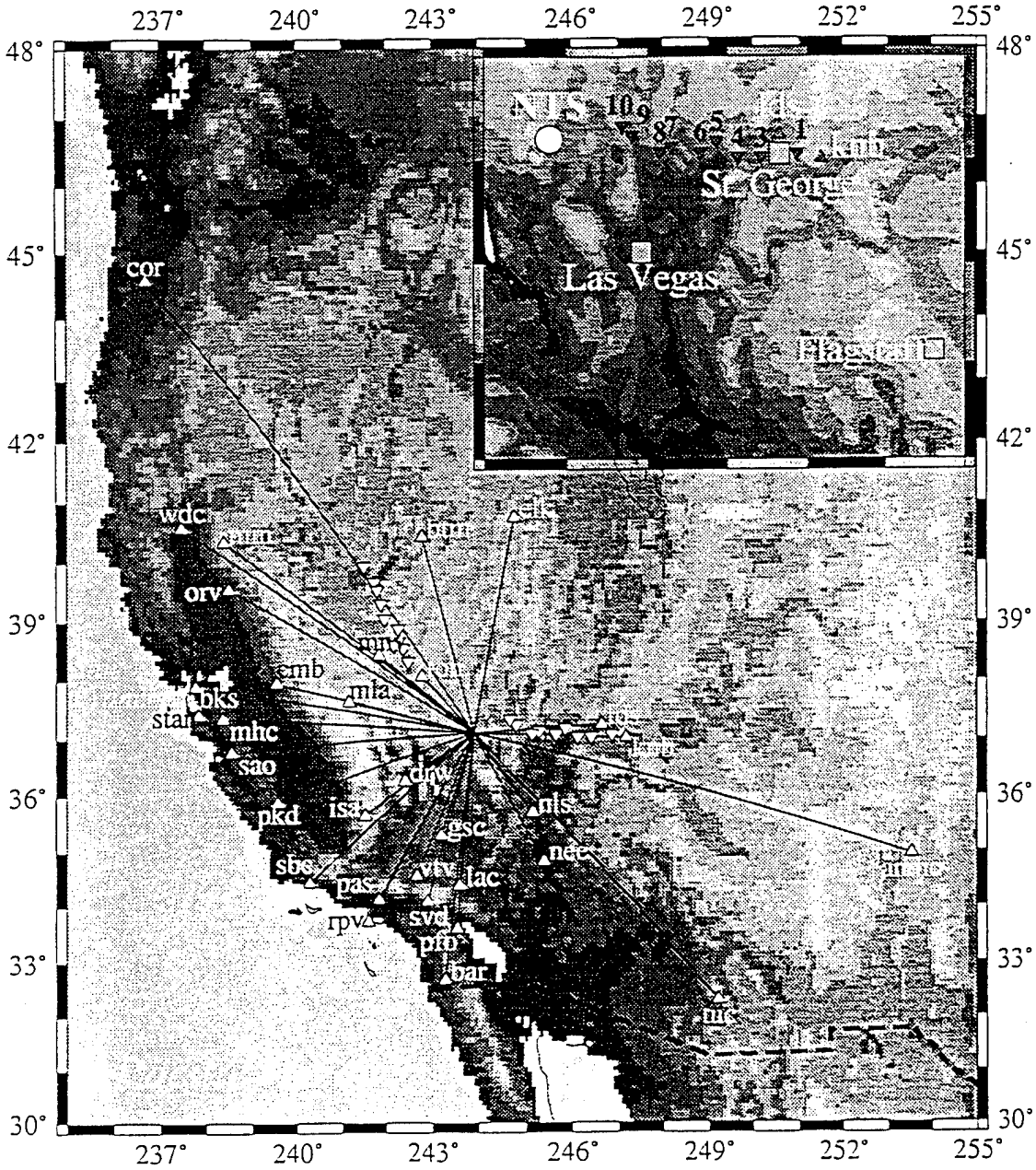

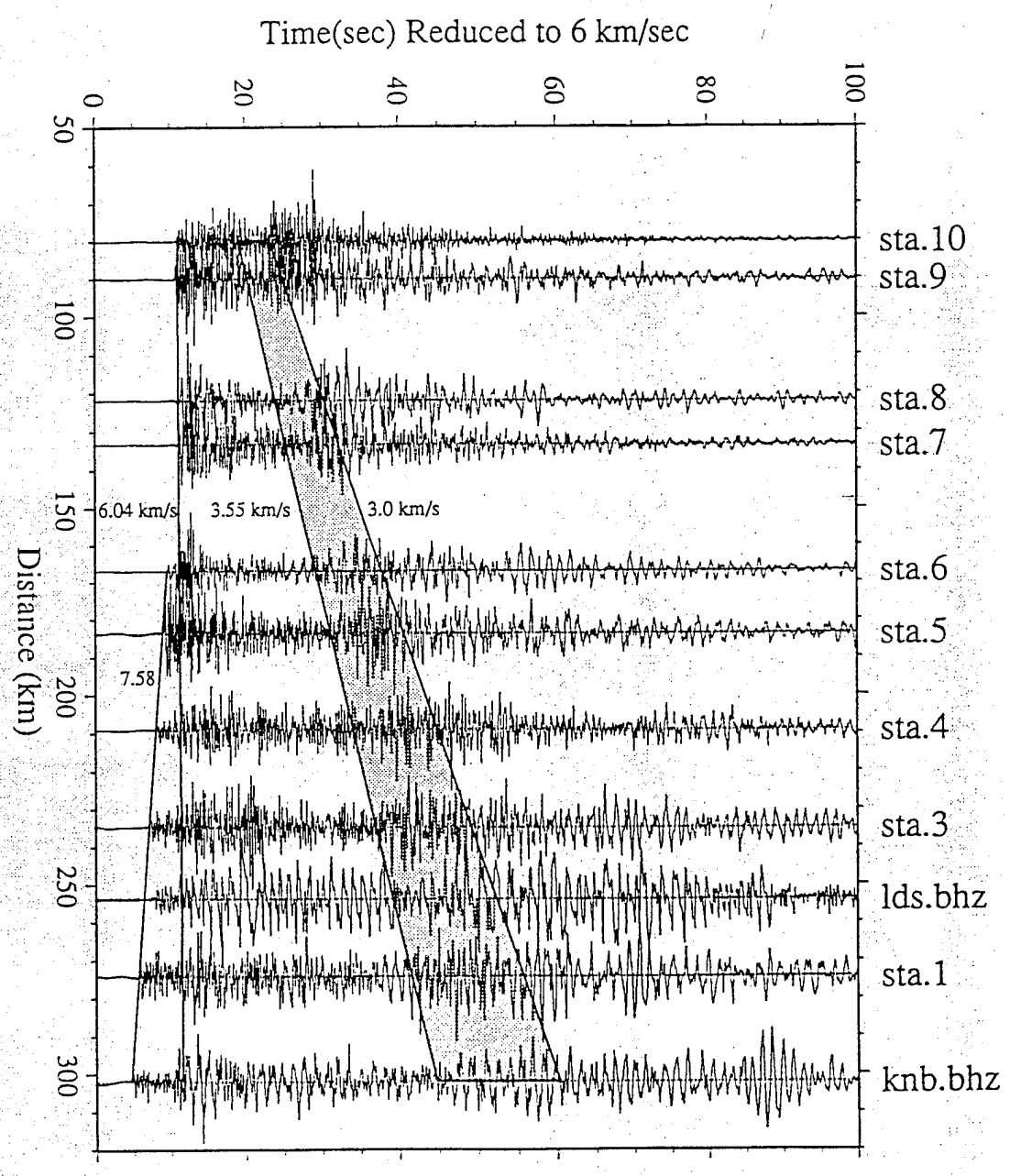
Time(sec) Reduced to 6 km/sec
0
20
40
60
80
100
Distance (km)
50
100
150
200
250
300
6.04 km/s
3.55 km/s
3.0 km/s
7.58
sta.10
sta.9
sta.8
sta.7
sta.6
sta.5
sta.4
sta.3
lds.bhz
sta.1
knb.bhz

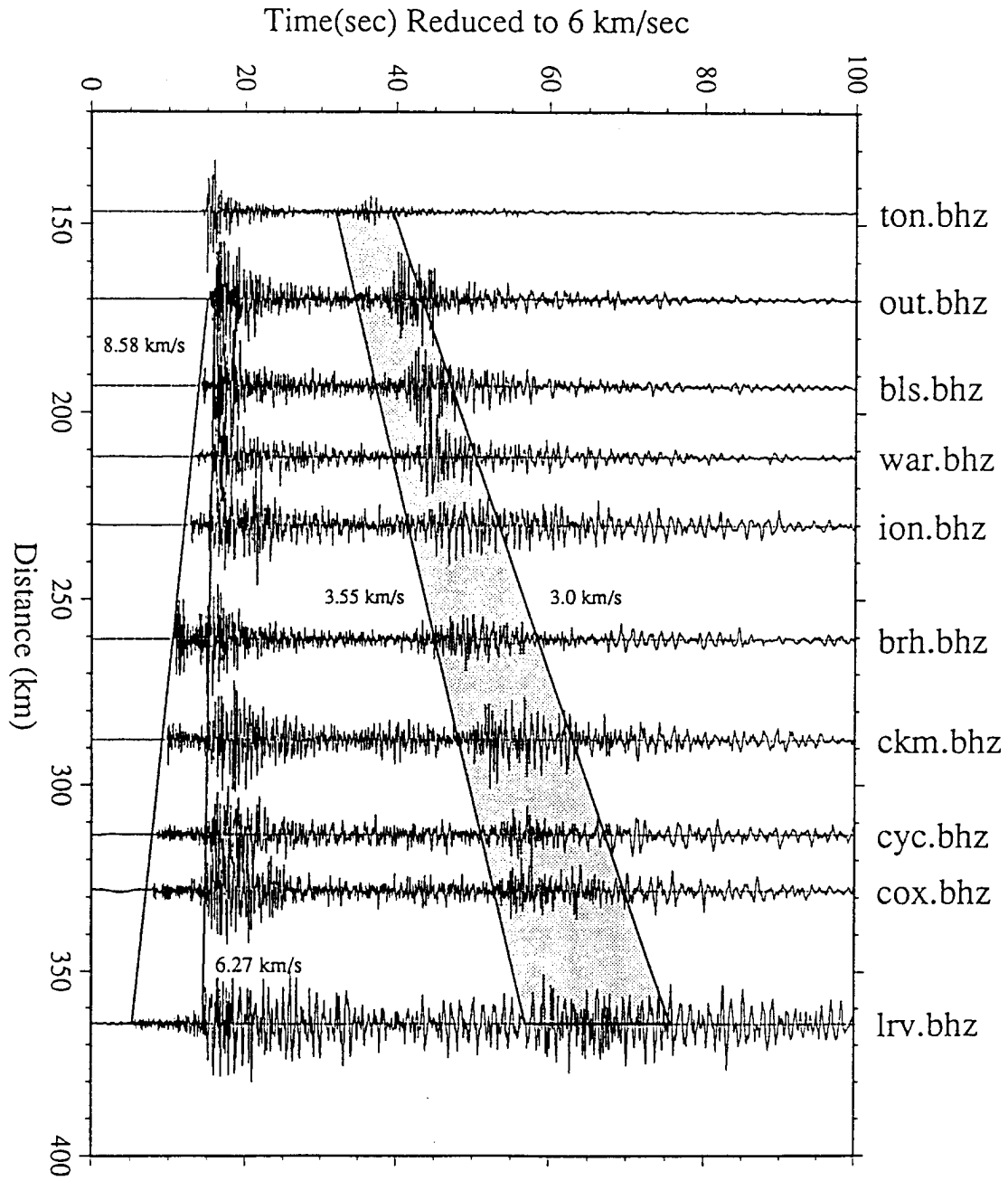
Time(sec) Reduced to 6 km/sec
0
20
40
60
80
100
Distance (km)
150
200
250
300
350
400
8.58 km/s
3.55 km/s
3.0 km/s
6.27 km/s
ton.bhz
out.bhz
bls.bhz
war.bhz
ion.bhz
brh.bhz
ckm.bhz
cyc.bhz
cox.bhz
lrv.bhz

Pn Ratio 0.1-10/2 to 4 Hz

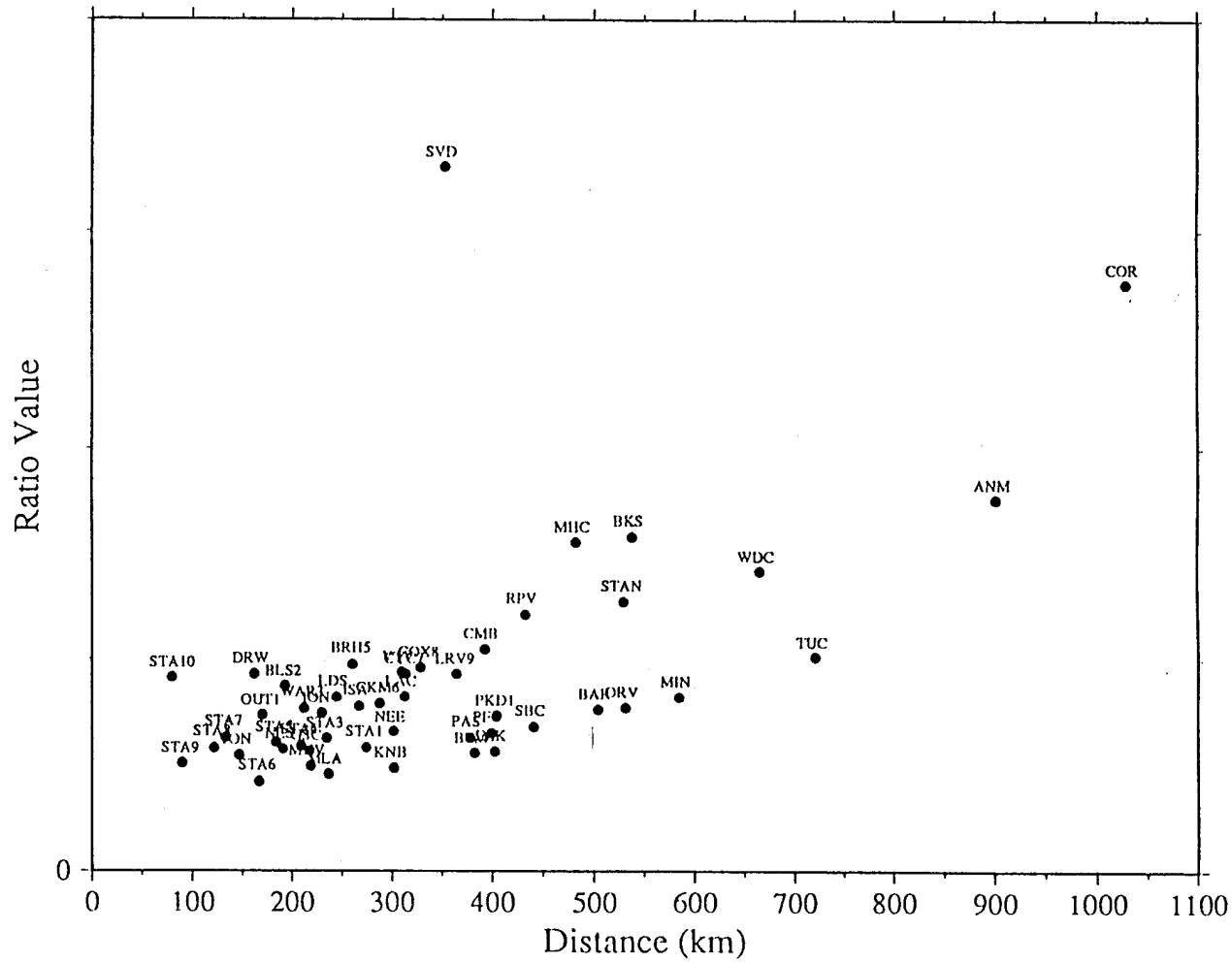

Lg Ratio 0.1-10/2 to 4 Hz

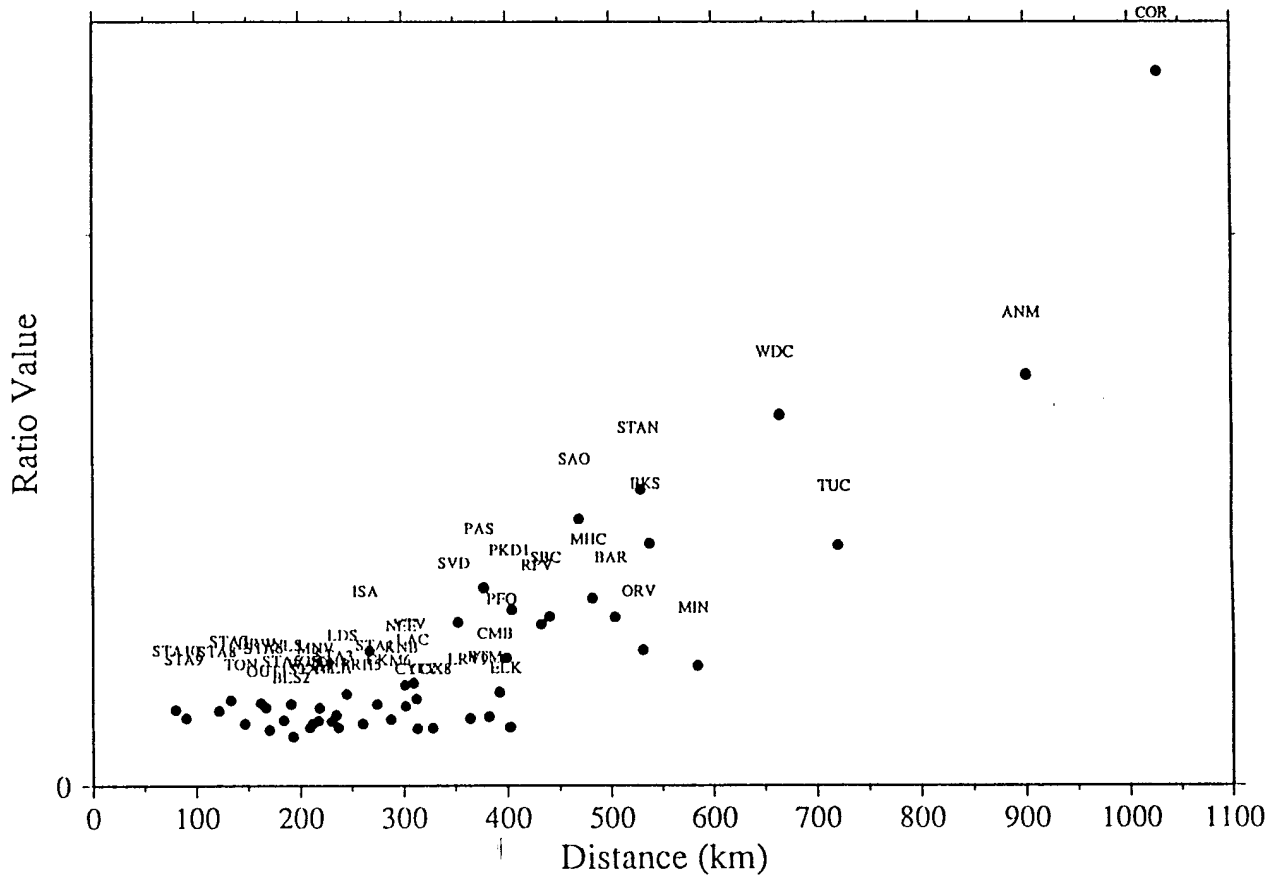

Lg (1-2)/Pn (4-6)

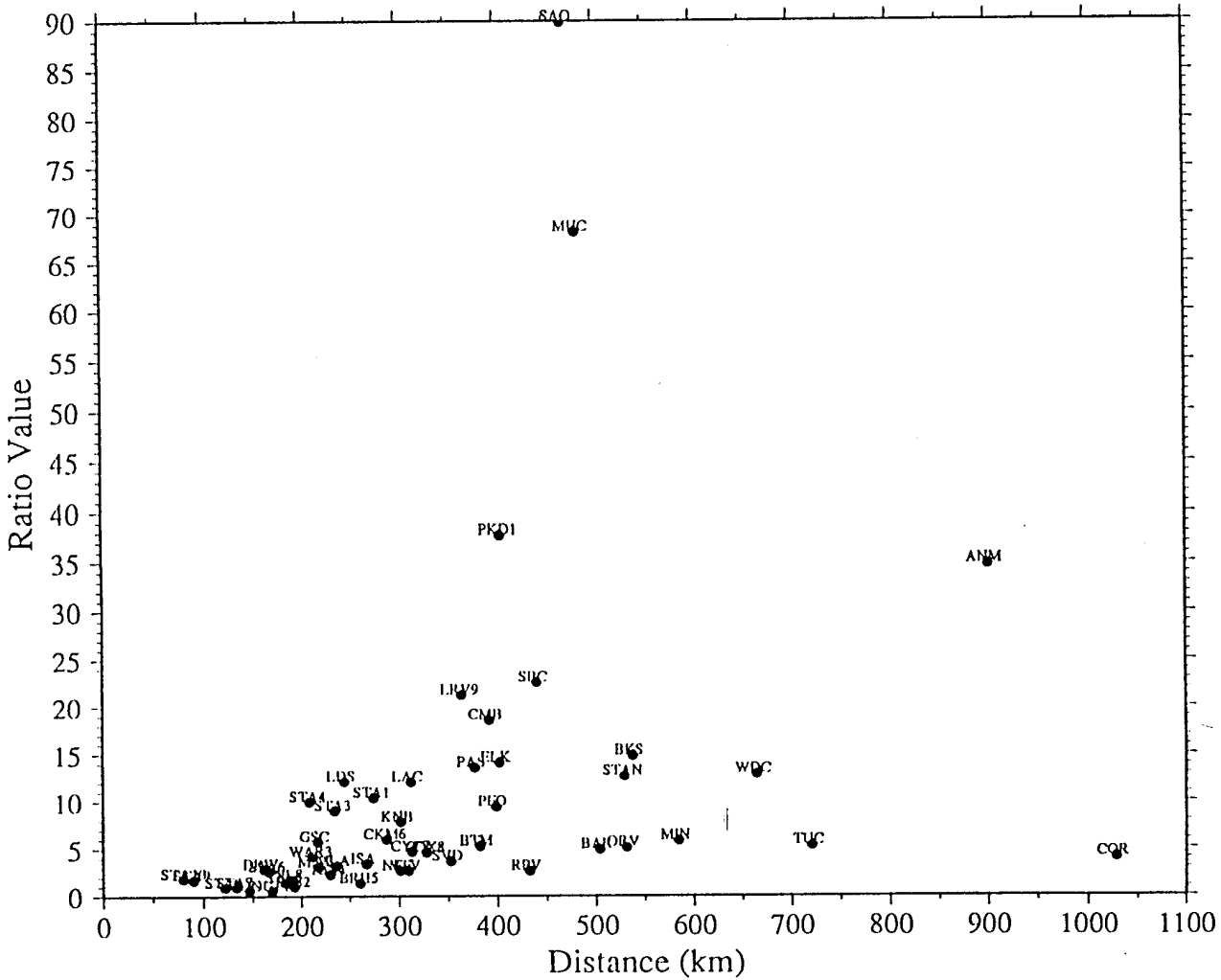
Ratio Value
Distance (km)
0
5
10
15
20
25
30
35
40
45
50
55
60
65
70
75
80
85
90
0
100
200
300
400
500
600
700
800
900
1000
1100
SAO
MUC
PKD1
ANM
SIC
LBW9
CMB1
BKS
STAN
WDC
LDS
LAC
PUO
KNB1
MIN
TUC
COR
RDV

Pn Comparison Between Hunter's Trophy and Chemical Kiloton

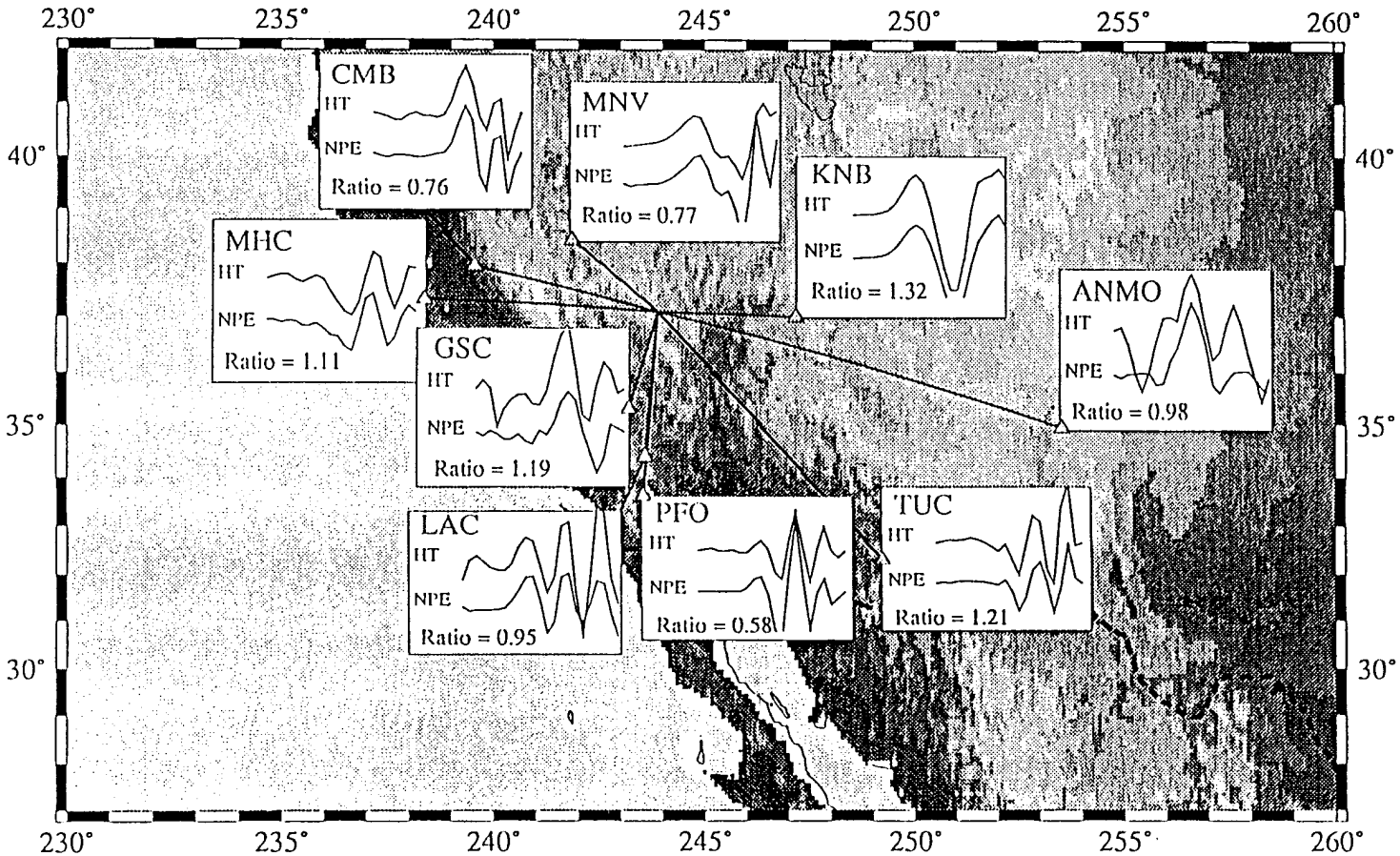

GMT Jun 4 16:30 Example 3

Pg Comparison Between Hunter's Trophy and Chemical Kiloton

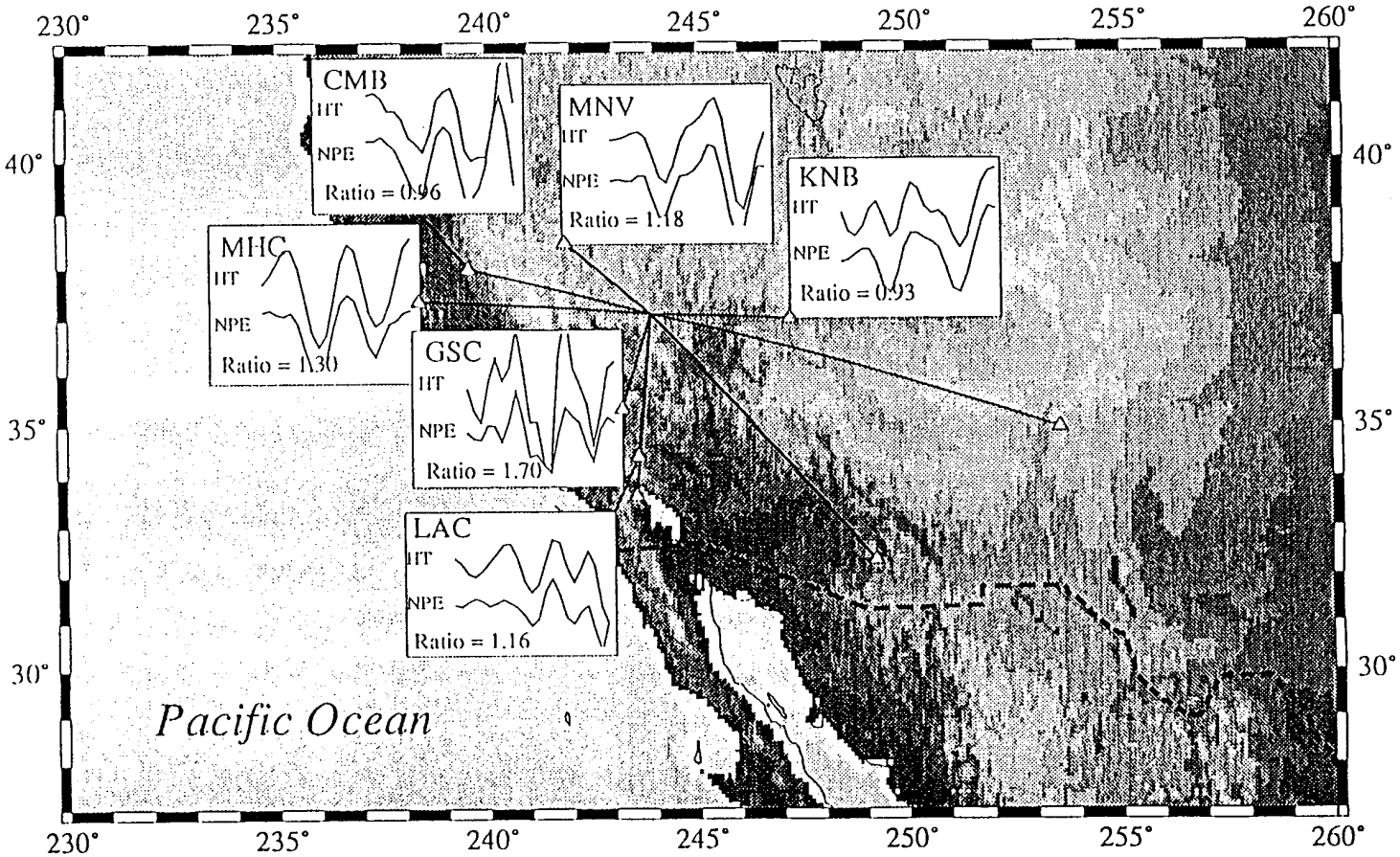

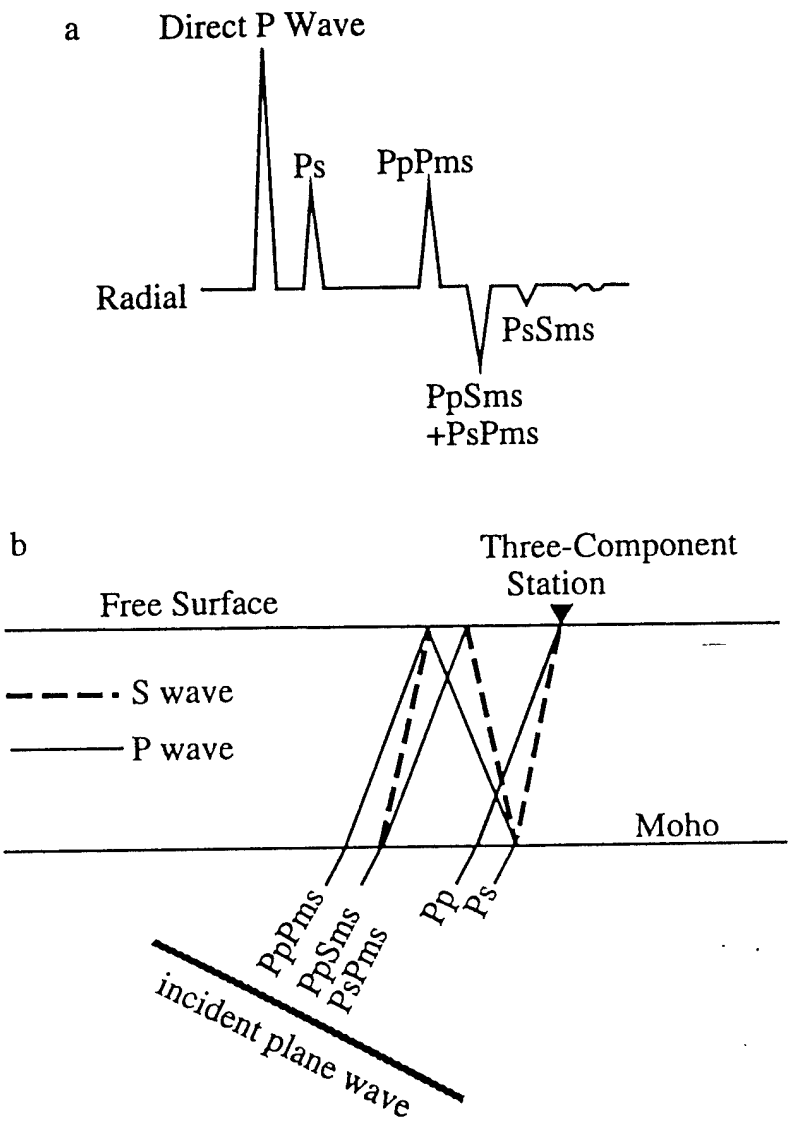
a
Direct P Wave
Ps
PpPms
Radial
PsSms
PpSms
+PsPms
b
Three-Component
Station
Free Surface
S wave
P wave
Moho
PpPms
PpSms
PsPms
Pp
Ps
incident plane wave